

DAVID A. HARDY

CASE FILE
COPY

DEPARTMENT OF
SPACE PHYSICS
AND
ASTRONOMY
RICE UNIVERSITY

HOUSTON, TEXAS 77001

(NASA-CR-141732) OBSERVATION OF LOW ENERGY
PROTONS IN THE GEOMAGNETIC TAIL AT LUNAR
DISTANCES M.S. Thesis (Rice Univ.) 127 p
HC \$5.75

CSCL 03B

N75-22251

Unclas

G3/93 19265

RICE UNIVERSITY

Observation of Low Energy Protons in the
Geomagnetic Tail at Lunar Distances

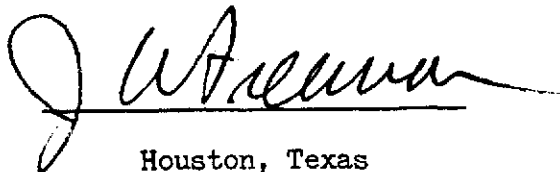
by

David Alfred Hardy

A THESIS SUBMITTED
IN PARTIAL FULLFILLMENT OF THE
REQUIREMENTS FOR THE DEGREE OF

MASTER OF SCIENCE

Thesis Directors Signature:

A handwritten signature in dark ink, appearing to read "J. W. Freeman", is written over a horizontal line.

Houston, Texas

September, 1974

NAS 9-5911

TABLE OF CONTENTS

page

CHAPTER ONE

1.1	Introduction.....	1
-----	-------------------	---

CHAPTER TWO

2.1	Description of Instrument.....	6
2.2	Design of Instrument.....	9
2.3	Location and Orientation.....	10
2.4	Data Conversion.....	11
2.5	The Explorer 35 Magnetometer.....	13
2.6	Method of Data Analysis.....	14

CHAPTER THREE

3.1	Introduction.....	17
3.2	Lunation 1.....	19
3.3	Lunation 2.....	22
3.4	Lunation 9.....	24
3.5	Lunation 13.....	26
3.6	Lunation 3.....	28
3.7	General Observations.....	28
3.8	Observational Conclusions.....	35
3.9	Theoretical Considerations.....	37
3.10	Further Analysis.....	41

OBSERVATION OF LOW ENERGY PROTONS IN THE
GEOMAGNETIC TAIL AT LUNAR DISTANCES

by

David Alfred Hardy

ABSTRACT

Using the three Suprathermal Ion Detectors stationed on the moon, we have detected a region of plasma flowing anti-sunward along the ordered field lines of the geomagnetic tail. This plasma flow is found within the tail, but exterior to the plasma sheet. It exhibits characteristics uniquely different from the other particle regimes traversed by the moon. The particles display an integral flux of from $.1$ to 9×10^7 ions/cm² sec ster, a bulk velocity of from 100 to 250 km/sec, temperatures in the range $.4$ to 5×10^5 degrees Kelvin and number densities between $.1$ and $5/\text{cm}^3$.

The magnetic field configuration for the times during which the particles were observed exhibits a direction and magnitude that is indicative of the lobes of the geomagnetic tail. In addition, no consistent deviation in the field is seen to correspond with the occurrence of the events. The events have an angular distribution extending over between 50 and 100 degrees.

Spatially the events extend over a wide region in both the Y_{sm} and Z_{sm} directions. Continuous observations of these particles are seen over distances as great as $17 R_e$ in the Y_{sm} direction and $12 R_e$ in the Z_{sm} direction. The majority of the encounters with

this flowing plasma, however, are found in a $12 R_e$ wide region adjoining the magnetopause. Also there are wide variations between tail passages as to the extent of time over which the particles are seen with an apparent correlation between the number of hours of observation and the Kp index averaged over these times.

It is proposed that these particles may have entered through the cusp region. The particles could then be convected down towards the neutral plane by $E \times B$ drift and eventually be accelerated by a neutral line to produce the particles in the plasma sheet.

CHAPTER ONE

1.1 Introduction

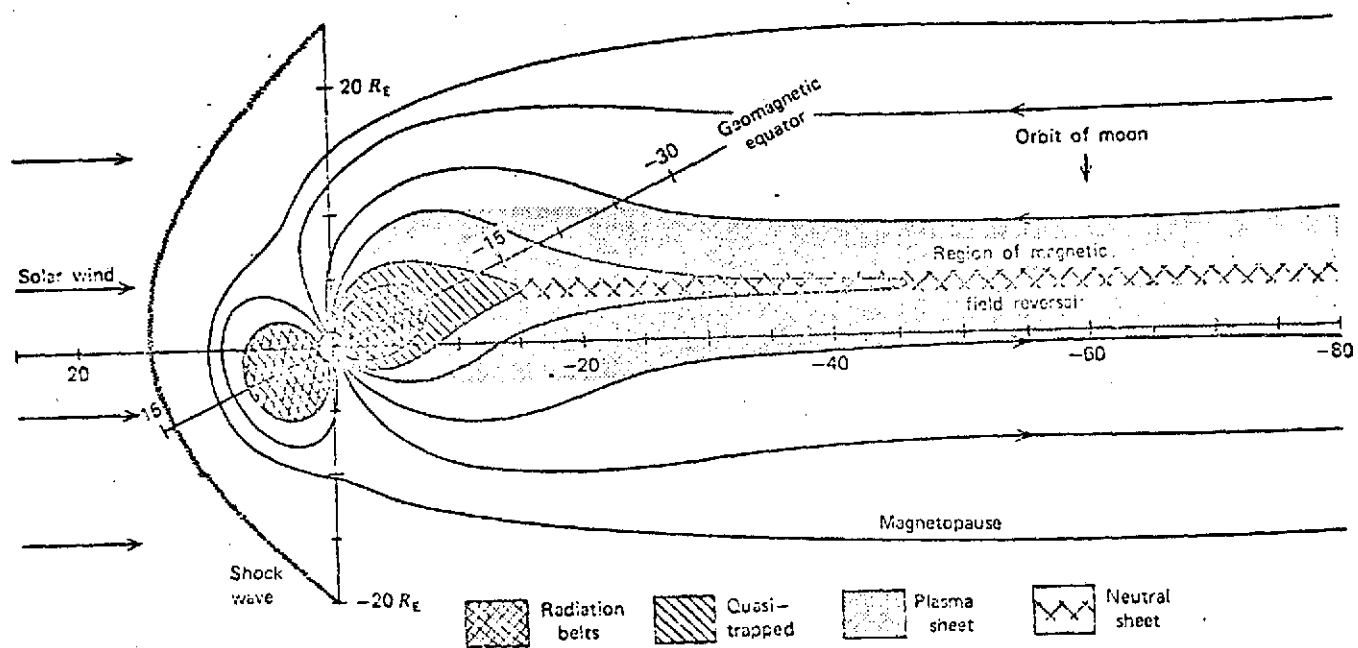
The near earth space environment is dominated by the interaction between the dipole magnetic field of the earth and the fully ionized plasma which flows outward from the sun's corona [the solar wind]. This interaction results in the production of particle reservoirs and currents systems which grossly distort the earth's field. The investigation as to the exact nature as to these processes has been and remains a fruitful area for research.

The general configuration for the region is shown in Figure 1.1. The plasma of the solar wind travels outward from the sun achieving a velocity of ~ 400 km/sec and a number density of $\sim 5/\text{cm}^3$ by the time it reaches the near earth region. Because of its high conductivity it carries with it the solar magnetic field lines. Since its speed is much greater than the Alfvén speed the flow is supersonic and a shock front is produced when this flow encounters the obstacle presented by the earth's magnetic field. This standoff shock is normally found $15 R_e$ in front of the earth. It thermalizes the plasma, i.e., it changes much of the flow energy into random thermal energy. These particles continuing to stream toward the earth form a region called the magnetosheath. These particles in the magnetosheath continue to compress the earth's field behind the shock until the increase in magnetic pressure of the earth's field balances the particle and field pressures of the flowing plasma. This region where the earth's field generally excludes the solar plasma is known as the magnetosphere with the boundary between the two regions being called the magnetopause.

Figure 1.1

Cross sectional representation of the earth's magnetosphere, the magnetosheath, bow shock, and solar wind. (Hess, 1968)

Figure 1.1



The magnetosphere is immensely complicated comprised as it is of a large number of interrelated field and particle regimes. Close to the earth the field is generally near to its dipole configuration. As one considers regions progressively more removed from the earth the deviation becomes more and more significant. One of the most remarkable aspects of this is the generally drawing out of the field lines from the polar caps to form an extended magnetic region known as the geomagnetic tail.

The tail is one of the most intriguing subjects in magnetospherics. Despite 14 years of research much of its basic nature remains unclear or disputed. Its possible existence was first proposed by Piddington (1960). He suggested that geomagnetic storms arose from the arrival of solar plasma which by pulling back the polar field lines to form a tail, would decrease the earth's field as is observed. Though such a theory failed to account for all the aspects of a geomagnetic storm, it did correctly show that streaming plasma could extend the polar field lines. The case for a continuous streaming plasma was considered shortly later by Johnson (1960).

The first observational evidence for such a region was provided by Explorer X (Heppner et al., 1963) when a basically antisunward pointing field was found just within the magnetopause at $22 R_e$. This was later confirmed by the Explorer XIV instruments (Cahill, 1964a) which mapped the field back to $16 R_e$. It was shown that the field was approximately dipolar out to ten earth radii. Beyond this there was substantial deviation observed with a generally tail like configuration at the satellites apogee ($16 R_e$). The final confirmatory evidence was provided by the IMP 1 Satellite which mapped the tail out to $34 R_e$.

(Ness, 1965). It was shown that the tail configuration commenced at $\sim 10 R_e$ and in all likelihood extended much beyond the $34 R$ to which the satellite's orbit extended. It now appears that the tail extends to at least $80 R_e$ with the theoretical models predicting a length anywhere from $100 R_e$ (Dungey, 1965) to $20 - 50 \text{ A.U.}$ (Dessler, 1965).

There exists as of the moment no theory which fully accounts for the nature of the tail's fields and particles. Its morphology, however, has been fairly well ascertained. It consists of two tubes of flux which are swept principally from the two polar caps. This sweeping back of magnetic field lines produces a null region or cleft in the front of the magnetosphere where the lines go from the closed dipole configuration to the streaming configuration of the tail. Between the two bundles there is a neutral sheet; a current sheet where the magnetic field magnitude is close to zero and across which the field vector changes directions by 180° (Ness, 1964). Surrounding the neutral sheet above and below is a region of warm plasma called the plasma sheet. In the near earth region it has a total thickness of $\sim 6 R_e$ at the median of the tail (Bame et al., 1966) with a flaring towards the magnetopause to approximately twice this value. The magnetic field magnitude is generally smaller in the plasma sheet than in the lobes with a gradual increase in the field magnitude as the distance perpendicular the neutral plane increases. There is also a general thinning of the plasma sheet for increasing distance away from the earth. It extends, however, at least as far as lunar distance (Rich, 1972).

As stated before the exact nature of the mechanisms which lead to the production of a tail configuration as described above are not known. Two, approaches, however, are generally popular. The first relies on a viscous interaction between the interplanetary and terrestrial fields in order to pull the field lines out to some distance behind the earth (Piddington, 1963). The other approach requires a direct connection of the field lines between planetary and interplanetary regimes. The interplanetary field lines would then tend to draw out the earth field lines as the plasma in which they are imbedded flows past the earth.

Though either of these mechanisms can describe the general distortion produced they have difficulty in accounting for the detailed nature of the region. The plasma sheet's origin, in particular, remains a considerable problem. Both a continuous particle source and an energizing mechanism are required to account for the existence of the particles. Although many theories have been proposed to account for this region none has been conclusively successful as of yet.

A new particle regime has been recently discovered which may shed some light on the problem of a source mechanism for the plasma sheet. The regime consists of a region of streaming plasma flowing along the ordered field lines of the high and low latitude lobes of the tail (Hones et al., 1972; Hones et al., 1973; Akasofu et al., 1973). This plasma, observed with the Vela satellites, exhibits fluxes only slightly less in intensity than those found in the magnetosheath. In addition these particles possess a bulk velocity of from 100 to 250 km/sec, number densities generally less than $1/\text{cm}^3$, and electron temperatures generally higher than those in the magnetosheath. (No exact representative numbers are given for the electron temperature

or number density in the articles cited above.) The observations from which these conclusions are derived were obtained at a distance of 18 earth radii down the tail. The particles at this distance are seen principally near the flanks of the tail with a maximum thickness of several earth radii and a thinning of the spatial extent with decreasing distance from the neutral plane. Since at 18 earth radii the phenomenon appears to consist of a boundary region between the magnetosheath and the tail it has been called the "boundary layer" by Akasofu.

Such a region of flowing plasma is important since it is at least potentially the observation of particles which have entered through the cleft and which further down the geomagnetic tail may be accelerated by a neutral line to produce the plasma sheet particles. Events which are similar to those observed by the Vela satellite have been observed at lunar distance by the Apollo Suprathermal Ion Detector Experiment (SIDE). It is in order to better understand these events and their relationship to the overall tail structure and maintenance that this study has been undertaken.

CHAPTER TWO

2.1 Description of Instrument

The data analyzed in this thesis was obtained from the three Suprathermal Ion Detector Experiments (SIDE) placed on the moon during the Apollo 12, 14, and 15 missions. These instruments, part of the Apollo Lunar Surface Experimental Package (ALSEP), are all basically of the same design. They consist of two particle detectors arranged in a side by side configuration. One, the Total Ion Detector (TID) is capable of discriminating positive ions by their energy per charge irrespective of mass. The other instrument, the Mass Analyzer (MA), is capable of discriminating positive ions according to both their energy and mass per charge.

The energy discrimination is accomplished in both devices through the use of a curved plate analyzer. This device consists of two curved plates with radii of curvature a and b , respectively ($a < b$) with a potential V_0 applied across the gap between them (see Figure 2.1). This V_0 produces a potential within the gap as a function of r given approximately by

$$V(r) = (V_0 \ln(r/a)) / \ln(b/a) ,$$

and an electric field,

$$E(r) = V_0 / r \ln(b/a) .$$

Figure 2.1

Trajectories for particles passing through a flat plate analyzer, a curved plate analyzer, and a Wien filter assuming that the voltages are arranged so that the particle may travel to the counter.

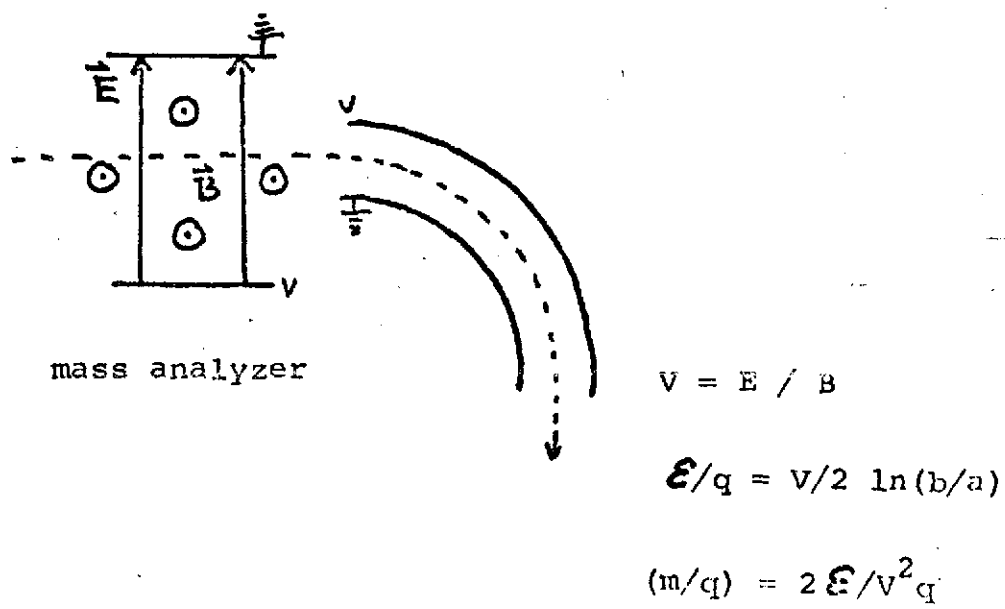
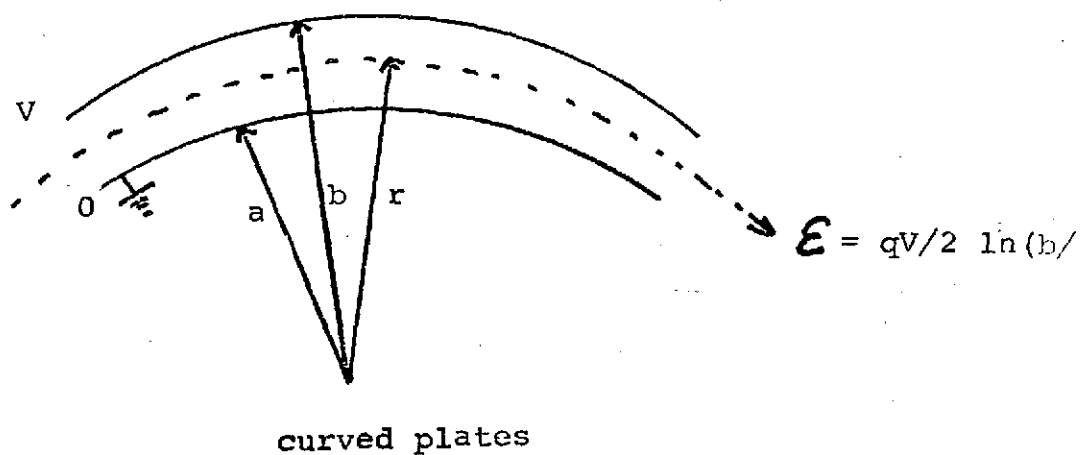
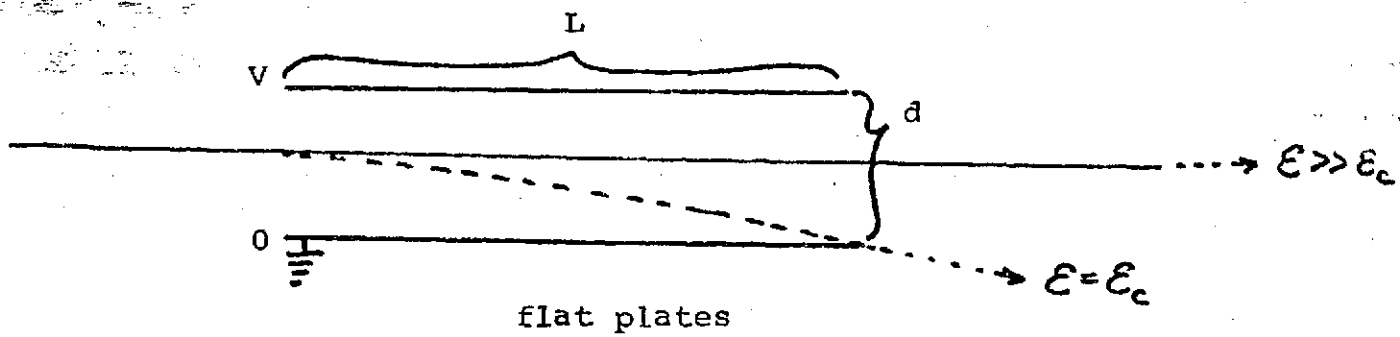


Figure 2-1

The incoming particles, collimated by the aperture for the device, enter the region of the curved plate travelling approximately perpendicular to the cross sectional area between the plates. In this region between the plates they are accelerated by the electric field and are thus made to travel in an arc of some radius r' . If the radius of curvature of this arc is within the limits of the curved plates, i.e., greater than a but less than b , the particles will travel through the device to the counter. This requirement for a particle to pass through the device is equivalent to a balancing between the centrifugal force produced by the particles circular motion

$$F_c = mv^2/r ,$$

and the force arising from the electric field

$$F_e = qE = qV_0/r \ln(b/a) .$$

This gives

$$F_c = F_e ,$$

or

$$mv^2/g = \text{Energy}/q = V_0/\ln(b/a) .$$

Since mv^2 is the kinetic energy of the particles, by varying V_0 , the instrument can be made to sample different energy ranges for the incident particles.

In the Mass Analyzer the mass discrimination is accomplished by using crossed electric and magnetic fields. The device consists of two parallel plates across which a voltage is applied and two permanent magnets arranged perpendicular to the plates. In general, particles entering the region where the two fields are operating will undergo displacement caused by both the electric and magnetic forces. This will tend to deviate the particle's trajectories so that they will not be observed. Only those particles for which the two forces are balanced will pass through without deviation and travel to the curved plate and therefore to the counter. The requirement for this to take place is that the Lorentz force be zero, i.e.,

$$q(\mathbf{E} + \mathbf{v} \times \mathbf{B}) = 0$$

$$\mathbf{v} = \mathbf{E}/\mathbf{B}$$

$$v = V_1/Bd$$

where V_1 is the potential across the plates and d the plate separation.

In the proceeding paragraph it was found that the condition for a particle to pass through the curved plate was that the centrifugal and electric force balance. This condition can be written as

$$m/q = V_0/\ln(b/a)v^2$$

Which after substituting for v^2 gives,

$$m/q = V_0 B^2 d^2 / \ln(b/a) V_1^2 .$$

The right hand side of this last equation contains only known quantities (B , d , b , and a) and voltages (V_0 and V_1) which can be varied. Therefore, by adjusting V_0 and V_1 the device can scan different mass ranges.

2.2 Design of Instrument

Figure 2.2 shows a schematic representation of the instrument; the upper section shows the Mass Analyzer and the lower section the Total Ion Detector. Both devices, as explained before, possess a curved plate analyzer for determining the energy of the particles. For the Mass Analyzer this is known as the Low Energy Curved Plate Analyzer (LECPA). It spans an energy range from .2 eV to 48.6 eV in six steps; 48.6 eV/q; 16.2 eV/q; 5.4 eV/q; 1.8 eV/q; .6 eV/q, and .2 eV/q. It is preceded by a Wien filter which produces the mass discrimination. At each energy the device steps through twenty mass channels. The Total Ion Detector's curved plate is called the High Energy Curved Plate Analyzer (HECPA). It measures the energy per charge of ions from 10 eV/q to 3500 eV/q in twenty steps; 10, 20, 30, 50, 70, 100, and 250 eV/q and then by increments of 250 eV/q up to 3500 eV/q.

In both cases the particles are counted by a Bendix channeltron[†], i.e., a channel electron multiplier. This device is held at a potential of 3.5 kilovolts in order to accelerate the particles after they leave the curved plate. This increases the detection efficiency of the channeltron by multiplying the number of secondary electrons emitted by the incident ion.

[†]Registered Trademark

The screen attached in front of the device is connected through a voltage stepping mechanism to a web like conducting screen laying on the lunar surface. This procedure couples the instrument electrically to the surface and thus leaves the region in front of the devices at a known voltage relative to the surface. The stepper voltage supply passes through 23 voltage steps from -27.7 volts to +27.7 volts with a change taking place everytime the instruments cycle through SIDE frame. This has been used extensively to determine the lunar surface potential in the magnetosheath (see Fenner et al., 1972). Figures 2.3 and 2.4 show the normal configuration and the deployed arrangement.

2.3 Location and Orientation

As stated previously the three instruments were stationed on the moon during the Apollo 12, 14, and 15 missions. The Apollo 12 instrument was deployed at longitude 23.5°W and latitude 3.0°S in the Ocean of Storms. It was stationed so as to look 15° west from the local vertical and approximately in the ecliptic plane. The Apollo 14 instrument was positioned 6° east of the Apollo 12 instrument at longitude 17.5°W and a latitude of 3.7°S in the Fra Mauro region. It was deployed with its look direction 15° due east from vertical again pointing approximately in the ecliptic plane. Since the two instruments are separated spatially by six degrees in longitude, the total difference in their look directions is 36° . The Apollo 15 instrument was deployed at a latitude of 26.11°N and a longitude of 3.65°E in the Hadley Rille area, i.e., more than 30° north of the other two instruments and 20° east of the Apollo 14 instrument. Its look direction is 15° east and 26° south of the local vertical so that it too points generally in

Figure 2.2

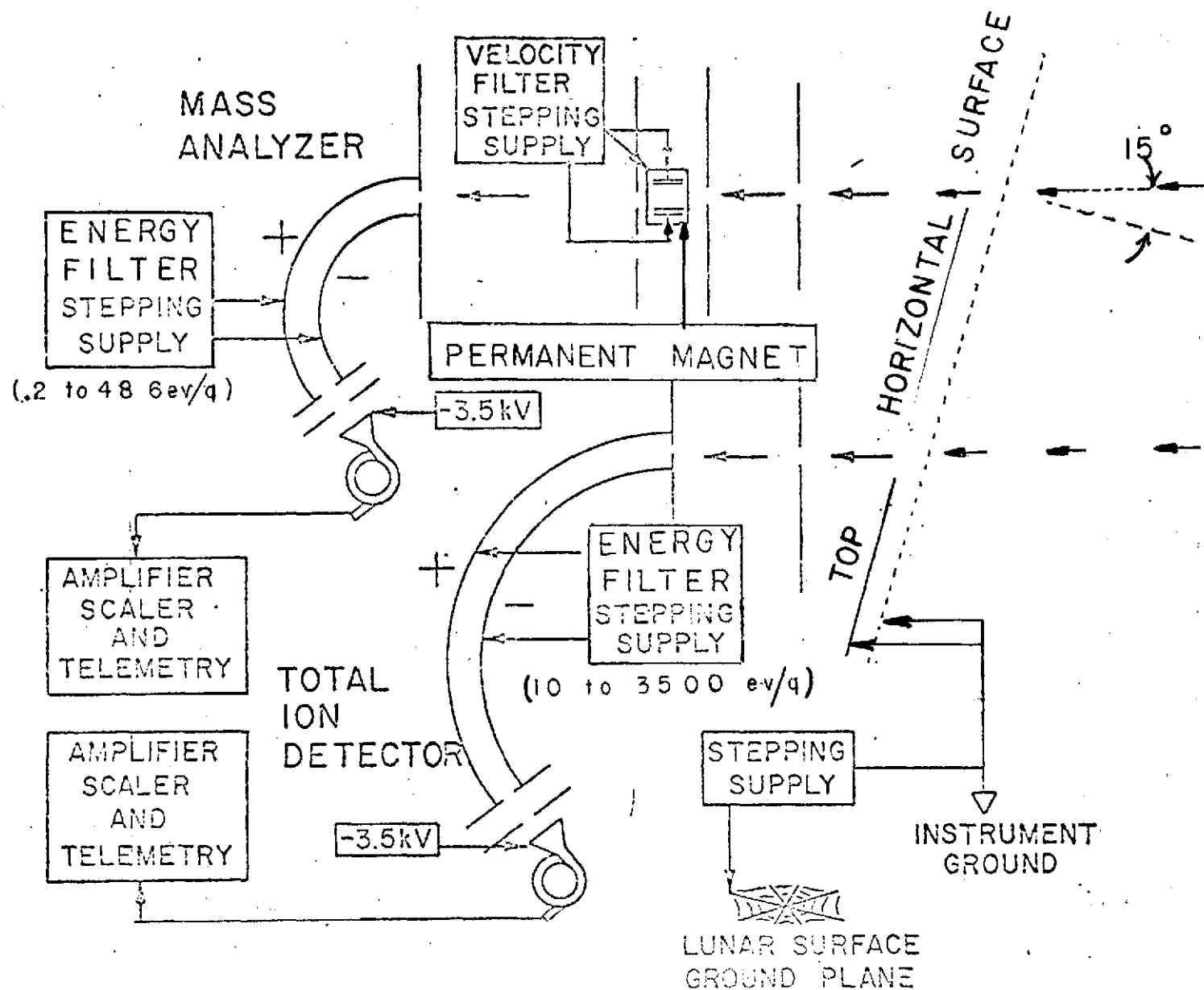
Schematic representation of the
of the operating components of the
SIDE.

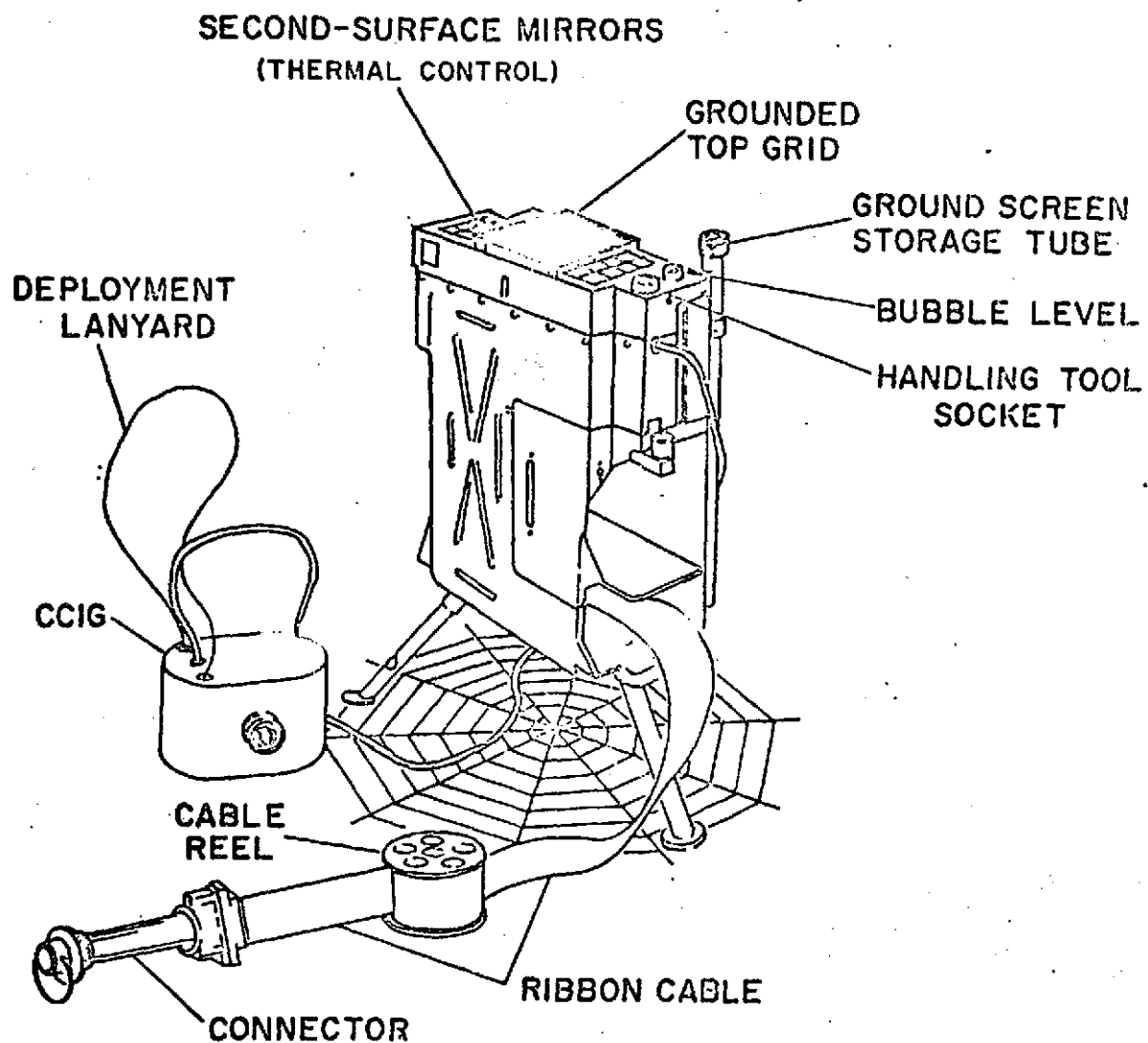
Figure 2.3

Deployed configuration for the
Apollo 12 SIDE.

Figure 2.4

Photographs of the deployed SIDE on
the moon.





DEPLOYED CONFIGURATION

Figure 2.3

ORIGINAL PAGE IS
OF POOR QUALITY

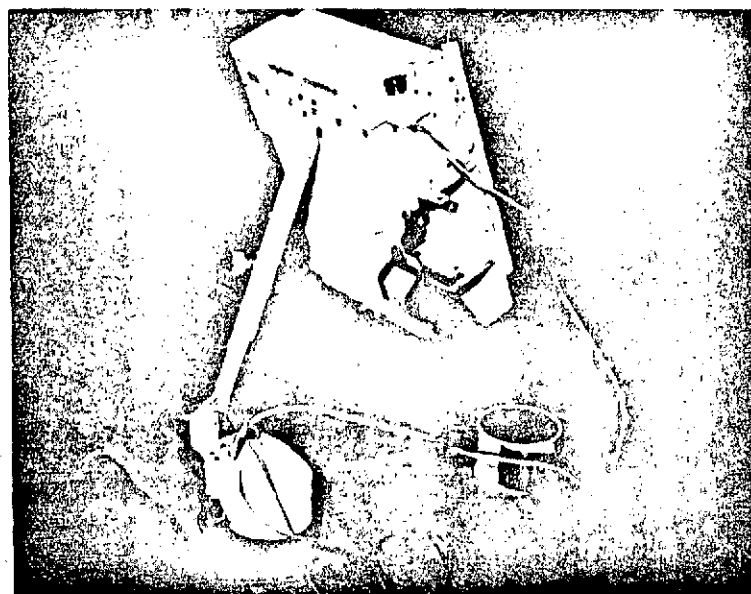
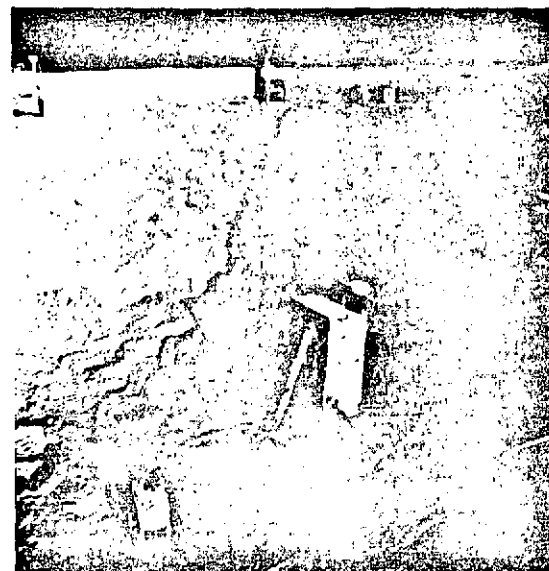


Figure 2.4

the ecliptic plane. Since it is 20° eastward of the Apollo 14 instrument while making the same angle eastward from the vertical as the Apollo 14 SIDE, the difference in their look direction is 20° . For the 12 and 15 devices the difference in look directions is 56° . Figure 2.5 shows the location of the instruments on the lunar surface. Figure 2.6 shows the look directions for the three instruments for various times throughout one complete lunation.

2.4 Data Conversion

The SIDE instrument accumulates data for 1.13 seconds in each channel of both the TID and MA. A period of .07 seconds is used after this 1.13 seconds to read out the data and adjust the instrument to the next channel. It takes, therefore, twenty-four seconds ($20 \text{ channel} \times 1.2 \text{ seconds/channel}$) to cover the twenty channels to produce a single mass or energy spectrum. What is returned in both cases is the channeltron recorded counting rate for the data accumulation period. Before these counting rates can be utilized they must first be converted into the actual differential flux observed by the instrument. To accomplish this conversion two quantities must first be known; the geometric factor for the instrument and the passband for particles in each channel. The latter of these two quantities, the passband, refers to the range in energy or mass which will be detected when the instrument is in a given channel. It is obvious, for instance, that the 50 eV channel of the TID will admit particles of energy other than exactly 50 eV/q. From the geometry of the curved plates one knows that particles with energy less than 50 eV/q can be seen by the channeltron if they enter the curved plate analyzer closer to the far

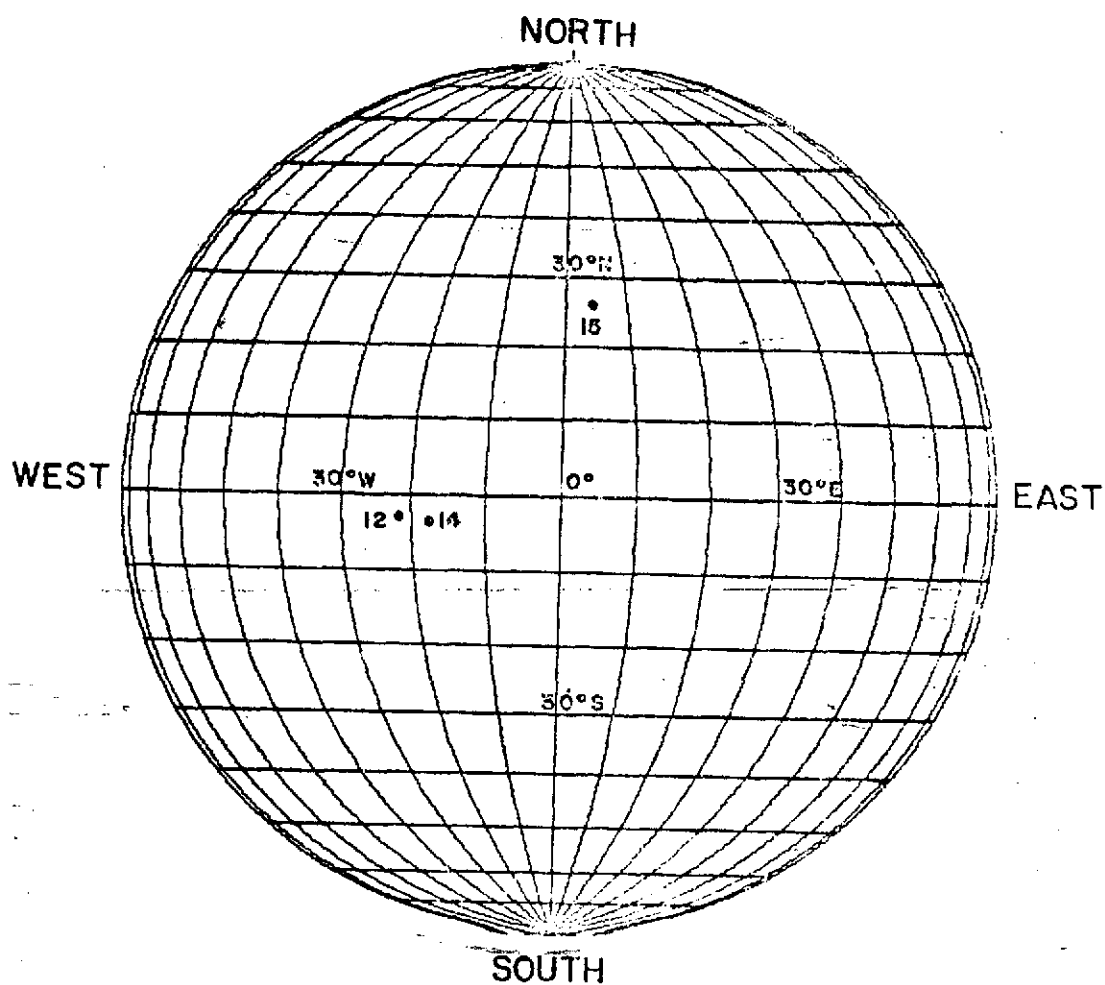
Figure 2.5

Location of the three SIDE's on the lunar surface.

Figure 2.6

Look directions of the three SIDE's during the course of one complete lunation.

MOON



	LONG	LAT	M	D	Y
APOLLO 12	23.4W	3.2S	11	19	69
APOLLO 14	17.4W	3.6S	2	5	71
APOLLO 15	3.6E	26.1N	7	31	71

Figure 2.5

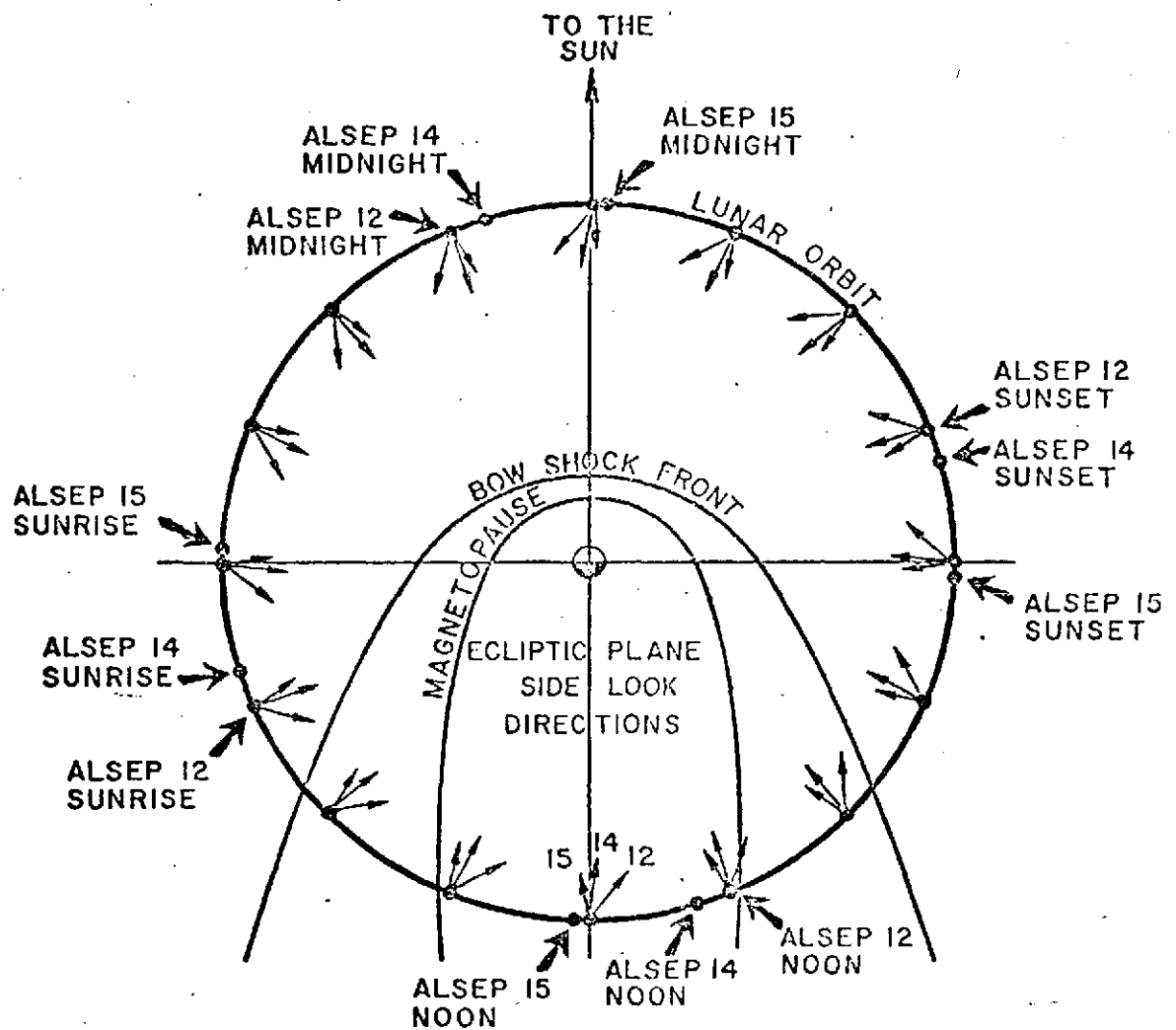


Figure 2.6

ORIGINAL PAGE IS
OF POOR QUALITY

plate. Similarly, higher energy particles can be detected if they enter closer to the inner plate. In a like manner with the Wien Filter, there exists some range in velocity where the deviation produced in the particle trajectory by the electric and magnetic fields will be sufficiently small so that the particles will pass through the filter to the curved plates and therefore potentially to the channeltron.

In general, one expects the counting rate to depend on the effective area of the detector, $A(E)$; the effective solid angle for observation, $\Omega(E)$; the detector efficiency, $\epsilon(E)$; the incident flux, $j(E, \Omega)$; and the passband, ΔE . All these quantities are expected to be energy dependent so that

$$CR(E) = A(E)\Omega(E)\epsilon(E)j(E, \Omega)\Delta E \quad .$$

It is difficult to measure $A(E)$, $\Omega(E)$, and $\epsilon(E)$ independently. Their product, however, known as the geometric factor, can be measured with greater ease,

$$G(E) = A(E)\Omega(E)\epsilon(E)$$

$$CR(E) = G(E)j(E)\Delta E \quad .$$

This means that if the geometric factor and bandwidth are known the differential flux can be calculated from the counting rate

$$j(E, \Omega) = CR(E)/G(E)\Delta E \quad .$$

From the extensive calibration performed on the instruments (Lindeman, 1973) a value of $G = 10^{-4} \text{ cm}^2 \text{ ster}$ and a bandwidth of 10% of the central energy for a given channel were calculated. The general conversion formula is, therefore

$$j(E) = CR(E)/.1(E)(G) = SFN(E)/.113(E)(G) ,$$

where $SFN(E)$ is the SIDE frame counts in a 1.13 second accumulation period. The uncertainty in this number is approximately $\pm 70\%$.

2.5 The Explorer 35 Magnetometer

The magnetic field data used in this thesis was obtained from the NASA/Ames Research Center fluxgate magnetometer aboard the Explorer 35 satellite and was provided by Dr. D. S. Colburn. The instrument has been described in detail by Mihalov et al. (1968). Briefly, however, it operates as follows. The device consists of three perpendicular detectors which make a measurement of the field every 6.14 seconds in each of three scales; 0-20, 0-60, and 0-200 gammas. These measurements are then spin demodulated onboard the spacecraft and telemetered back to earth. The data used in this analysis comprises 81.8 second averages of this data plotted in solar equatorial coordinates; a system in which the xy plane is tilted 7° to the solar ecliptic plane.

The magnetometer is stationed onboard the Explorer 35 satellite which has been orbiting the moon since 1967. The satellite has an aposelene of 5.42 lunar radii ($1.425 R_e$) and a periselene of 1.44 lunar radii ($.378 R_e$) with the plane of the orbit generally in the ecliptic.

There are several difficulties with the data. First, the satellite possesses no onboard recorder thus there is a loss of data when the satellite is occulted by the moon and telemetry coverage is cut off. Second, there is a weakness in the onboard batteries which results often in the sudden loss of data when the solar panels are either in the shadow of the moon or the earth. Thirdly, the satellite lost its reference in longitude. The data is internally consistent and merely appears shifted by some unknown angle in longitude. This offers no difficulty in the tail since the true angle can be found to within 10° by comparing the longitude angle of the field as reported by the satellite to the known field longitude in the lobes of the tail (180° or 360°).

The data presents one other difficulty. There is a distance varying between .378 and 1.425 R_e between the point at which the magnetic field is measured and the point where the particle flux is measured. This can produce a time difference between when an event, such as a magnetopause crossing, is seen in the magnetic field and when it is observed in the spectra observed by SIDE.

2.6 Method of Data Analysis

The calculation of parameters from the data; integral flux; bulk velocity, temperature, and number density, were accomplished by numerically integrating over the experimentally derived distribution function. To do this the counting rates in the twenty energy channels were averaged over one SIDE cycle (6 full spectra) and the background was subtracted. Then by dividing by the bandwidth and the geometric factor the comparable differential flux was calculated. The differential

flux spectrum was then converted into the distribution function by converting the energy channels into their equivalent velocity channels and multiplying the flux by the conversion factor $m_p^2/2E_1$. Theoretically the parameters can be approximated by taking the moments of the distribution function $f(v)$

$$\text{Integral flux} = I = \int j(E, \Omega) dE$$

$$\text{Bulk velocity} = V_b = \int f(v) v d^3v / N$$

$$\text{Thermal speed} = V_T = \int (v - v_b)^2 f(v) d^3v / N$$

$$\text{Number density} = \frac{I \Omega'}{V_b}$$

where Ω' = the angular extent over which the event is isotropic and N is the particular number density.

The actual numerical method employed utilizes the following summed approximations

$$V_b = \frac{\sum_i f(v_i) v_i (v_{i+1} - v_{i-1}) / 2}{\sum_i f(v_i) (v_{i+1} - v_{i-1}) / 2}$$

$$T = \frac{(m/2k) \sum_i f(v_i) (v_i - v_b)^2 (v_{i+1} - v_{i-1}) / 2}{\sum_i f(v_i) (v_{i+1} - v_{i-1})}$$

$$I = \frac{\sum_i j(E_i) (E_{i+1} - E_{i-1}) / 2}{\sum_i f(v_i) (v_{i+1} - v_{i-1}) / 2}$$

where the summation is taken over the twenty energy or velocity channels of the TID.

In order to equate the integral $(1/N) \int v f(v) d^3v$ to the bulk ve-

locity one must make the assumption that the contribution to the velocity from the thermal motion of the particles is negligible compared to the contribution from the flow motion. Since our instruments are fixed relative to the lunar surface, we have no easy, direct method of ascertaining that this assumption is justified for the fluxes of interest in this study. We find, however, that the results derived using this assumption are consistent with observations of the flow made at lesser X_{sm} distances with the Vela and HEOS satellites. The assumption, therefore, appears to be self-consistent. Such a method is, however, obviously inapplicable in the plasma sheet where the vast majority of the energy is in the thermal motion of the particles.

This assumption is further supported by observations of the same particles by the ALSEP Solar Wind Spectrometer (SWS). For several events for which data is available from both the SIDE and SWC, Dr. Goldstien (private conversation) has been able to confirm that the plasma is indeed flowing approximately antisunward with velocities commensurate to those measured by the SIDE's.

locity one must make the assumption that the contribution to the velocity from the thermal motion of the particles is negligible compared to the contribution from the flow motion. Since our instruments are fixed relative to the lunar surface, we have no easy, direct method of ascertaining that this assumption is justified for the fluxes of interest in this study. We find, however, that the results derived using this assumption are consistent with observations of the flow made at lesser X_{sm} distances with the Vela and HEOS satellites. The assumption, therefore, appears to be self-consistent. Such a method is, however, obviously inapplicable in the plasma sheet where the vast majority of the energy is in the thermal motion of the particles.

This assumption is further supported by observations of the same particles by the ALSEP Solar Wind Spectrometer (SWS). For several events for which data is available from both the SIDE and SWC, Dr. Goldstien (private conversation) has been able to confirm that the plasma is indeed flowing approximately antisunward with velocities commensurate to those measured by the SIDE's.

CHAPTER THREE

3.1 Introduction

The three Suprathermal Ion Detectors stationed at the Apollo 12, 14, and 15 sites observe intense fluxes of low energy protons (LEP's) associated with the passage of the moon through the geomagnetic tail. These fluxes appear in the data as a significant increase in the counting rate in the Total Ion Detectors' eight lowest energy channels which span an energy range from 10 to 500 electron volts. The most prominent events are centered in the 50, 70, or 100 eV channels. The events range in duration from as short as five minutes to as long as a full day or more with wide variations in the intensity and frequency of occurrence with time within a given tail passage as well as between separate tail passages.

The particle fluxes to be considered in this thesis, were positively identified as having a composition which is primarily protons. This fact was ascertained by the observation of significant peaks in the mass channels for protons in the Mass Analyzer of the Apollo 15 instrument. (see Figure 3.1_A) No real counts for other particle species besides protons have, as yet, been detected above the background of the instrument. The other peaks seen in Figure 3.1 have not been confirmed to be statistically significant.

In the present analysis fifteen lunations of tail data have been used covering all the lunations in 1972 from the 28'th of January and the first three lunations of 1973. Altogether these orbits provided observations for 265 LEP events comprising almost two hundred hours of data. The location in time of these events was obtained through the use of Apollo 14 data exclusively. Verification of the

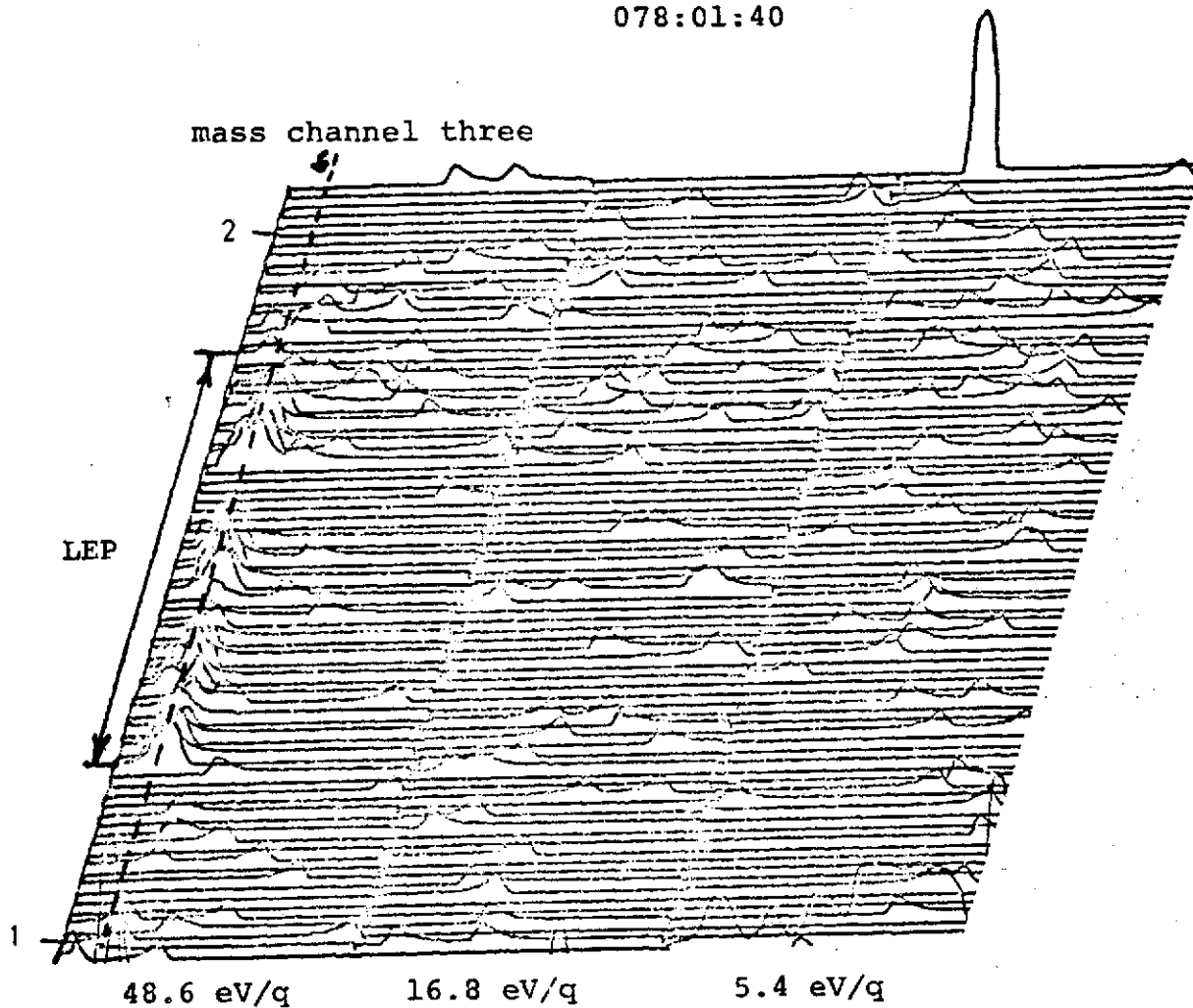
Figure 3.1a

Plot of the counting rates for the 48.6 eV/q, 16.2 eV/q, and 5.4 eV/q channels of the Apollo 15 Mass Analyzer. The plot shows a sustained period of observation of particles in the third mass channel. Counts in this channel represent particles of 1 amu.

Figure 3.1b

Plot of the positive ion plasma parameters showing the entry of the moon into the magnetotail.

078:01:40



076:00:40

FIGURE 3.1a

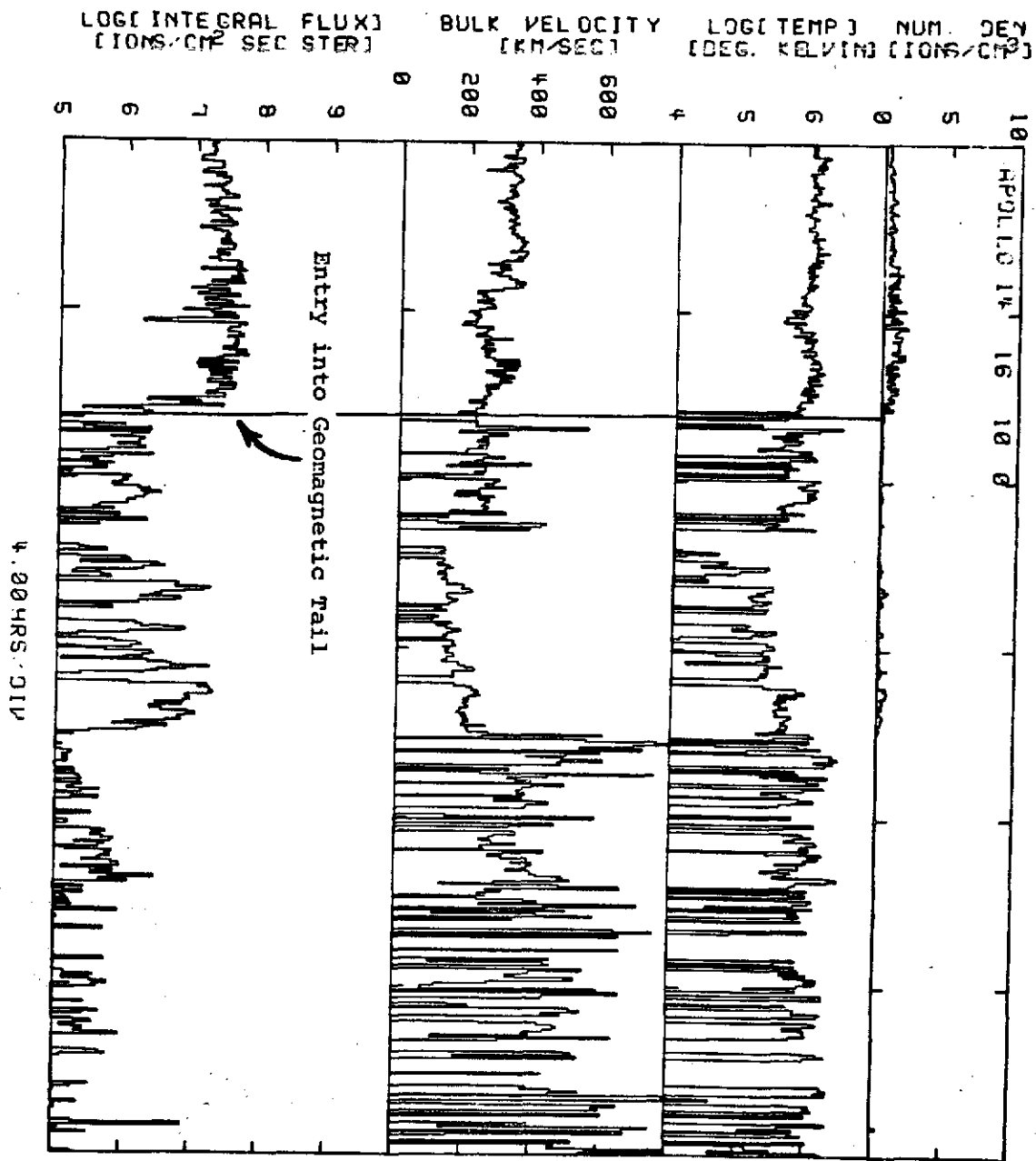


Figure 3.1b

4.00 HRS. CIP

occurrence of the events was accomplished by checking against Apollo 12 and 15 data where it existed. No cases have yet been found where the verification failed when simultaneous data from the other instruments was available. Similarly there were never observations of events in the Apollo 12 and 15 instruments which were not seen at the same time by Apollo 14. It should also be noted that no significant time difference in onset or falloff of the LEP events were observed with comparable data from the three instruments.

In Table 1 are listed the approximate times for entry and exit of the moon from the geomagnetic tail, the total times to the nearest hour the moon was in the tail, the number of hours of the tail passage dominated by the observation of low energy protons (LEP), and what percentage of the tail passage this comprises. The times of entry and exit cannot be determined exactly since the bulk motion of the magnetopause tends to cause multiple crossings of the moon in and out of the tail. An approximation as to the times of entry and exit from the tail was nonetheless determined by noting the final falloff or initial rise in the integral flux as well as the point of disappearance or appearance of the characteristic magnetosheath spectrum. Where possible this was further verified by the use of the Explorer 35 magnetometer data.

An example of such a tail entry is seen in Figure 3-1b taken from the first lunation of 1973 for the Apollo 14 instrument. We have calculated in this graph the logarithm of the integral flux and temperature as well as the bulk velocity and number density, all as functions of time. A sudden drop off in the integral flux is observed on day 16 GMT 1640 accompanied by a falloff in the bulk velocity and number density. This coupled with the disappearance of the magnetosheath spectrum indicates entry into the tail.

Table 1

Lunation	Time of moons entry into tail	Time of moons exit from tail	Hours moon in the tail	Hours of LEP events	percentage of tail domi- nated by LEP's
1	023:12:00	031:07:00	88	16.167	18.37
2	057:23:00	062:03:00	94	14.50	15.42
3	088:20:37	091:12:21	72	42.683	59.28
4	117:22:41	121:03:40	100	16.350	16.35
5	147:00:00	151:05:00	101	2.10	2.00
6	176:19:45	180:00:00	79	3.083	3.90
7	205:19:01	210:01:00	102	13.650	13.38
8	235:10:00	238:22:20	84	5.667	6.75
9	264:21:42	268:10:00	75	21.132	26.84
10	294:22:00	298:03:00	77	8.00	10.39
11	324:00:01	327:15:00	87	6.232	7.16
12	352:06:20	357:00:40	90	3.81	4.01
13	016:17:00	020:01:00	81	11.733	14.49
14	046:07:22	050:03:00	92	17.117	18.66
15	076:09:00	079:04:00	62	17.533	28.28

Of the fifteen lunations studied, Explorer 35 data has been obtained for the four tail passages of interest; three in 1972 (lunations 1, 2, and 9) and one in 1973 (lunation 13). In order to present a clear picture as to the detailed nature of the events studied, these lunations will be presented in greater detail. One other lunation (lunation 3) for which magnetic data is not available but which exhibits events of interest will also be presented in some detail.

3.2 Lunation 1

The first tail passage of interest lasts from approximately day 28 GMT 1200 to day 32 GMT 0700. The general behavior of the data for this tail passage is shown in Figures 3.2 and 3.3. In these graphs, the twenty energy channels have been plotted along the x axis with an equal space between each channel. In the y direction is plotted the logarithm of the average counting rate in each channel and in the z direction is plotted time. Each line represents a twenty minute average of the data.

Referring to Figure 3.2 one sees that four LEP events are observed in the 18 hours following the moons entry into the tail at GMT 1245 on day 28. These LEP events, having durations of from 1.5 to 4 hours, are distinct from the magnetosheath in that significant counts are only seen for the energy channels below 500 eV/q. The forty hour period following their disappearance at GMT 0742 on day 29, displays only occasional significant counts in the higher energy channels of the TID ($E > 250$ eV/q). These are interpreted as encounters with the plasma sheet.

Figure 3.3 shows the remaining portion of the tail passage. Four prominent LEP events are seen, the first occurring approximately 20 hours prior to the moons re-entry into the magnetosheath. The most important fact to notice is that the periods of observation of the LEP events are found in close conjunction to, but separated from, times when the plasma sheet is observed, i.e., simultaneous observations of LEP spectra and plasma sheet spectra are not seen.

In Figure 3.4 the location of the events has been plotted in solar magnetospheric coordinate. On the inbound side (solar magnetospheric longitude less than 3.14 radians) the events span a distance of approximately $12 R_e$ in the Y_{sm} direction and approximately $9 R_e$ in the Z_{sm} direction with the longest continuous event traversing $\sim 5 R_e$ in the Z_{sm} direction and $\sim 2.25 R_e$ in the Y_{sm} direction. Similarly on the outbound side (solar magnetospheric longitude greater than 3.14 radians) the events cover distances of $\sim 18 R_e$ in the Y_{sm} direction and $\sim 9 R_e$ in the Z_{sm} direction with the longest event covering distances of $Y_{sm} \sim 4 R_e$ and $Z_{sm} \sim 2 R_e$.

One may make estimates of the integral flux, bulk velocity, temperature and number density as discussed previously. Figures 3.5 and 3.7 show these parameters for the LEP events observed in this first lunation, (the shaded areas show periods of observation of the LEP's). One sees that the encounter of the instrument with the initial of these low energy events is accompanied by a rapid decline in the bulk velocity and temperature from 250 km/sec to 120 km/sec and from $1.5 \times 10^6 K$ to $2 \times 10^5 K$, respectively. Taken as a group these inbound LEP events exhibit an integral flux intensity of approximately .1 to 1×10^7 ions / cm^2 -sec-ster and a bulk velocity on the order of 100 to 200 km/sec,

with temperatures varying between .8 and 4×10^5 K and number densities of $\sim .2/\text{cm}^3$. Similar behavior is seen in the data for the outbound portion of this tail passage. The main difference is that the integral flux is greater during this period reaching a value as high as 9×10^7 ions $\text{cm}^2\text{-sec-ster}$. This increase produces no noticeable change in the temperature or bulk velocity of the LEP's. The number density is, however, increased close to an order of magnitude to between 1 and $2.5/\text{cm}^3$.

Figures 3.6 and 3.8 show the magnetic field configuration during approximately the same portions of the tail passage as in Figures 3.5 and 3.7. The latitude, longitude and magnitude of the field have been plotted in solar equatorial coordinates as functions of time. Again the periods where the LEP events were observed have been shaded. The lowest panel displays the differential flux in the 100 eV channel with the background not subtracted. This channel was chosen since it represents the approximate region of the peak of the energy spectrum for the LEP events.

One sees that the tail is well ordered for the entire span over which the LEP events were observed inbound. Specifically, no deviations in the field can be seen to correlate with either the appearance or disappearance of the LEP events. Such an orderly and steady configuration indicates that the moon was in the high latitude lobe of the tail during this entire period. This is further supported by the fact that the first neutral sheet crossings is not seen until GMT 1258 on day 29 and the actual cross over to the low latitude region does not take place until GMT 1200 on day 30; long after the last of the inbound LEP events. Similar behavior is seen for the outbound events.

Figures 3.2&3.3

Plots showing the counting rates in the 20 channels of the Total Ion Detector for the tail passage in lunation 1. Periods in which the moon encountered the plasma sheet (PS), magnetosheath (MS), and low energy protons (LEP) have been labeled.

Figure 3.4

The position of the moon in solar magnetospheric coordinates has been plotted for the times during which LEP's are observed. The arrow points to the location for the event during which significant spectral variation in the low energy protons was observed.

Figures 3.5&3.7

Two and one half minute averages of the plasma parameters have been plotted for the times during which LEP events occurred in the tail passage of lunation 1. The approximate period over which the LEP events occurred has been shaded.

Figures 3.6&3.8

The latitude, longitude, and magnitude of the magnetic field have been plotted in solar ecliptic coordinates as functions of time for the periods of the LEP events. The longitude correction angle is approximately 50 degrees. The times for the LEP events have been shaded. The lowest panel gives the differential flux in the 100 eV/q channel without the background subtracted.

Figure 3.9

The time behavior of the spectra for the first LEP event outbound in lunation 1 is shown in four spectra which span the event. The time at the top of each graph refers to the start time for the spectrum to which the arrow does not point. Each spectrum is a ten minute average.

APOLLO 14 1972
START TIME 28 9 1
20 MIN AV
24.00HR/DIV

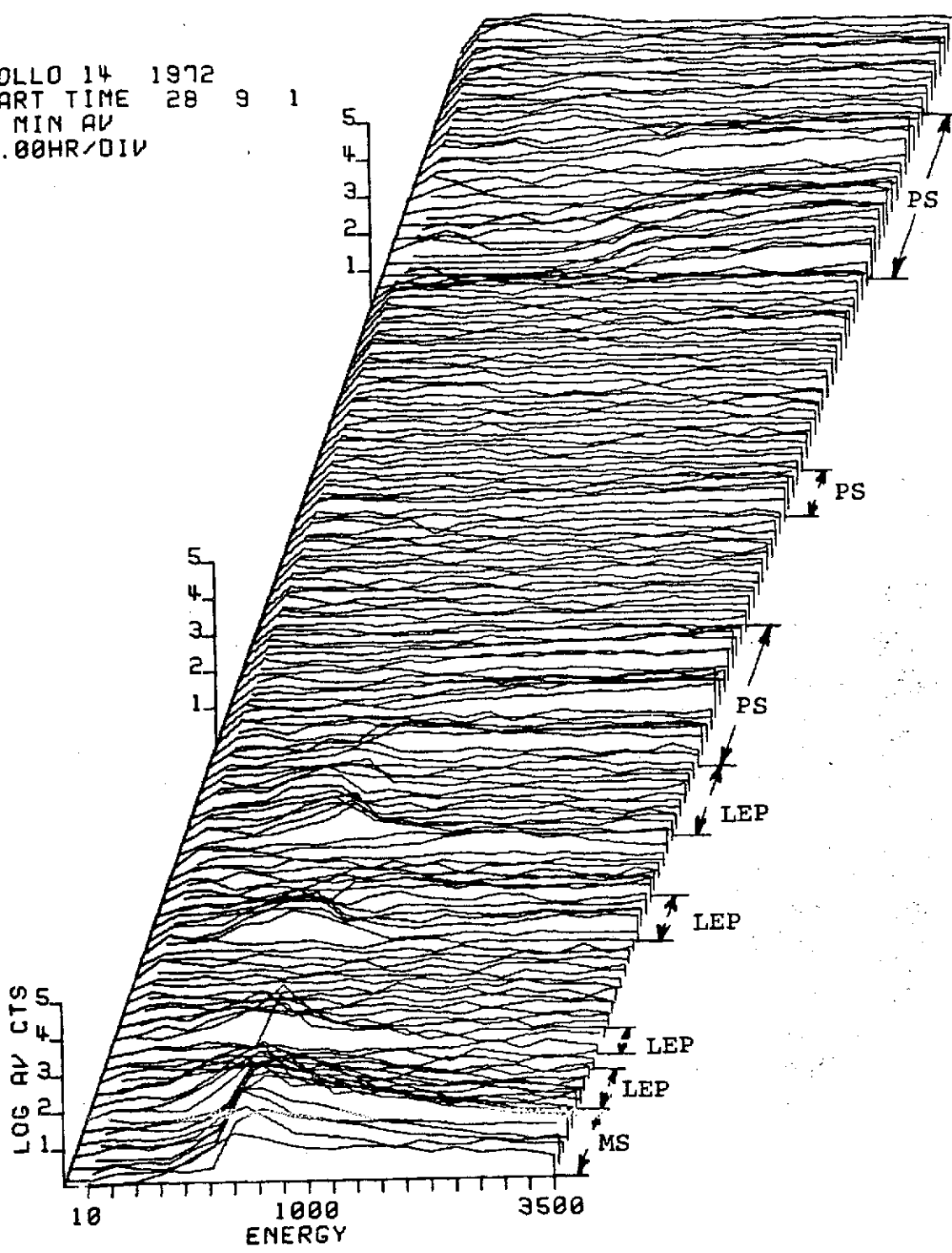


Figure 3.2

APOLLO 14 1972
START TIME 30 21 1
20 MIN AV
24.00HR/DIV

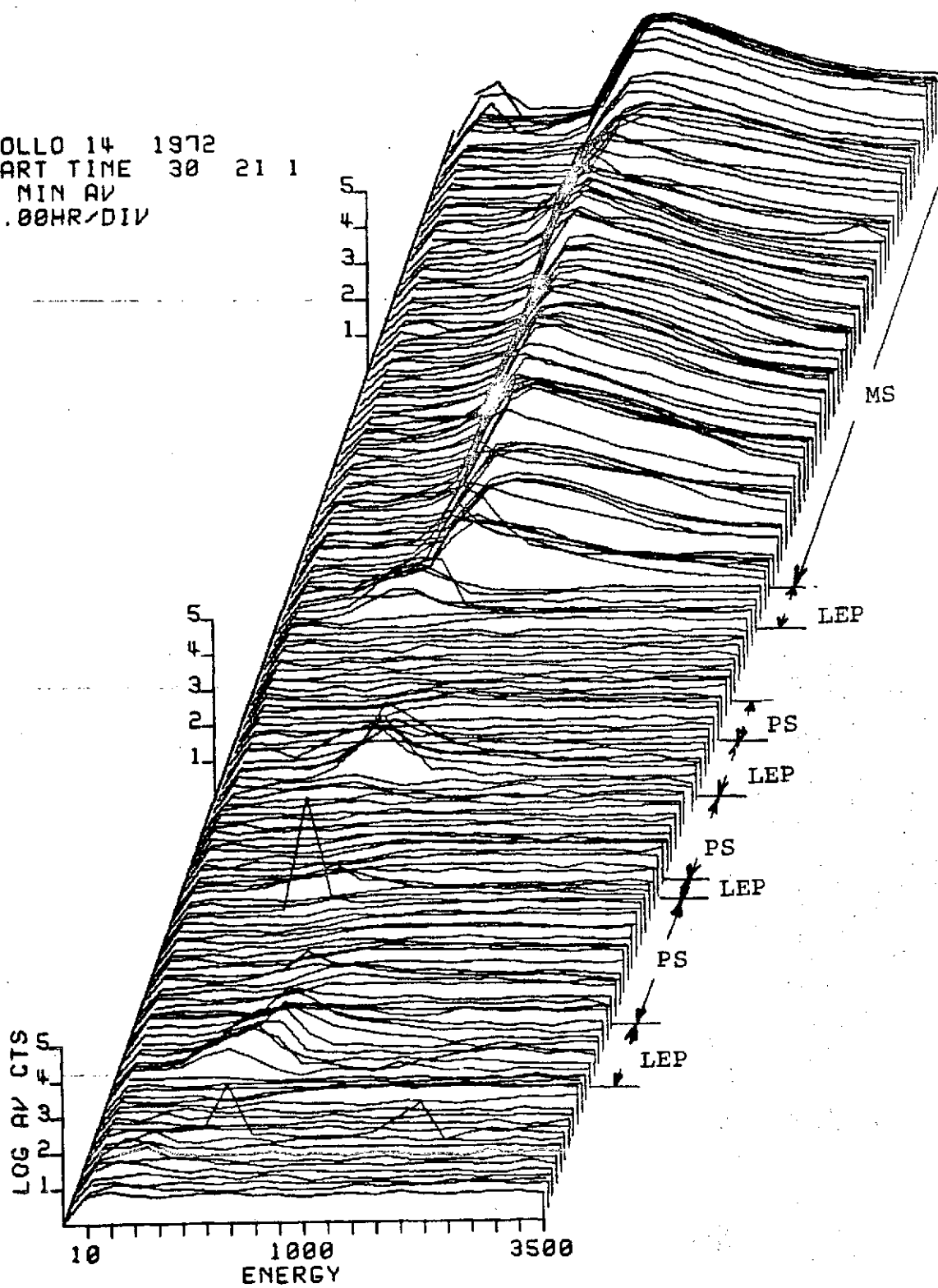


Figure 3.3

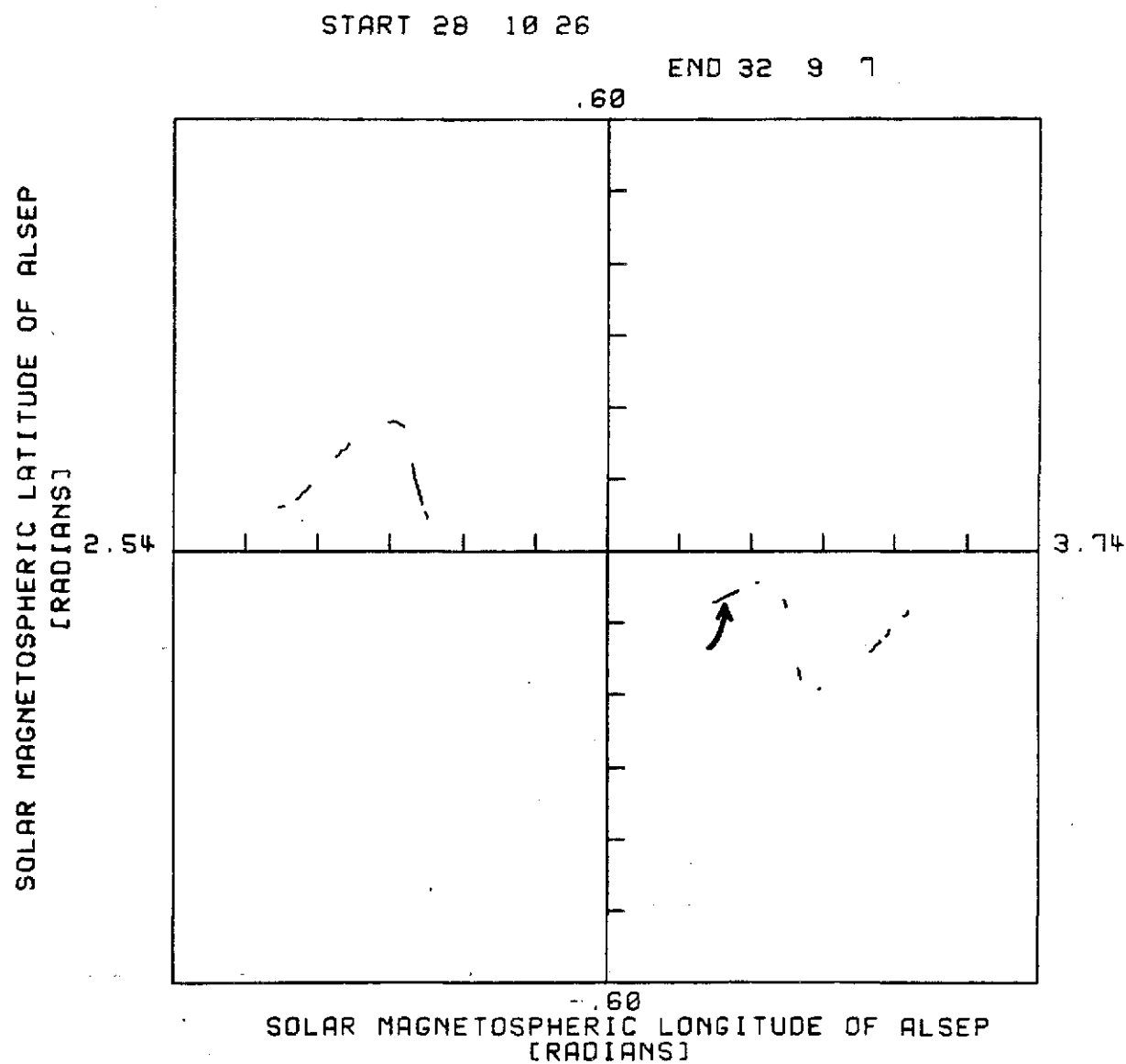
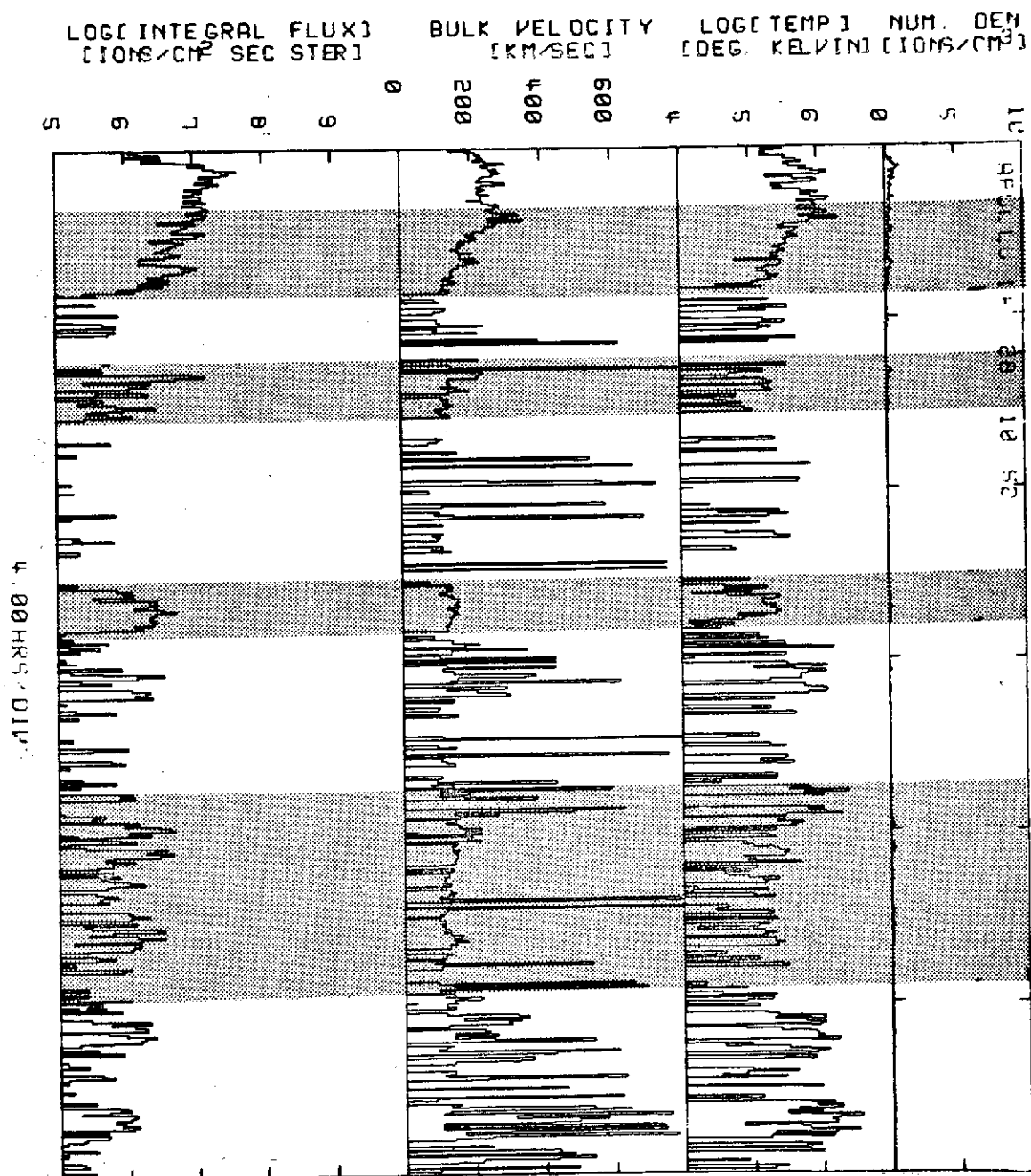


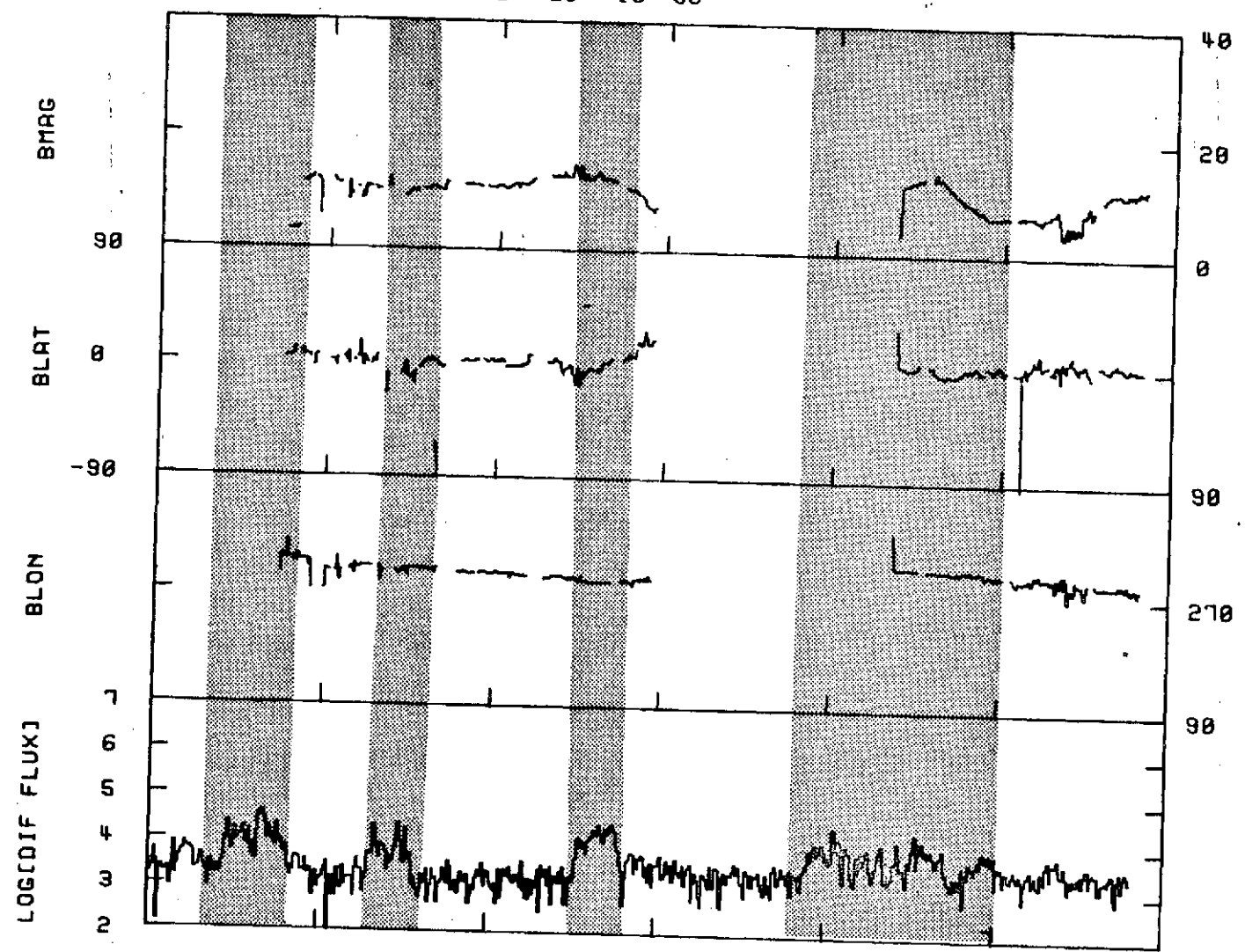
Figure 3.4

Figure 3.5



APOLLO 14 1972 28 10 58

Figure 3.6



4 HR/D IV

Figure 3.7

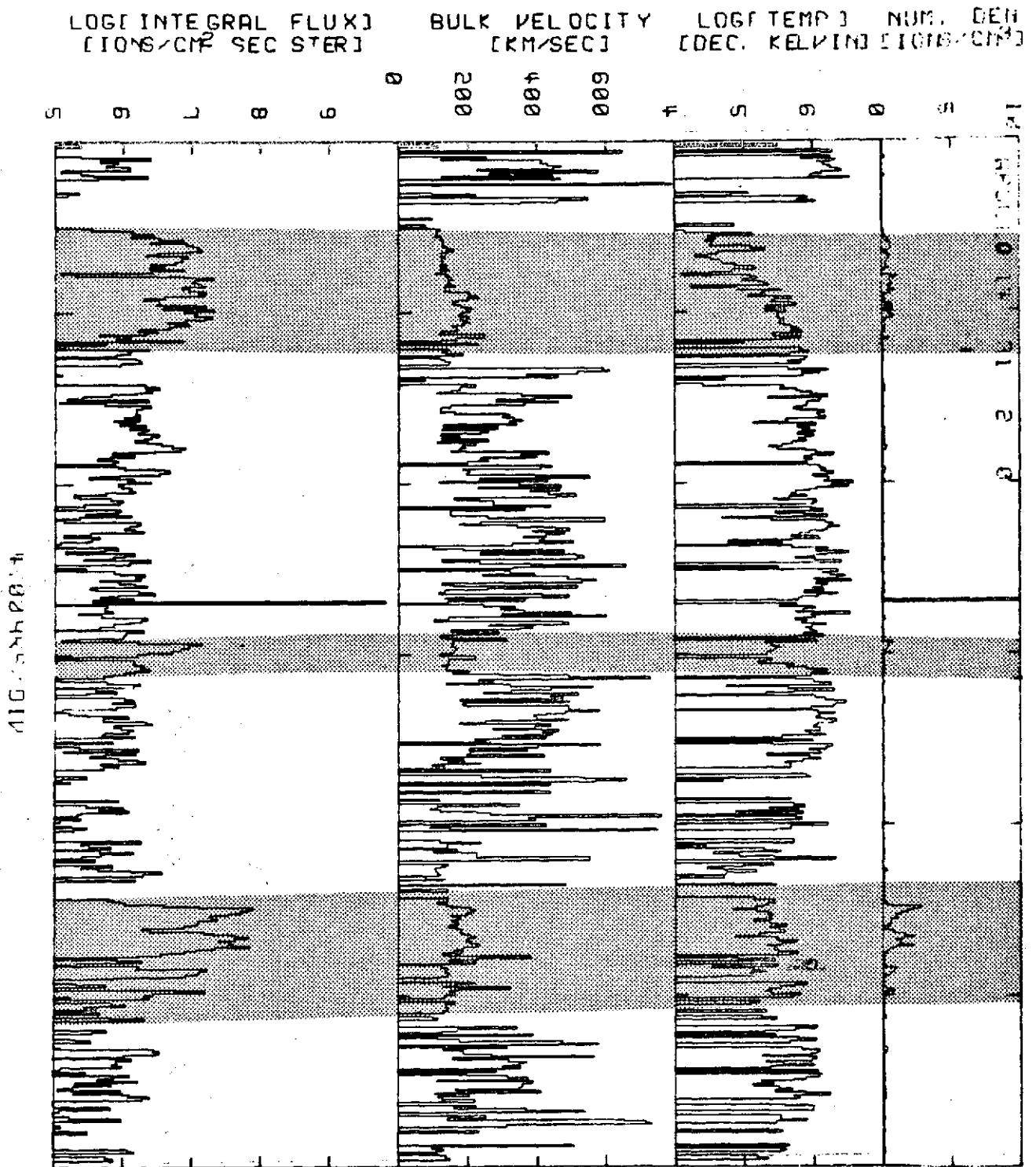
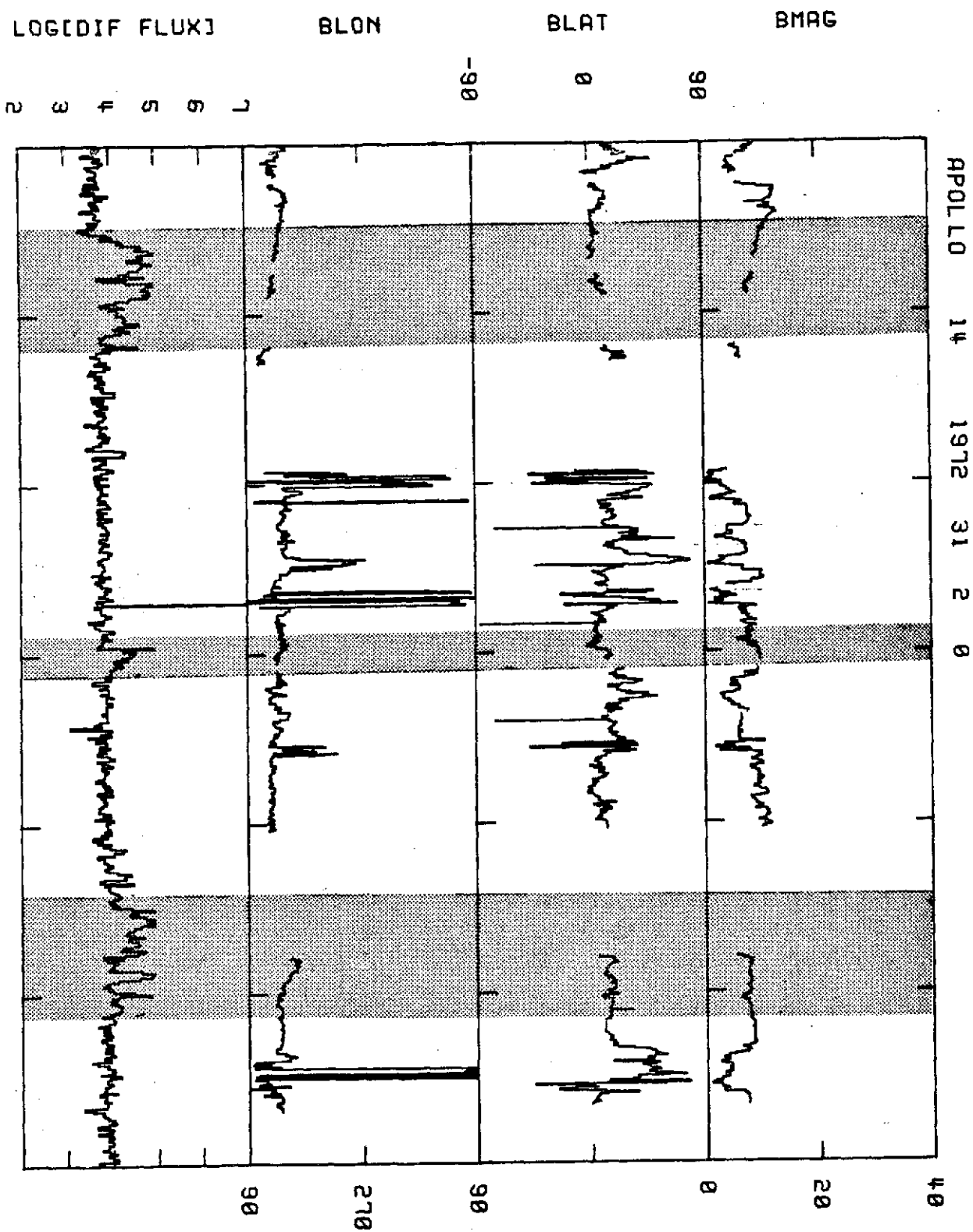


Figure 3.8



4 HR 014

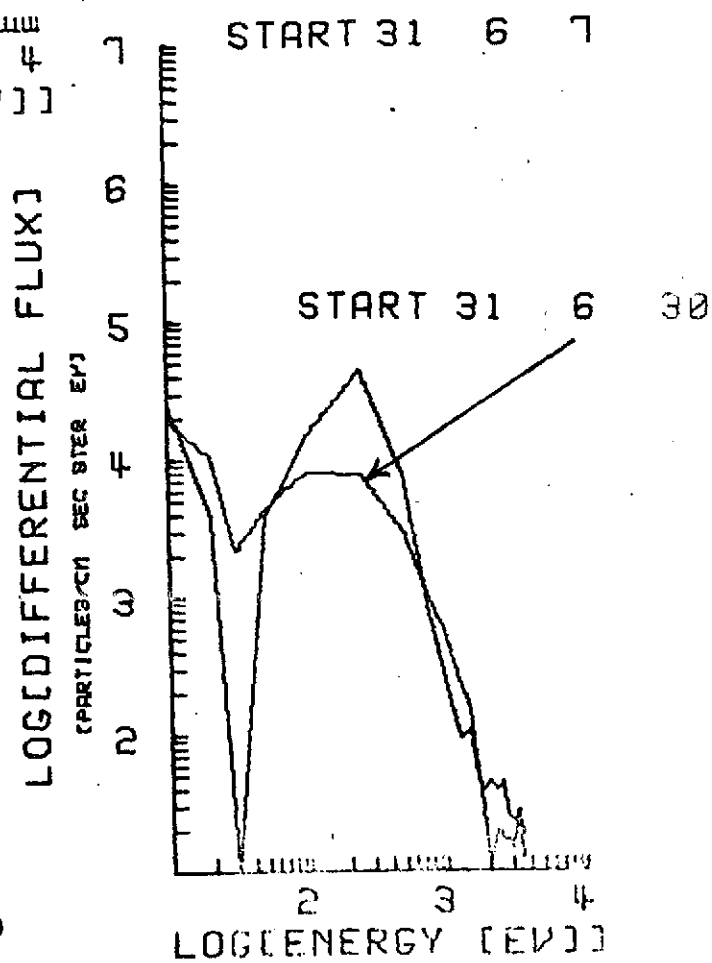
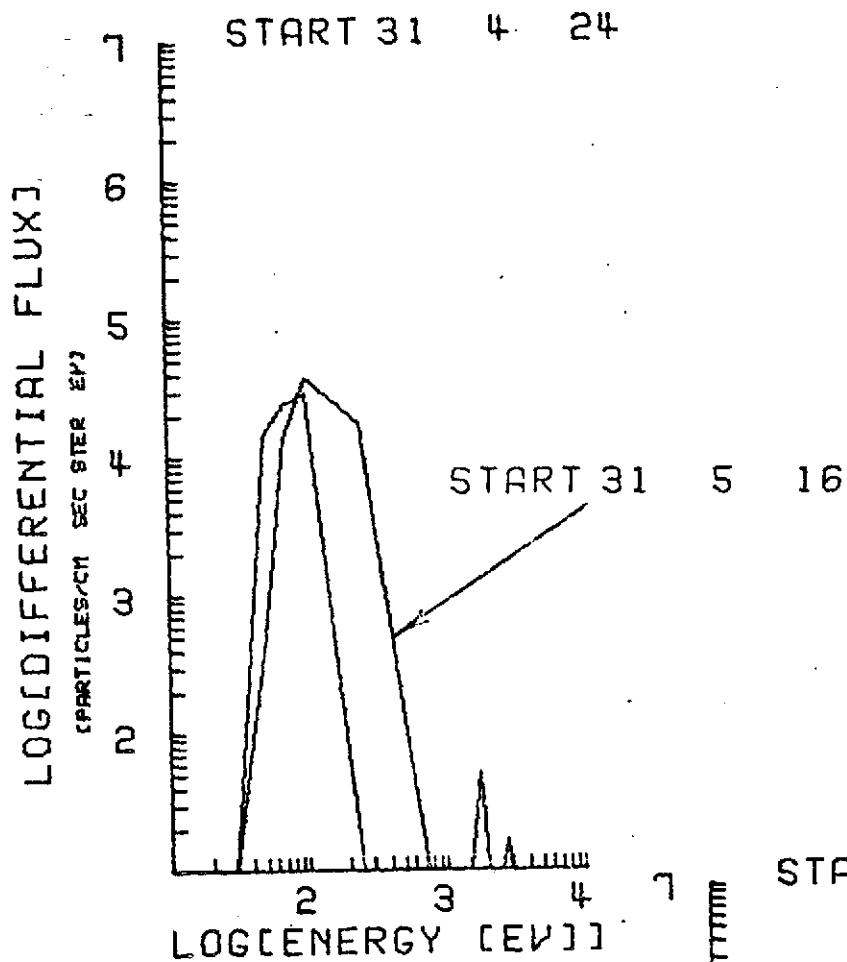


Figure 3.9

The LEP events for this lunation exhibit little time variation as to their spectral characteristics, showing a peak centered normally in the 100 eV region with a maximum differential flux of from 2 to 5×10^5 ions/cm²-sec-ster-eV. The one exception to this behavior is found in the LEP event which runs from GMT 0406 to GMT 0656 on day 31 which exhibits a shifting of the peak towards higher energy and a hardening of the general spectrum during the course of the event.

This behavior is shown in Figure 3.9. Four spectra are shown in this illustration; the first taken at the onset of the LEP event and the other three spaced over the next two hours. All four spectra are ten minute averages of the data. These show clearly the broadening of the spectrum out to energies greater than three kilovolts and the gradual shifting of the peak from 100 eV to a value in the range of 250 eVs. Figures 3.4 and 3.8 show that the instrument was moving towards the neutral sheet during the period of this LEP event, encountering the neutral sheet approximately three hours after the cessation of the event. This is further supported by the fact that the moon is seen to enter the plasma sheet immediately after the LEP event terminates.

3.3. Lunation 2

Figures 3.10 and 3.11 show the counting rates observed by the Apollo 14 instrument for the third tail passage of 1972. As before a series of low energy events are observed for approximately one day following the entry of the moon into the tail. The time after this exhibits significant counts only in the higher energy channels of the TID which, as before, indicates that the instrument is in the plasma sheet. Such observations dominate the vast majority of the time for

this passage with the only LEP events observed outbound found close to the magnetopause bracketed by times dominated by sheathlike spectra. The corresponding spatial locations are shown in Figure 3.12.

Parametrically these LEP events display little significant difference from those of the previous lunation (see Figures 3.13 and 3.15). The only point that should be pointed out is the high number density (approximately $2.5/\text{cm}^3$) associated with the outbound LEP events.

As in the previous lunation the LEP events are found to occur in the well ordered field regions of the lobes of the tail. (Figures 3.14 and 3.16.) Inbound the behavior of the field during the LEP events shows little variation, displaying a lobe like configuration. Outbound the behavior is more unusual. On day 61 GMT 1800 the moon enters a region of disorganized field reflective of the magnetosheath (see Figure 3.16). This is verified by the simultaneous observation of characteristic magnetosheath spectra by the SIDE. This behavior is maintained until GMT 1932 when the Explorer 35 satellite reenters a region of ordered field. This is followed at GMT 2100 by the advent of a LEP event seen in Figure 3.16 as a rise in the differential flux in the 70 eV channel. This LEP event last until day 62 GMT 0400. The field data is unfortunately discontinuous during this period making it impossible to be definitive as to the field configuration for the entire LEP event. When, however, field data is again available, after the end of the LEP event, it is seen that the moon is once more in the magnetosheath. The one other LEP event taking place in the period covered by Figure 3.16 is also seen to correspond with the entering of the moon into the ordered tail field region from the magnetosheath at GMT 0632.

Figures 3.10&3.11

Counting rates for the Apollo 14 TID for the second tail passage of 1972 showing the moon's encounters with the plasma sheet (PS), magnetosheath (MS), and low energy proton regions. (LEP)

Figure 3.12

The location of the moon in solar magnetospheric coordinates has been plotted for the times in the tail passage of lunation 2 during which the LEP events were observed. (.1 radian = $6 R_e$)

Figures 3.13&3.15

Two and one half minute averages of the plasma parameters have been plotted for the periods during which LEP events were observed in the 2nd tail passage of 1972. Shaded regions correspond to periods of observation of the LEP events.

Figures 3.14&3.16

Latitude, longitude, and magnitude of the magnetic field are plotted in solar ecliptic coordinates as functions of time for the period during which LEP events were observed in the 2nd tail passage of 1972. The differential flux in the 100 eV/q channel is plotted in the lowest panel without the background subtracted. The correction angle for the longitude is again 50 degrees.

Figure 3.17

Four plots of the differential flux spectra for the period of transition of the moon from the LEP region into the magnetosheath. The time at the top of each plot refers to the start time for the spectrum to which the arrow does not point. Each spectrum represents a ten minute average.

APOLLO 14 1972
 START TIME 57 12 1
 20 MIN AV
 24.00HR/DIV

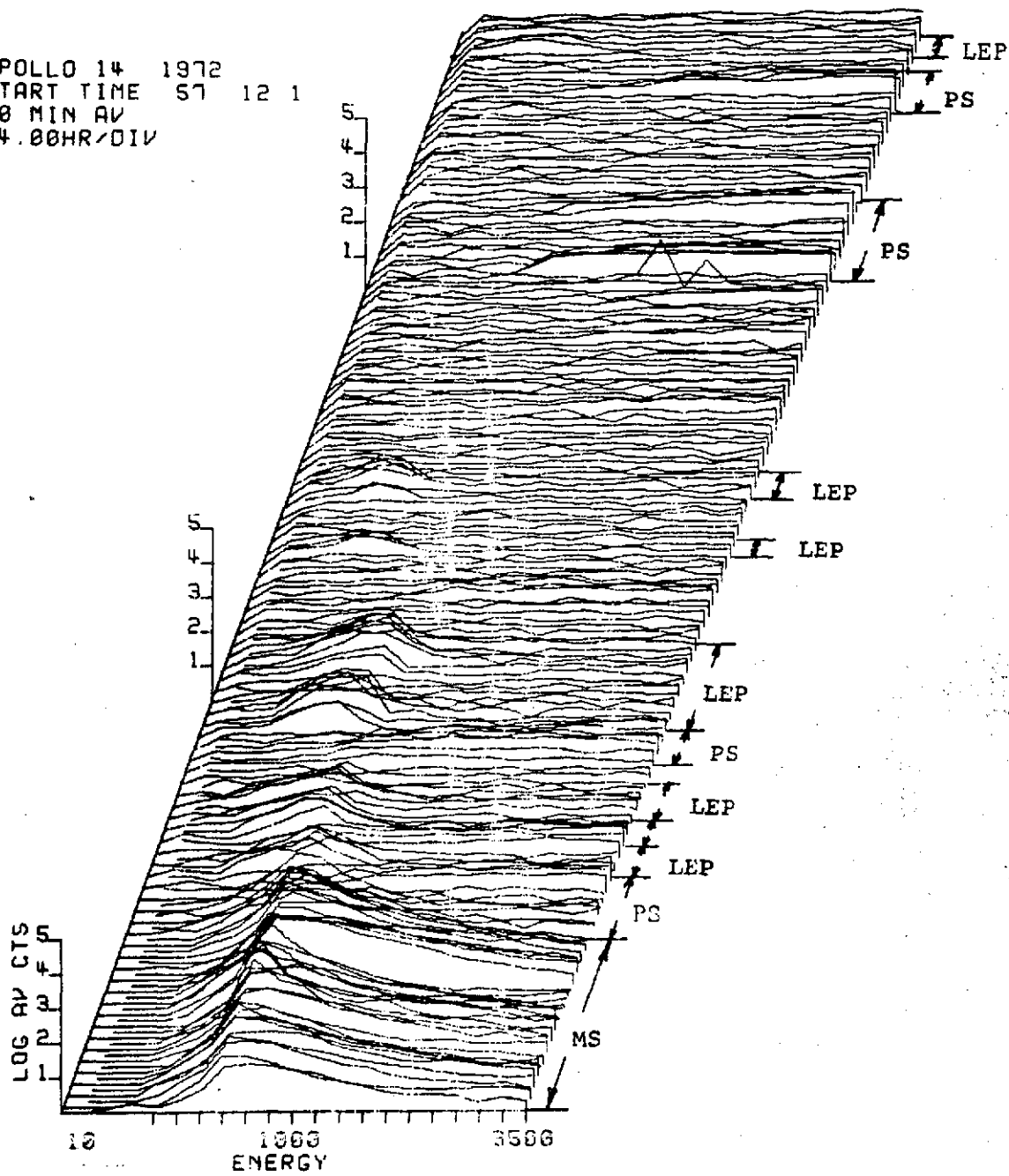


Figure 3.10

APOLLO 14 1972
START TIME 60 0 0
20 MIN RV
24.00HR/DIV

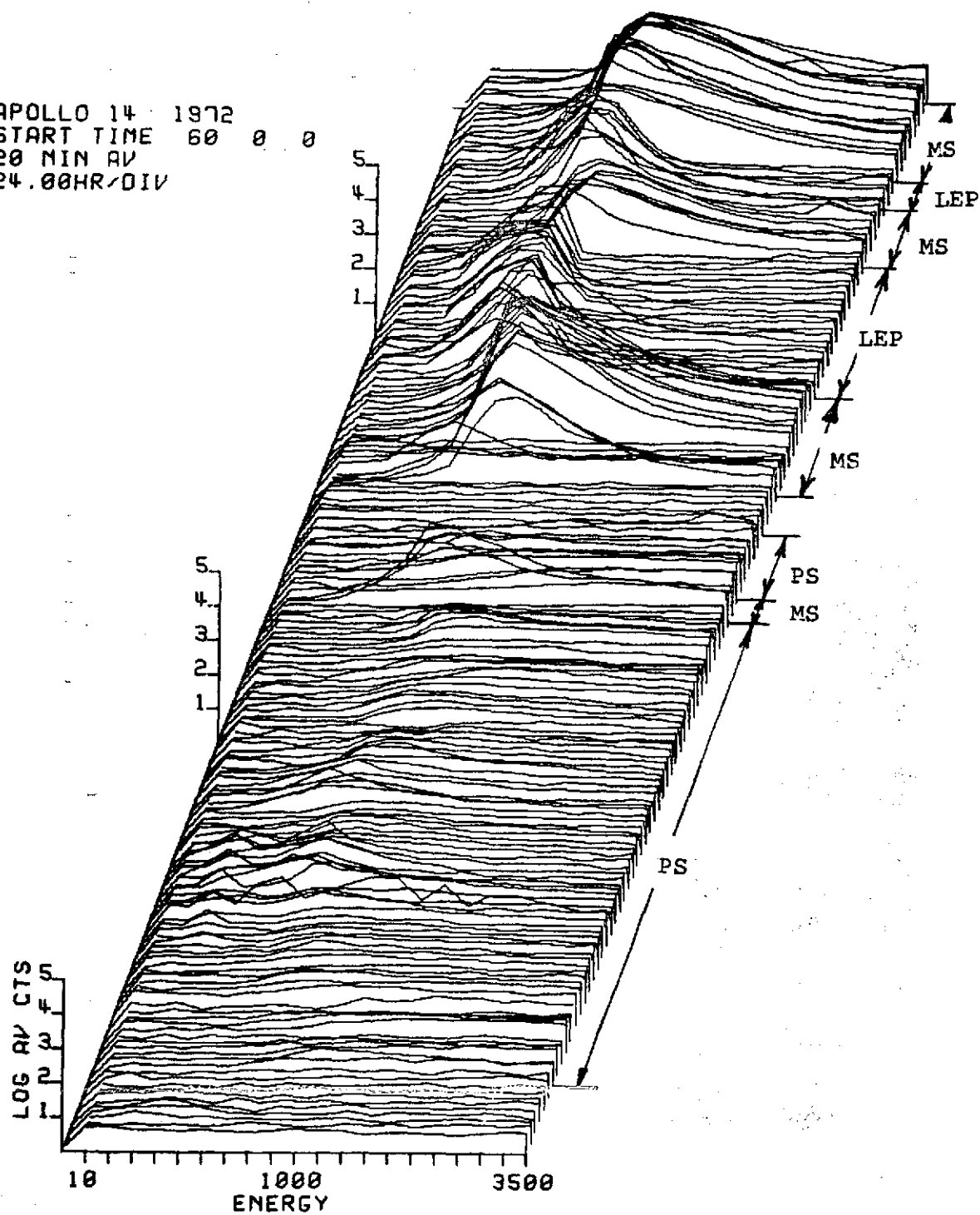


Figure 3.11

START 57 19 25

END 62 9 6

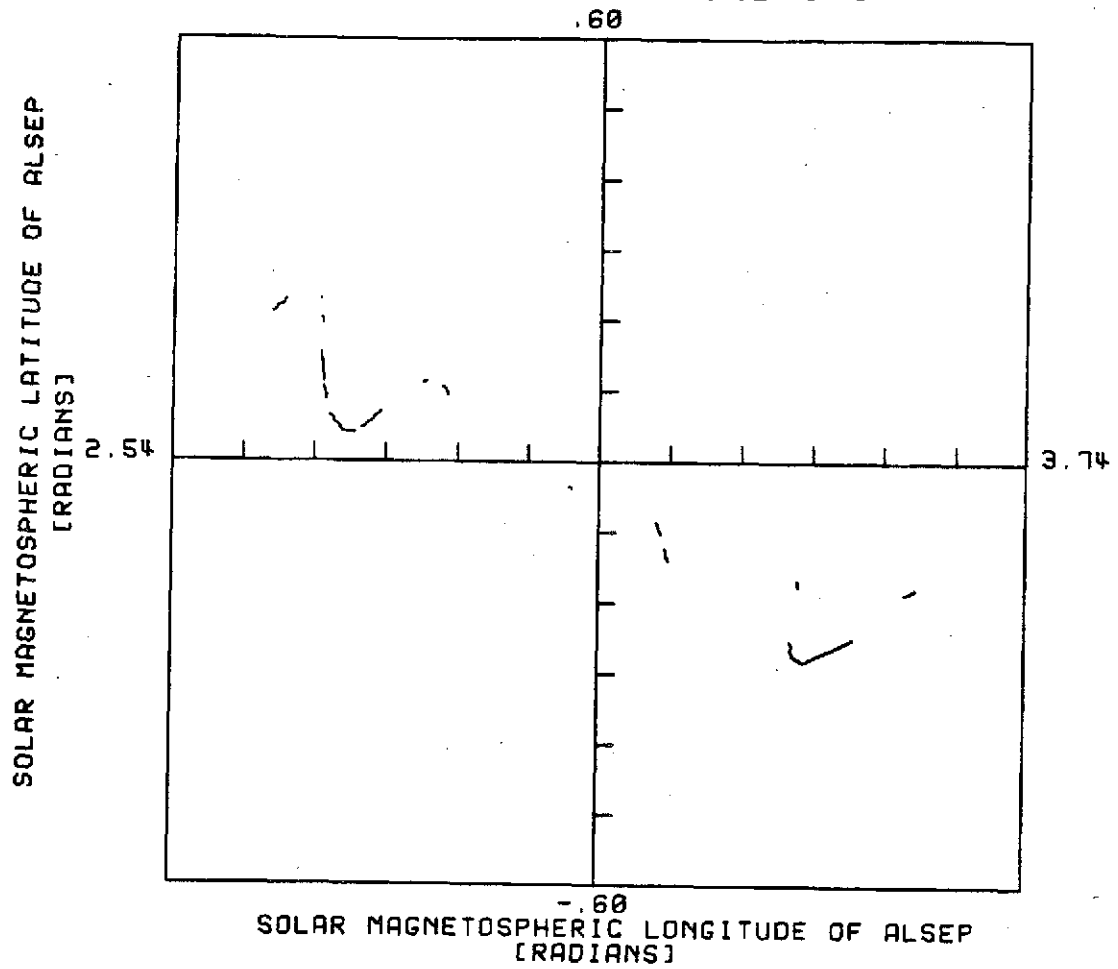


Figure 3.12

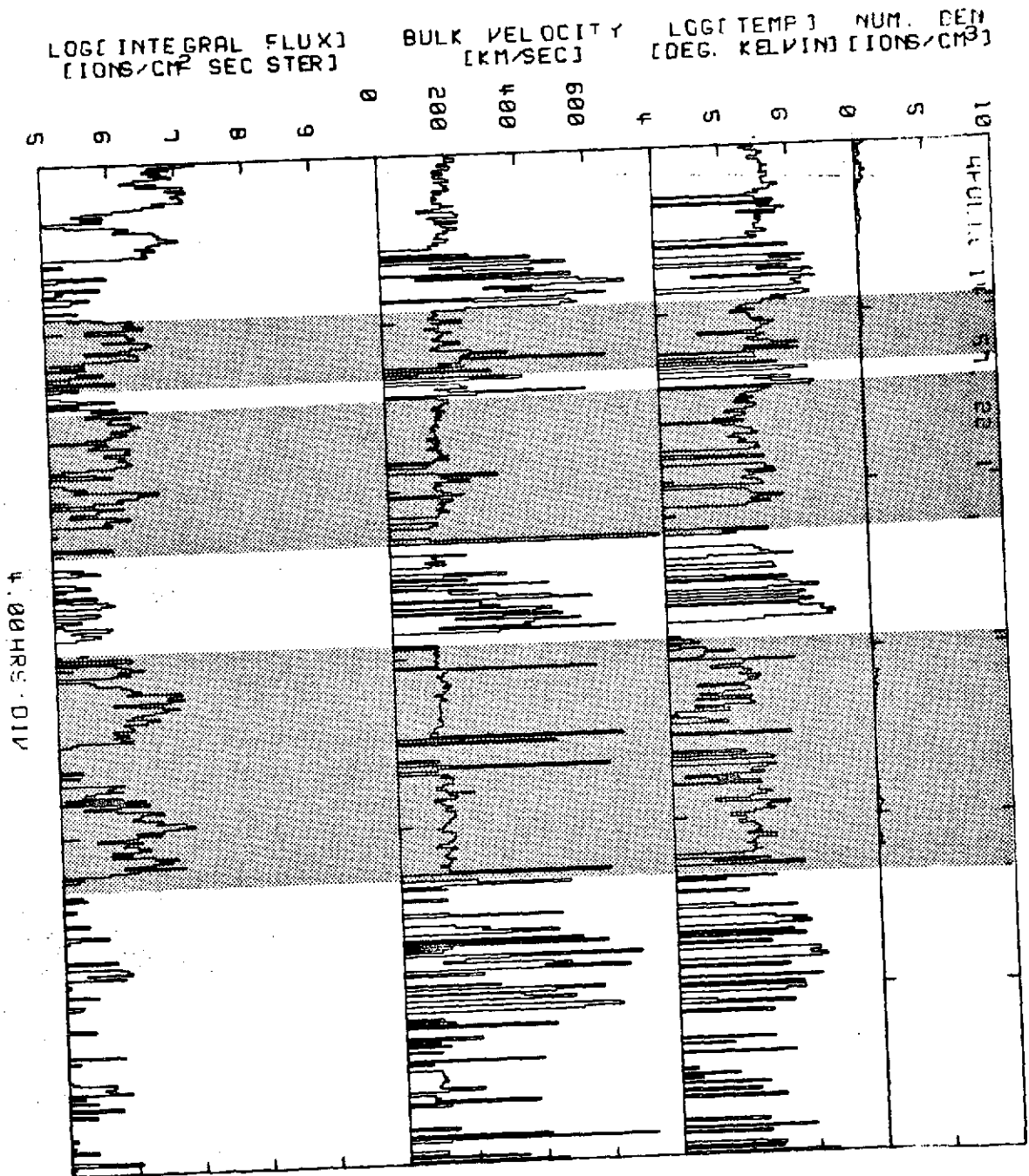


Figure 3.13

APOLLO 14 1972 58 0 0

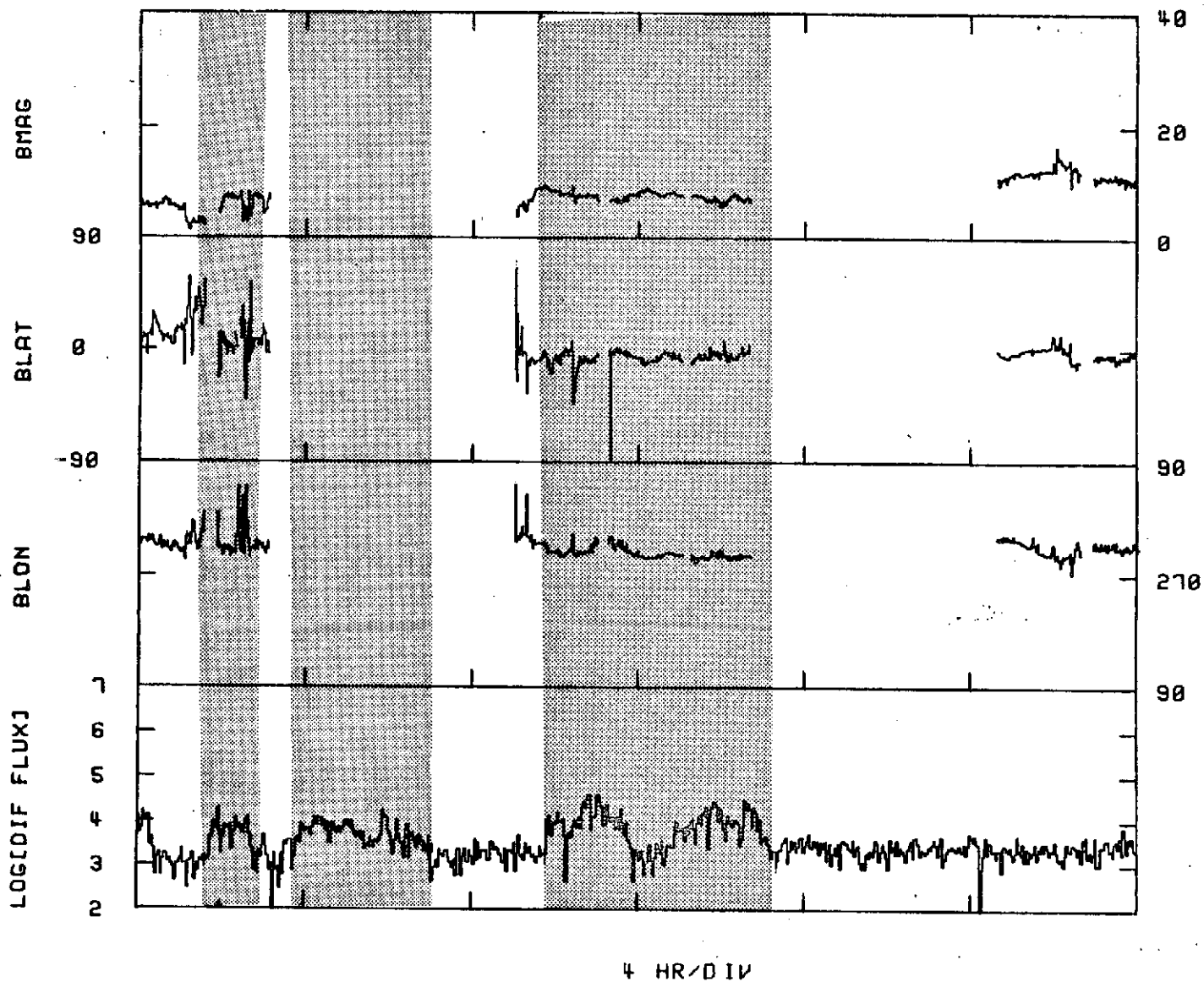
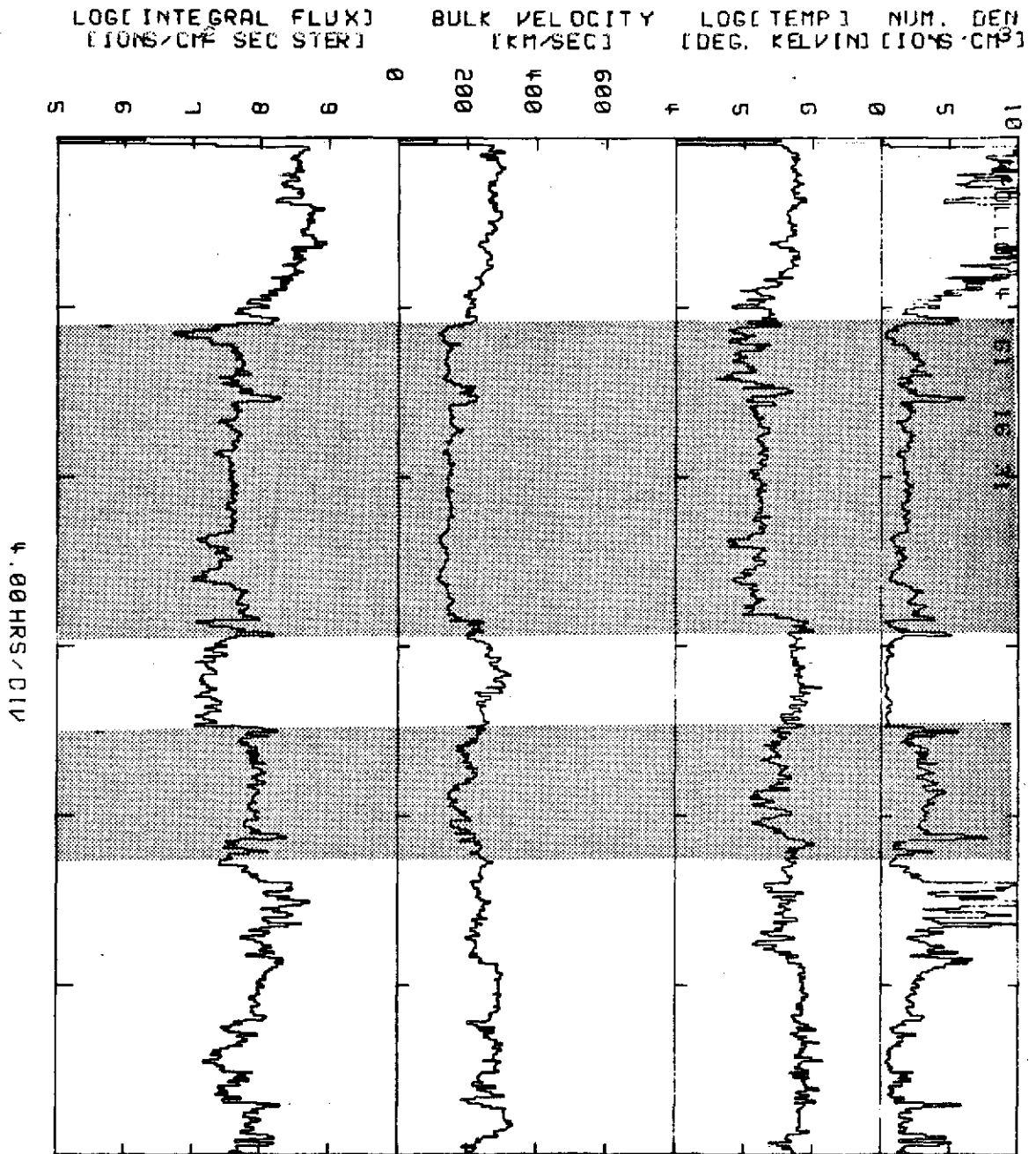


Figure 3.14

Figure 3.15



APOLLO 14 1972 61 16 30

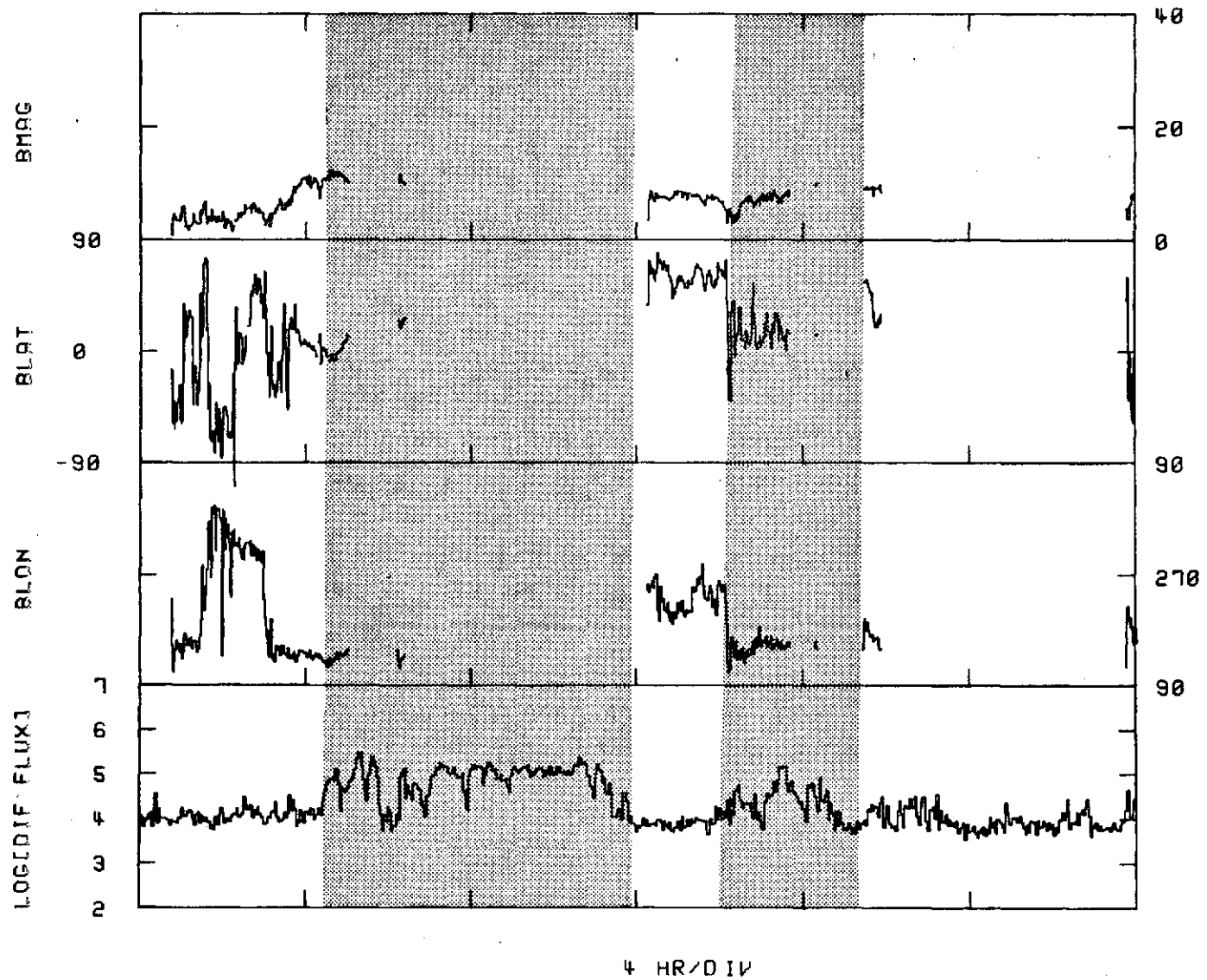


Figure 3.16

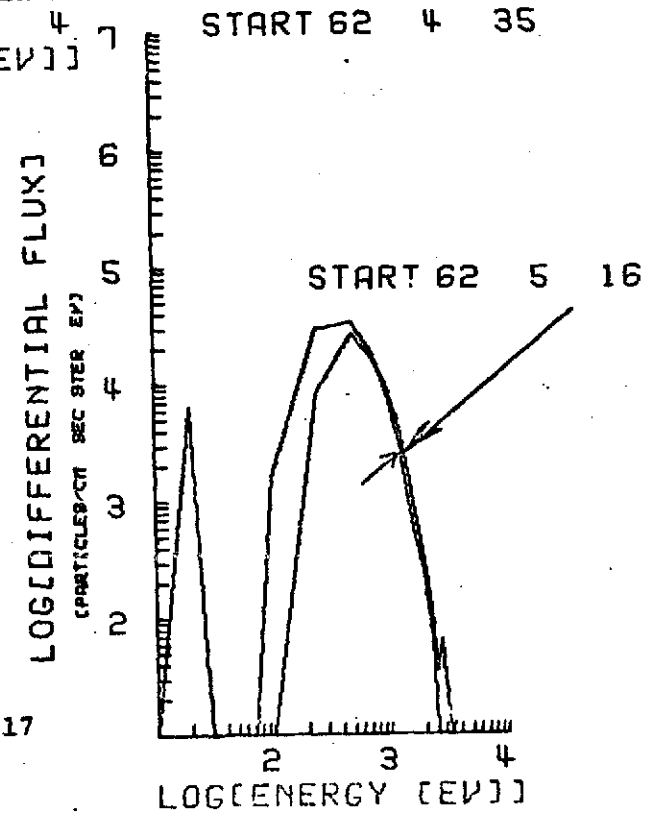
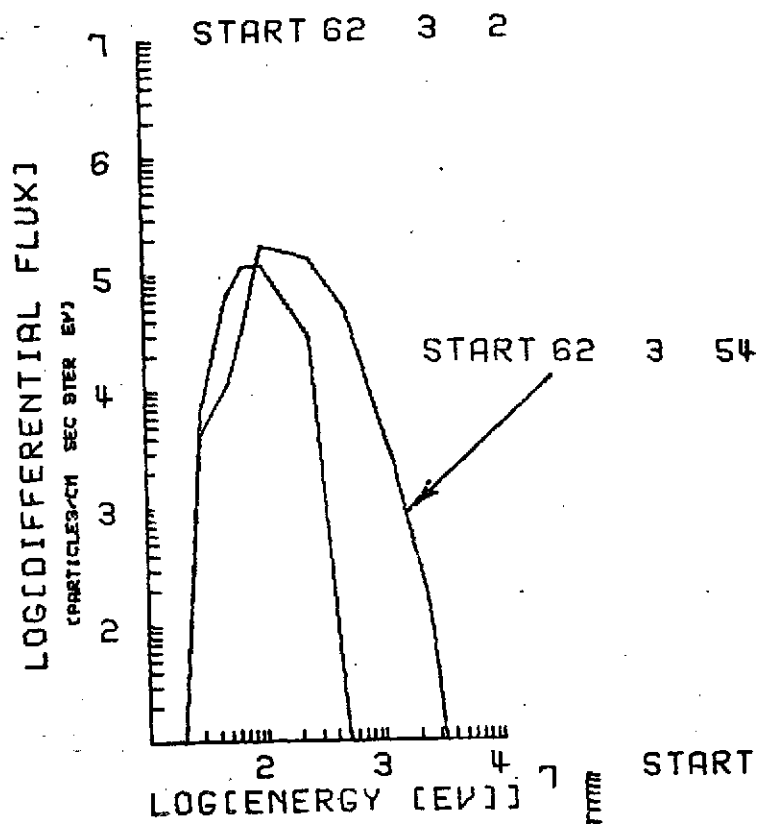


Figure 3.17

The time history of the spectra for the first of the LEP events outbound is shown in Figure 3.17. Representative spectra are presented; the first showing the spectrum during the middle of the LEP event and the other three showing the rapid transition into the magnetosheath. The former is characterized by its narrowness and its peak in the 100 eV channel. The other three show a shifting in the peak towards higher energy and a broadening of the spectrum into all the higher energy channels of the detector. At the same time there is a decrease in the magnitude of the differential flux at the peak. All this is suggestive of some interaction between the two particle regimes across the magnetopause.

3.4 Lunation 9

Lunation 9 contains the longest period for observation of the LEP events for which magnetic data has been obtained. Figures 3.18 and 3.19 show the general behavior of the data for this tail passage. As before, on the inbound portion of the passage the low energy events occur over a period of approximately 18 to 24 hours after the initial passage of the moon into the tail. The observation of these LEP events is terminated by the entry of the moon into the plasma sheet. The plasma sheet is seen to dominate the inbound portion of the tail passage. Outbound, however, only one brief encounter with the plasma sheet is observed, the rest of the time being dominated by a long period of continuous observation of the LEP's. Parametrically and spatially the LEP events follow the same pattern established in the previous lunations. (See figures 3.20, 3.21, 3.33, and 3.35.)

The magnetic field configuration for the times of observation of LEP events for this lunation are shown in Figures 3.22, 3.24, and 3.26. Magnetic data is not available for the times of the LEP events inbound. Figure 3.22 does show, however, the ordering of the field as the moon enters the tail. The outbound LEP events can be verified to take place on well ordered field lines. Figure 3.24 shows that when the LEP's were encountered in day 267 the moon was in the high latitude lobe of the tail. As before, the abrupt increase in the flux of 100 eV particles produces no change in the field direction. The magnitude of the field appears, however, to change dependent on the intensity of the event. Magnetic data is available for the period of these LEP events starting at GMT 1230. The advent of the first event after this time shows a decrease of ~ 4 gammas in the magnitude of the field as the intensity of the LEP event approaches its maximum and a subsequent return to a field strength of 21 gammas as the LEP event dies away. The field strength is again observed to fall off with the commencement of the next event at GMT 1800. The magnetic field data is discontinuous in the middle of this LEP event and this variation of the field magnitude is not observed during the next LEP event when data for the field is available. This could be a result of the fact that the LEP events where this variation in magnitude is not observed are a factor of four lower in their integral flux than those events in this lunation where the variation was observed.

Figures 3.18&3.19

Twenty minute averages for the twenty channels of the TID plotted as a function of time for the tail passage of lunation 9. The encounters of the moon with the plasma sheet (PS), magnetosheath (MS), and low energy proton regions (LEP) are labeled in the figures.

Figure 3.20

The portions of the lunar orbit for lunation 9 during which low energy protons were observed. The positions are calculated in solar magnetospheric coordinates. (.1 radian = $6 R_e$)

Figures 3.21,3.23&3.25 The plasma parameters for the times of the low energy proton events are plotted as a function of time for lunation 9. Shaded areas shows the times when the LEP's were observed.

Figures 3.22,3.24&3.26 The magnetic field configuration for the times of the low energy events is plotted as a function of time. The lowest panel gives the differential flux in the 100 eV/q channel of the TID without the background subtracted. The correction in longitude is 20 degrees. The shaded regions show the times of encounter of the LEP's

APOLLO 14 1972
START TIME 264 6 4
20 MIN AV
24.00HR/DIV

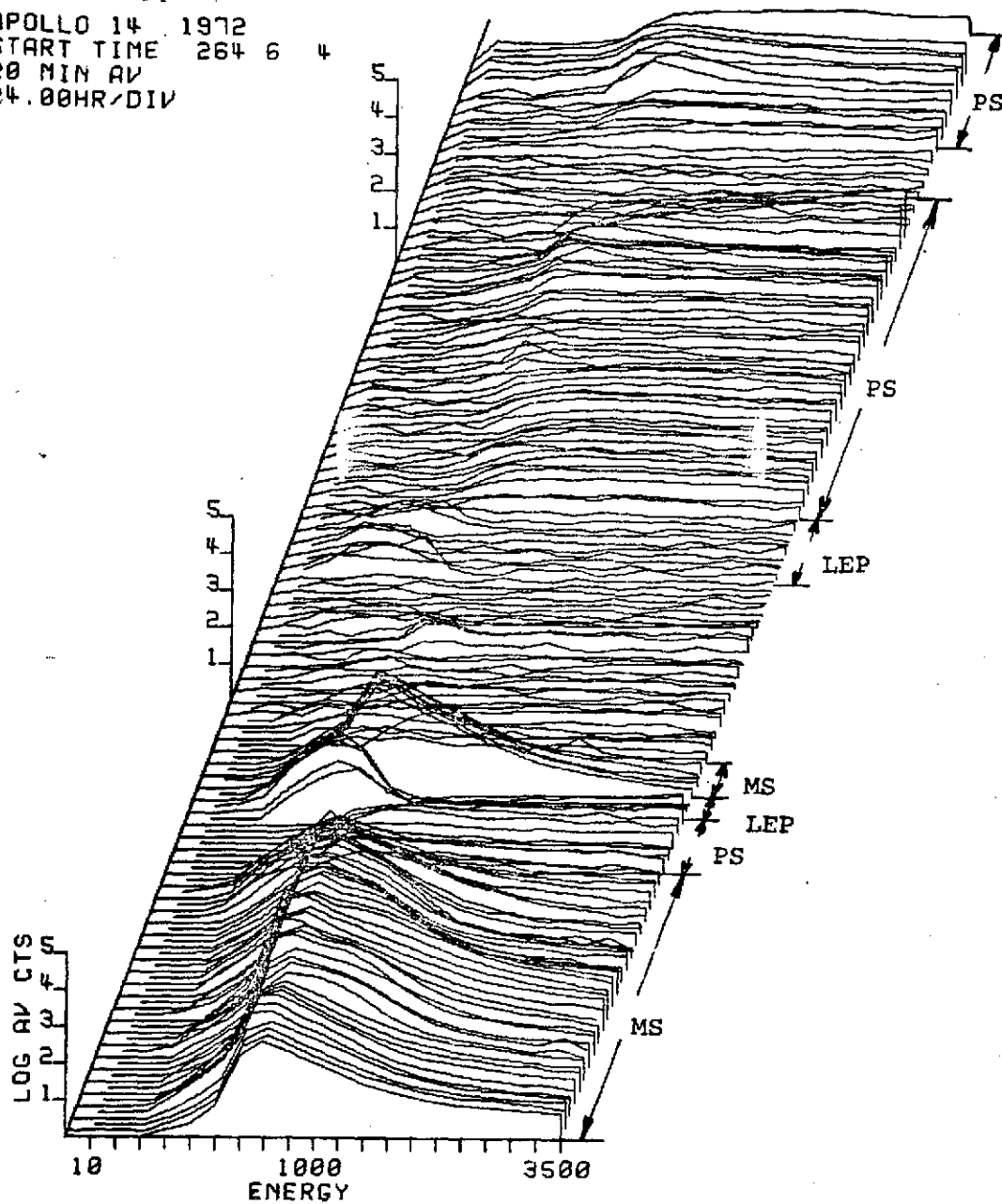


Figure 3.18

APOLLO 14 1972
START TIME 266 21 1
20 MIN AV
24.00HR/DIV

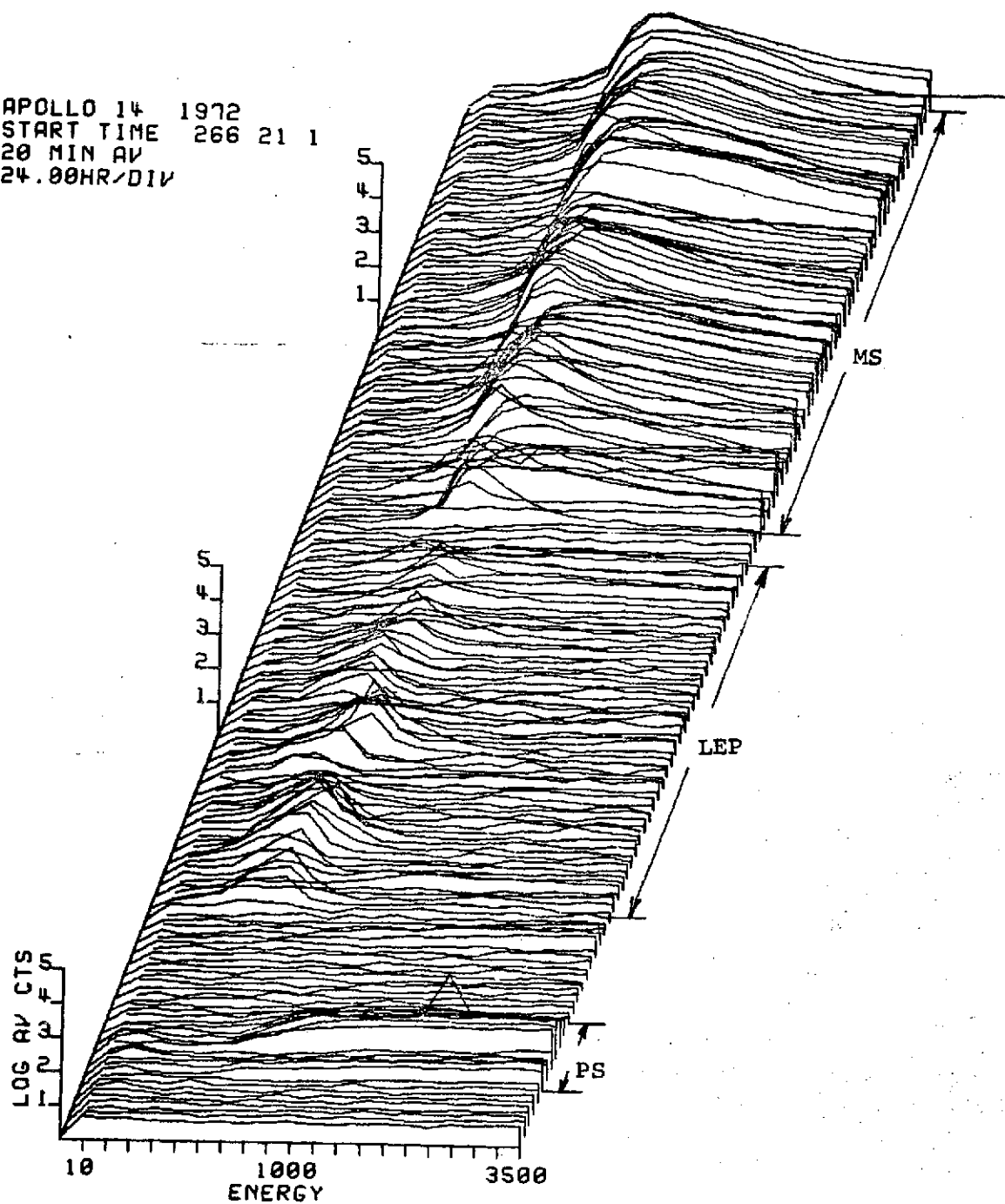


Figure 3.19

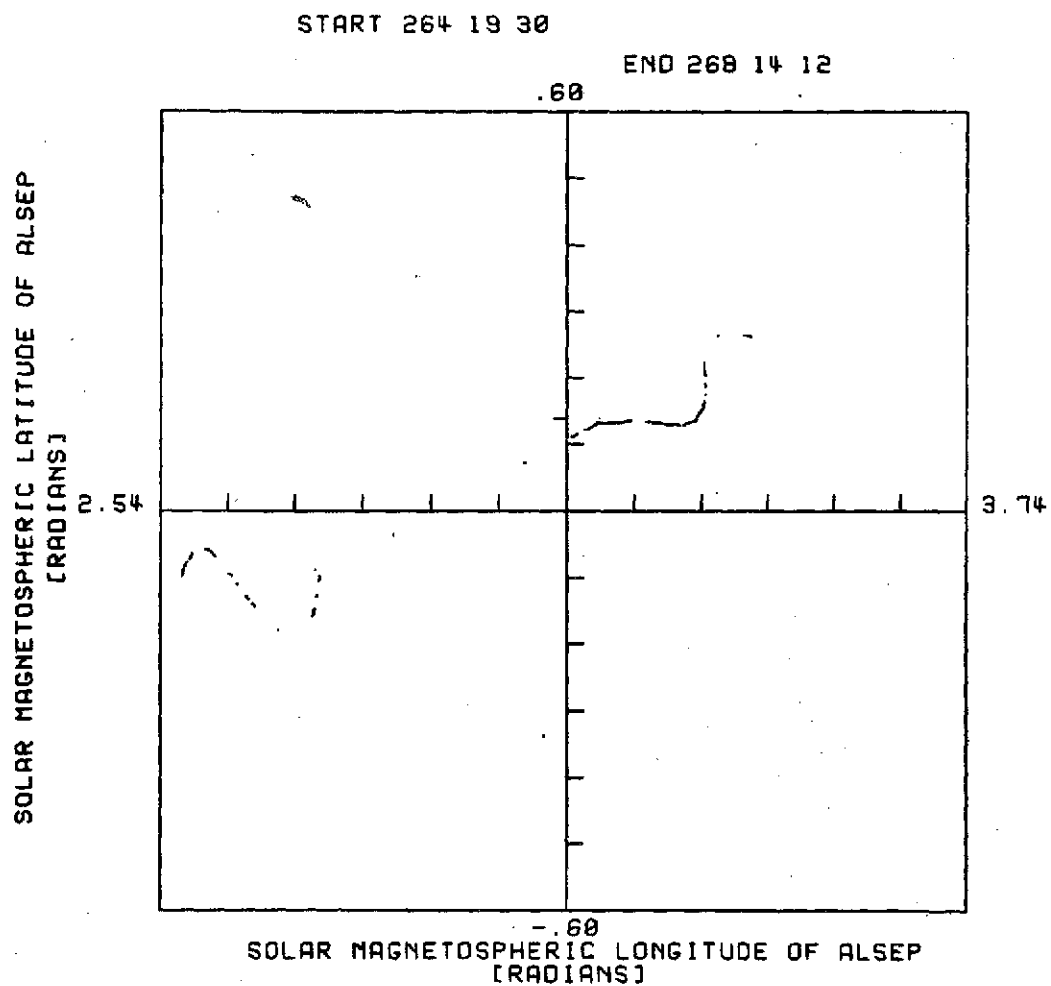


Figure 3.20

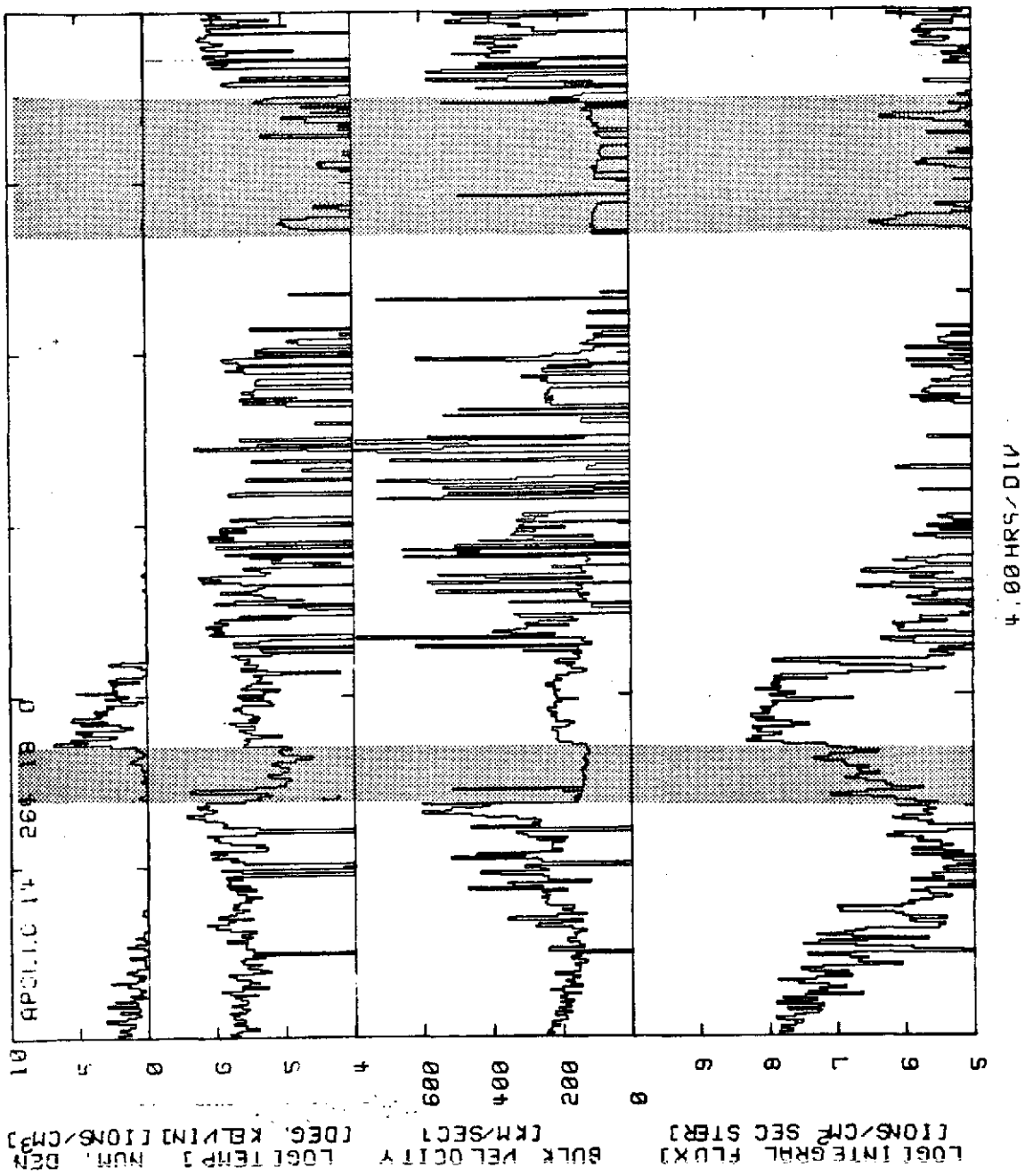
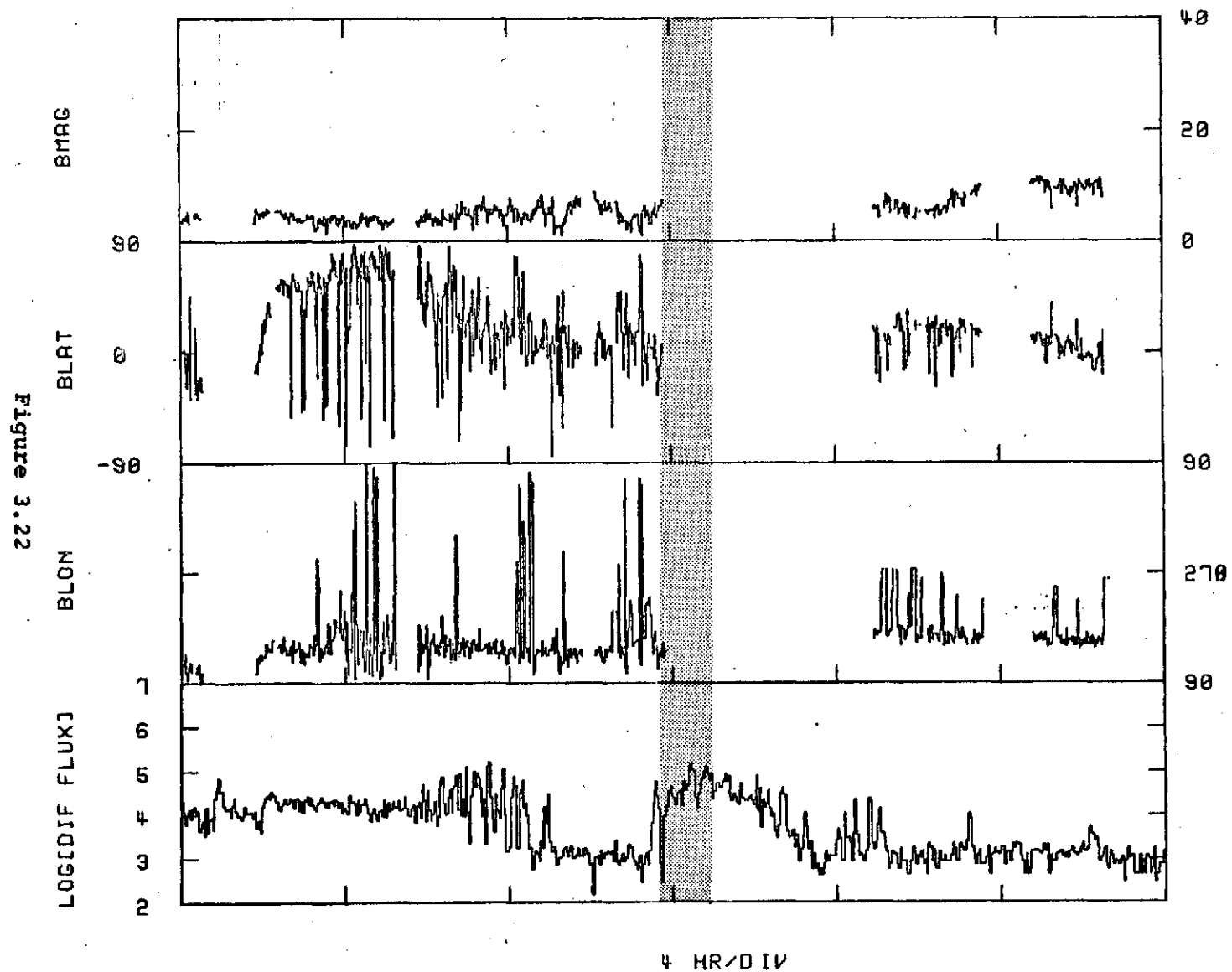
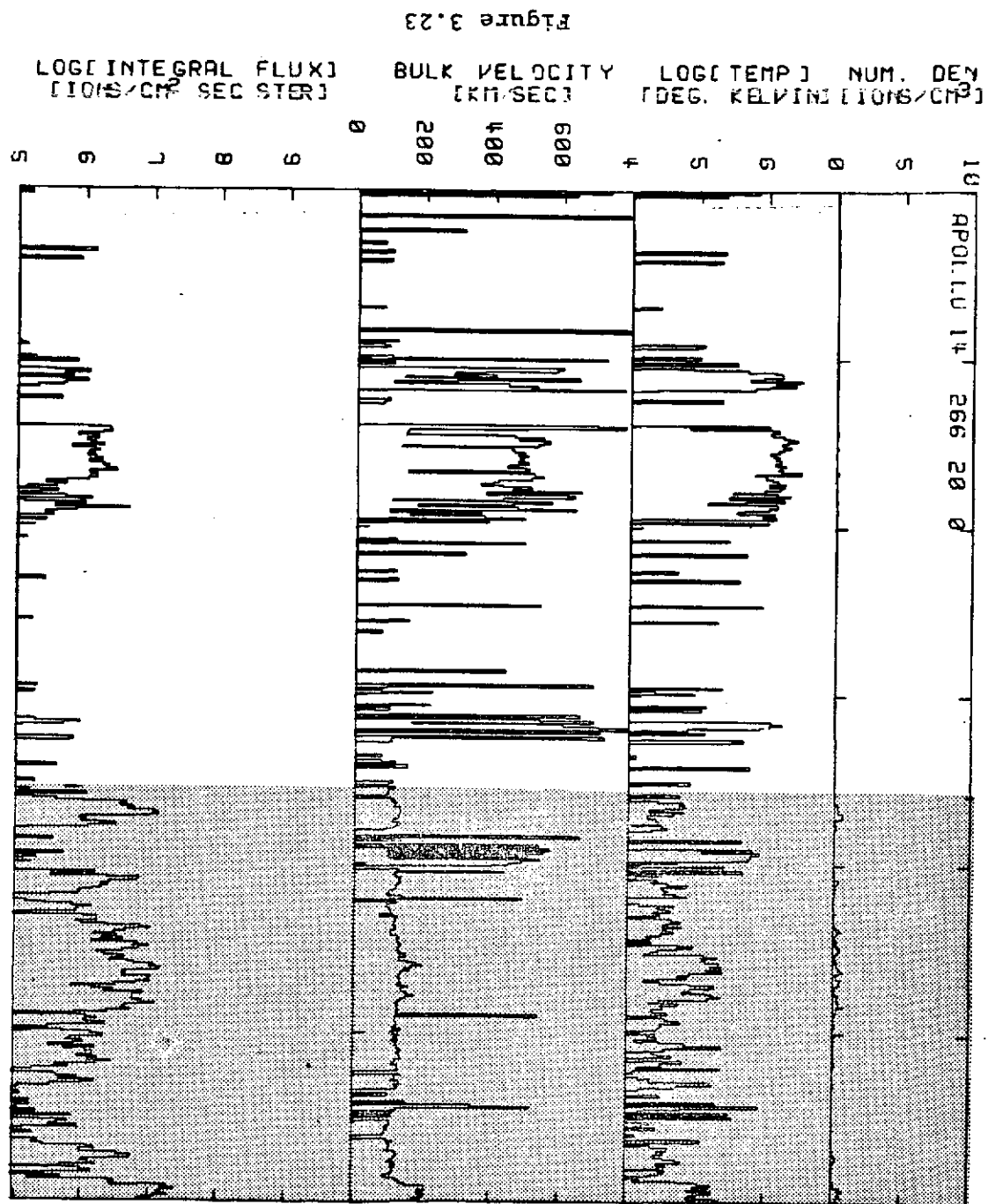


Figure 3.21

APOLLO 14 1972 264 12 0





APOLLO 14 1972 266 20 1

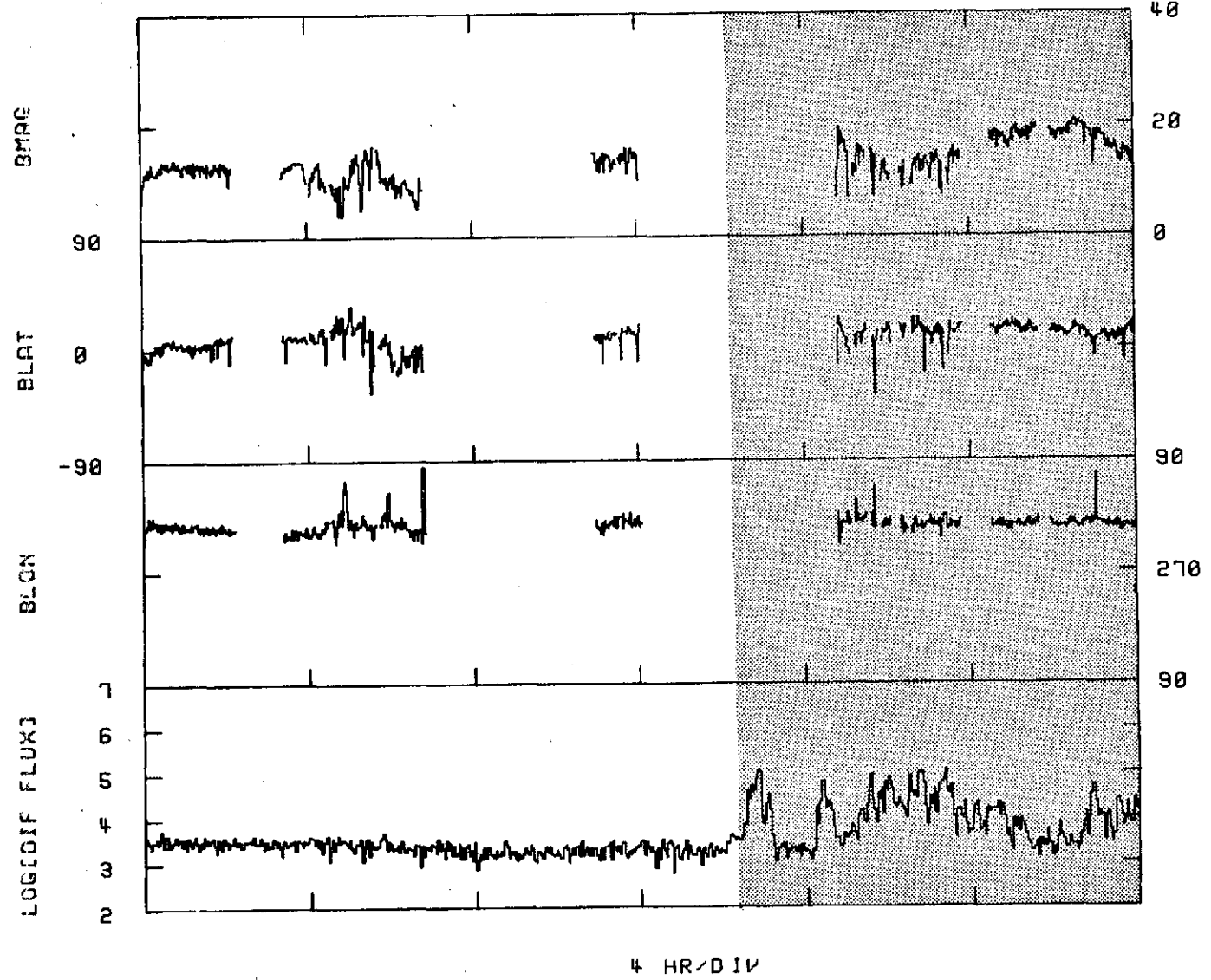
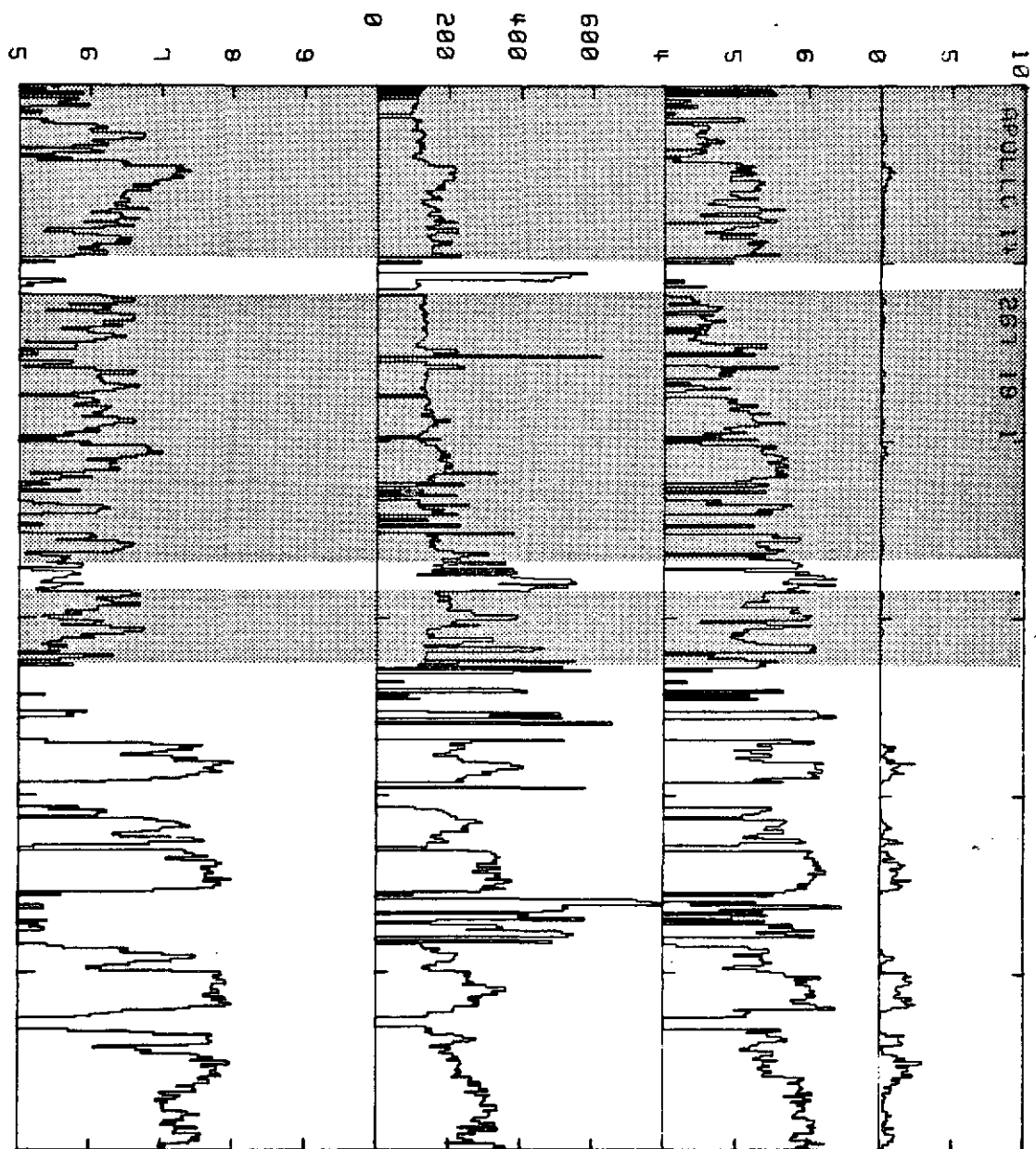


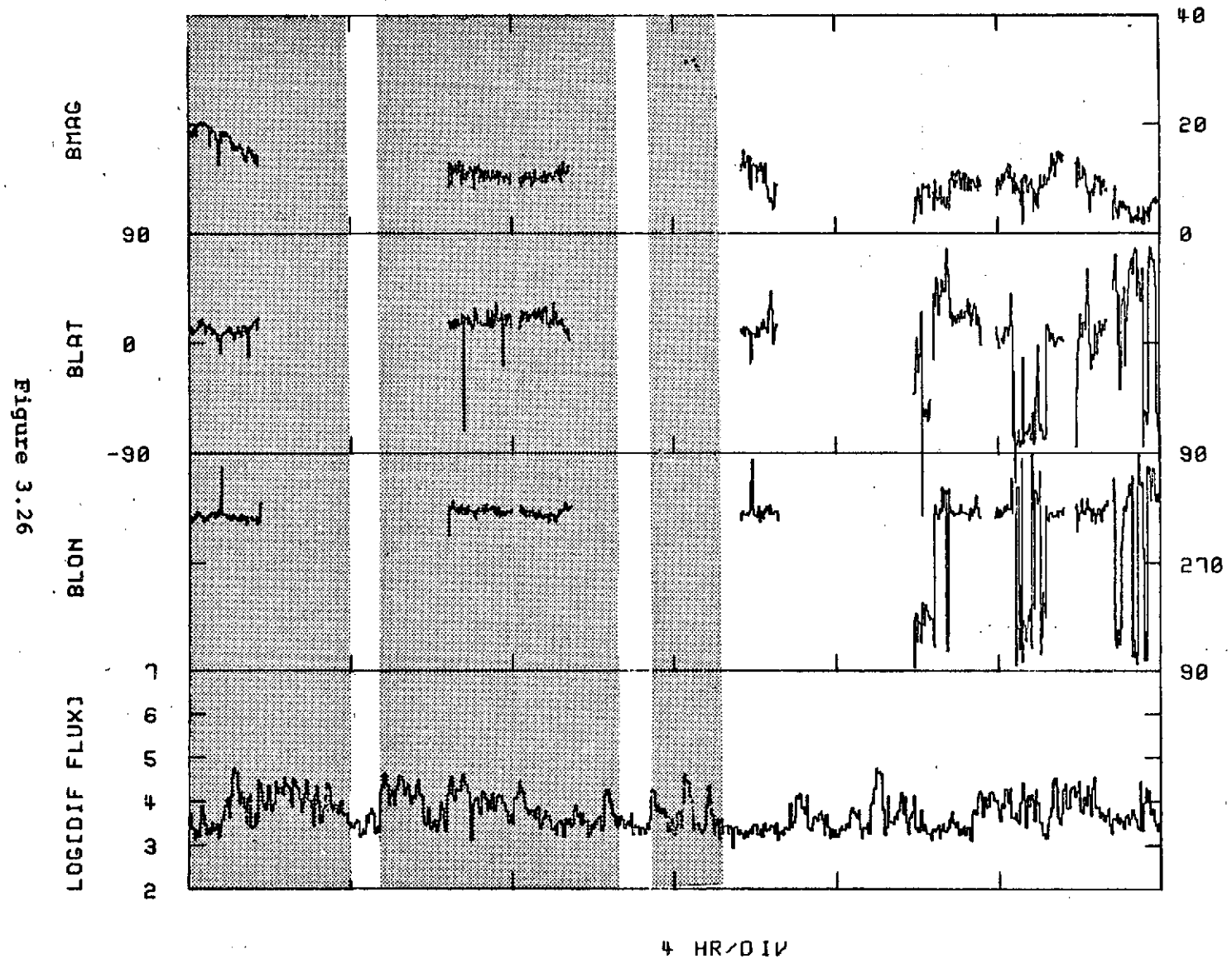
Figure 3.24

LOG[INTEGRAL FLUX]	BULK VELOCITY	LOG[TEMP]	NUM. DEN
[IONS/CM ² SEC STER]	[KM/SEC]	[DEG. KELVIN]	[IONS/CM ³]



4. 60 HRS. 31V

APOLLO 14 1972 267 18 0



3.5 Lunation 13

Lunation 13 exhibits two LEP events which are of note. Figures 3.27 and 3.28, which illustrated the general nature of the Side data for this tail passage, show that the two LEP events are observed during periods close to those times when the moon encounters the magnetopause. For regions deeper in the tail the plasma sheet is seen to be the principle particle regime encountered.

The behavior of the LEP events display considerable time variation. Figure 3.29 shows the inbound behavior of the plasma parameters. The crossing into the tail is clearly seen in the sharp falloff in the integral flux at ~ GMT 2000. This is followed at GMT 2800 by the appearance of the low energy ions. The LEP event exhibits a shifting towards higher energy and temperature as the event proceeds. The bulk velocity starts at 120 km/sec and appears to nearly double during the course of the event with a similar doubling of the temperature during the same period. During this period the moon was moving towards the theoretical location of the neutral sheet (Figure 3.33). At the termination of the event the moon enters the plasma sheet as witnessed in Figure 3.29 by the drop in integral flux and the rise in bulk velocity and temperature.

Figure 3.31 shows the characteristics of the events on the outbound portion of the tail passage. The first LEP event commences on day 19 GMT 1300 with the phenomenon being observed continuously over the next eight hours. As in the inbound case a shifting towards higher energy is observed. Over the course of the two hours prior to the disappearance of the event there is a rise in the bulk velocity from ~ 120 km/sec to ~ 350 km/sec with a corresponding rise in

temperature from 5×10^4 K to 1.5×10^6 K. This appears to correspond to a re-entry of the moon into the magnetosheath. Several short events are seen following the moons re-entry into the tail at GMT 2000 on day 19. There duration is ~ 1 hour. The moon re-enters the magnetosheath abruptly at 0130 on day 20.

Magnetically one can verify that the moon enters the ordered field region at GMT 1800 on day 16 (Figure 3.32). Data is unfortunately discontinuous over the period of the inbound events. One sees that the field is ordered at the beginning of the event but, due to the lack of data no definitive statements can be made as to the field configuration for the entire time of the phenomenon. Outbound data is available starting at GMT 1300 on day 19. (Figure 3.33.) The field is seen to be well ordered for the LEP events in this region. The only anomaly is a sudden doubling of the field strength in an approximately twenty minute periods commencing at GMT 1858 on day 19. This coincides within ten minutes with a five fold increase in the integral flux and a commensurate increase in the number density to $2.5/\text{cm}^3$. At the same time the bulk velocity is seen to remain constant and the temperature to drop an order of magnitude to a value of $\sim 5 \times 10^4$ K. From spectra it appears that the moon re-enters the magnetosheath at GMT 1918 day 19. Comments on the remaining events are not possible because of the lack of data.

The behavior of the outbound LEP event can be better understood in terms of the spectral variation with time. The eight spectra shown in Figures 3.34 and 3.35 cover the period for the phenomenon and show the spectral transition into the magnetosheath.

Figures 3.27&3.28

counters

Twenty minute averages of the counting rates in the twenty channels of the TID plotted as a function of time for the tail passage of lunation 13. The encounters of the moon with the plasma sheet (PS), magnetosheath (MS), and low energy proton regions (LEP) are labeled in the figures.

Figures 3.29&3.31

Plasma parameters for the times of the LEP events for the tail passage of lunation 13. Two and one half minute averages are plotted as functions of time for integral flux, bulk velocity, temperature and number density. Shaded regions correspond to periods during which the LEP's are observed.

Figures 3.30&3.32

The magnetic field configuration plotted in solar ecliptic coordinates for the times of the low energy proton events in lunation 13. The lowest panel gives the differential flux in the 100 eV/q channel with the background not subtracted. The longitude correction is approximately 50 degrees. The shaded areas show the times of encounter of the LEP's.

Figure 3.33

Location of the moon in solar magnetospheric coordinates for the times when the low energy protons were encountered in lunation 13. (.1 radian = $6 R_e$)

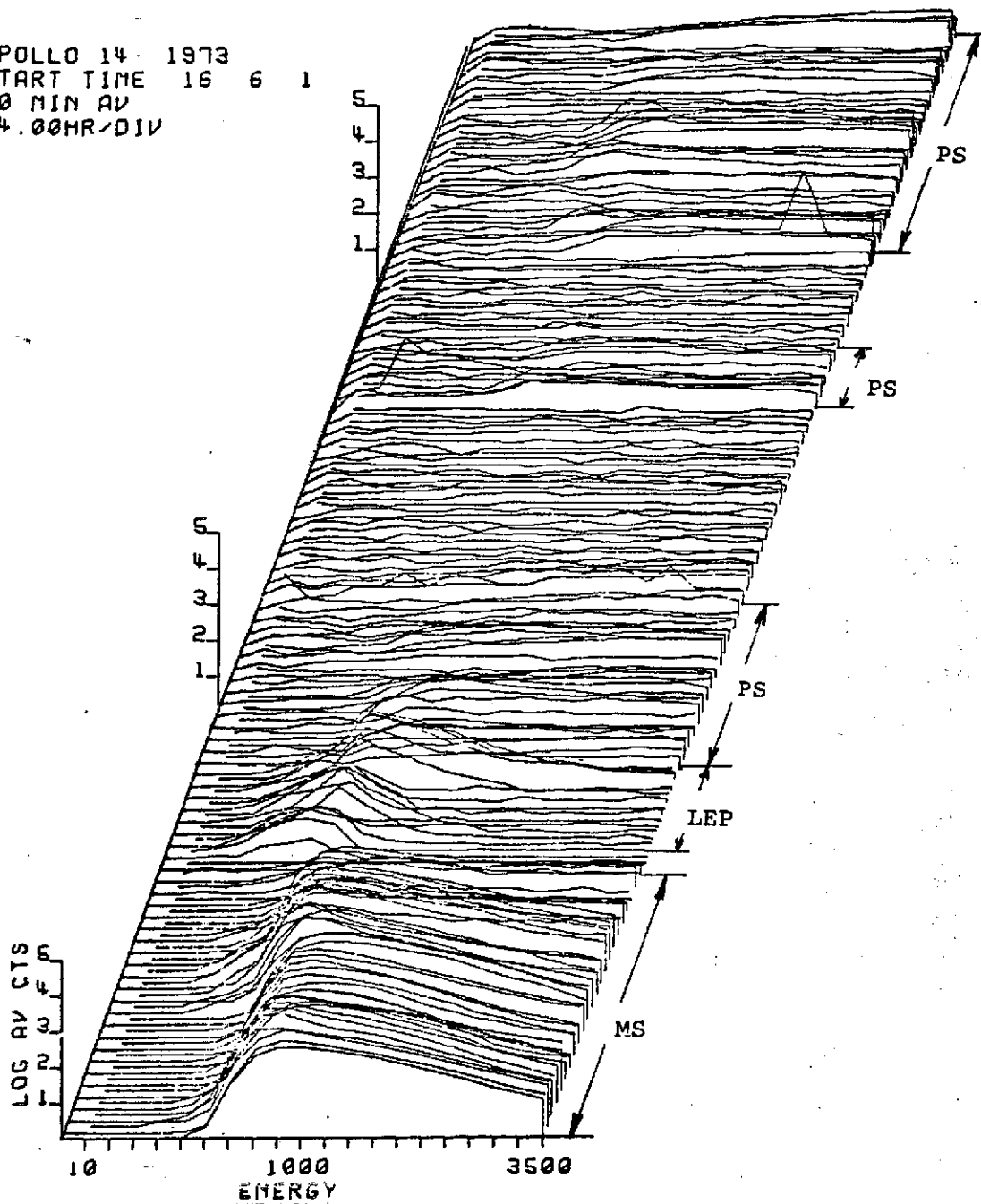
Figure 3.34

Comparative spectra for the three different particle regimes encountered by the moon during the tail passage of lunation 13.

Figure 3.35&3.36

Eight spectra are plotted showing the behavior of the outbound LEP event as the moon enters the magnetosheath. The time at the top of each plot refers to the start time of the spectrum to which the arrow does not point. All spectra are ten minute averages of the data.

APOLLO 14 1973
START TIME 16 6 1
20 MIN AV
24.00HR/DIV



APOLLO 14 1973
START TIME 18 17 3
20 MIN AV
24.00HR/DIV

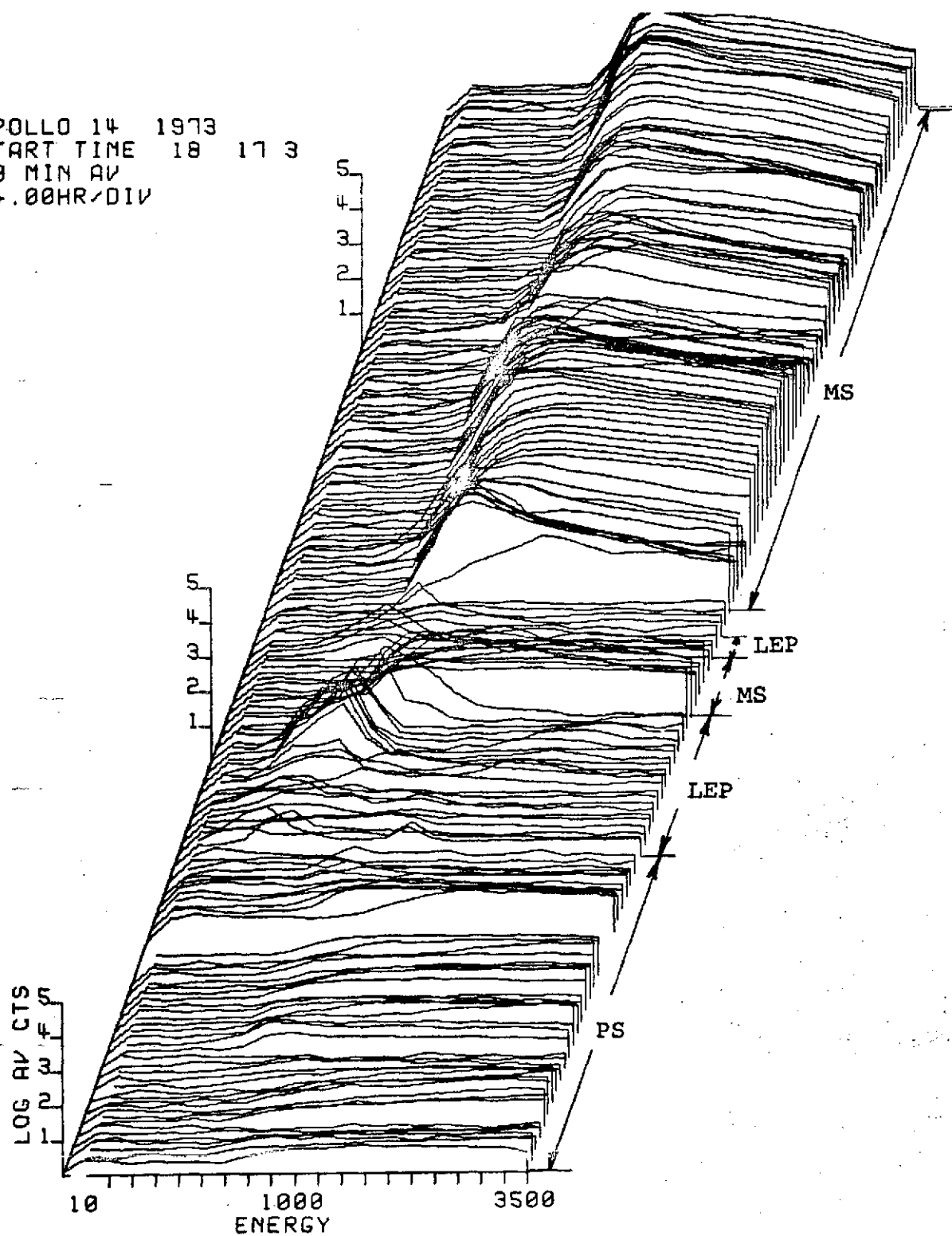


Figure 3.28

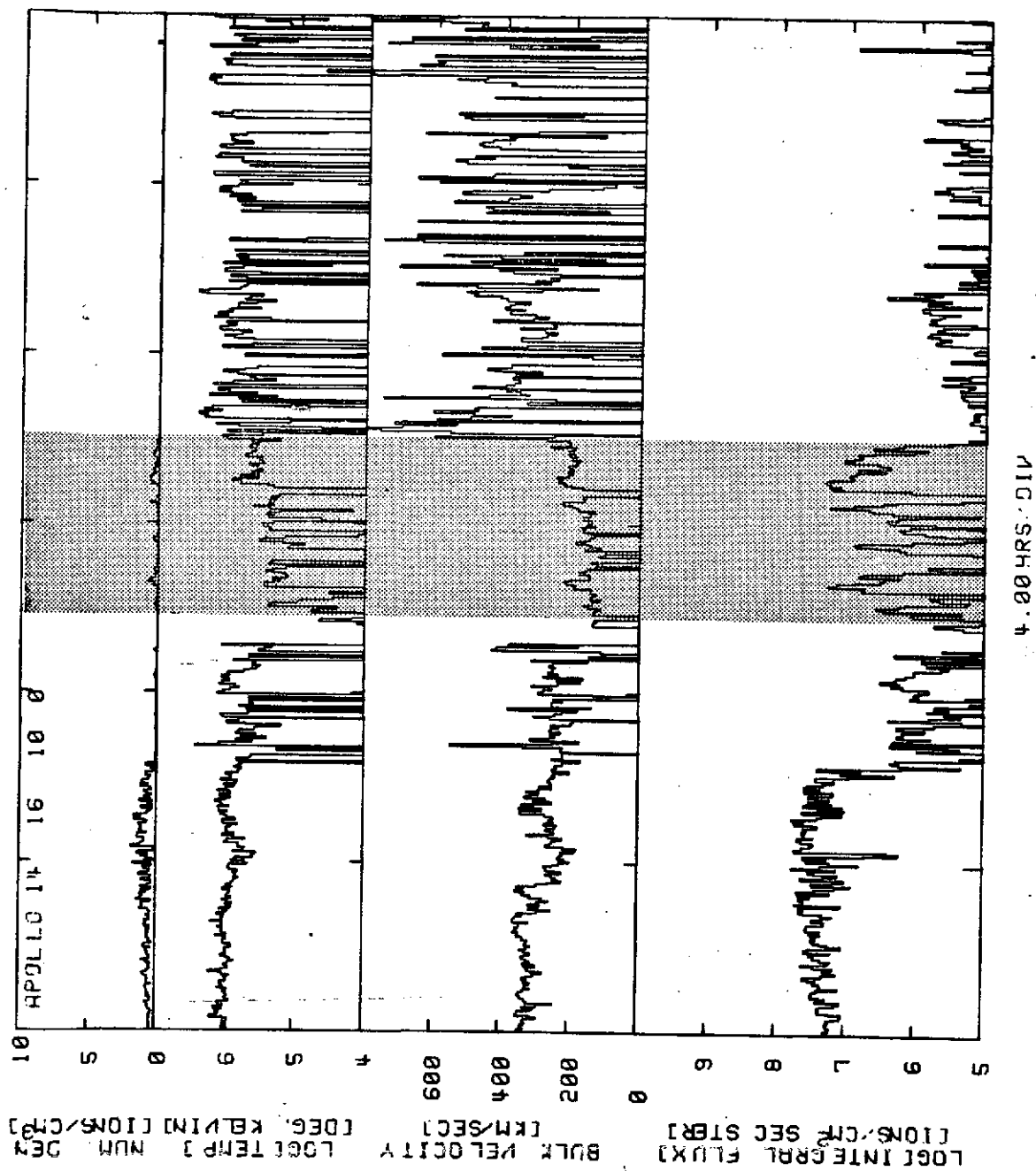


Figure 3.29

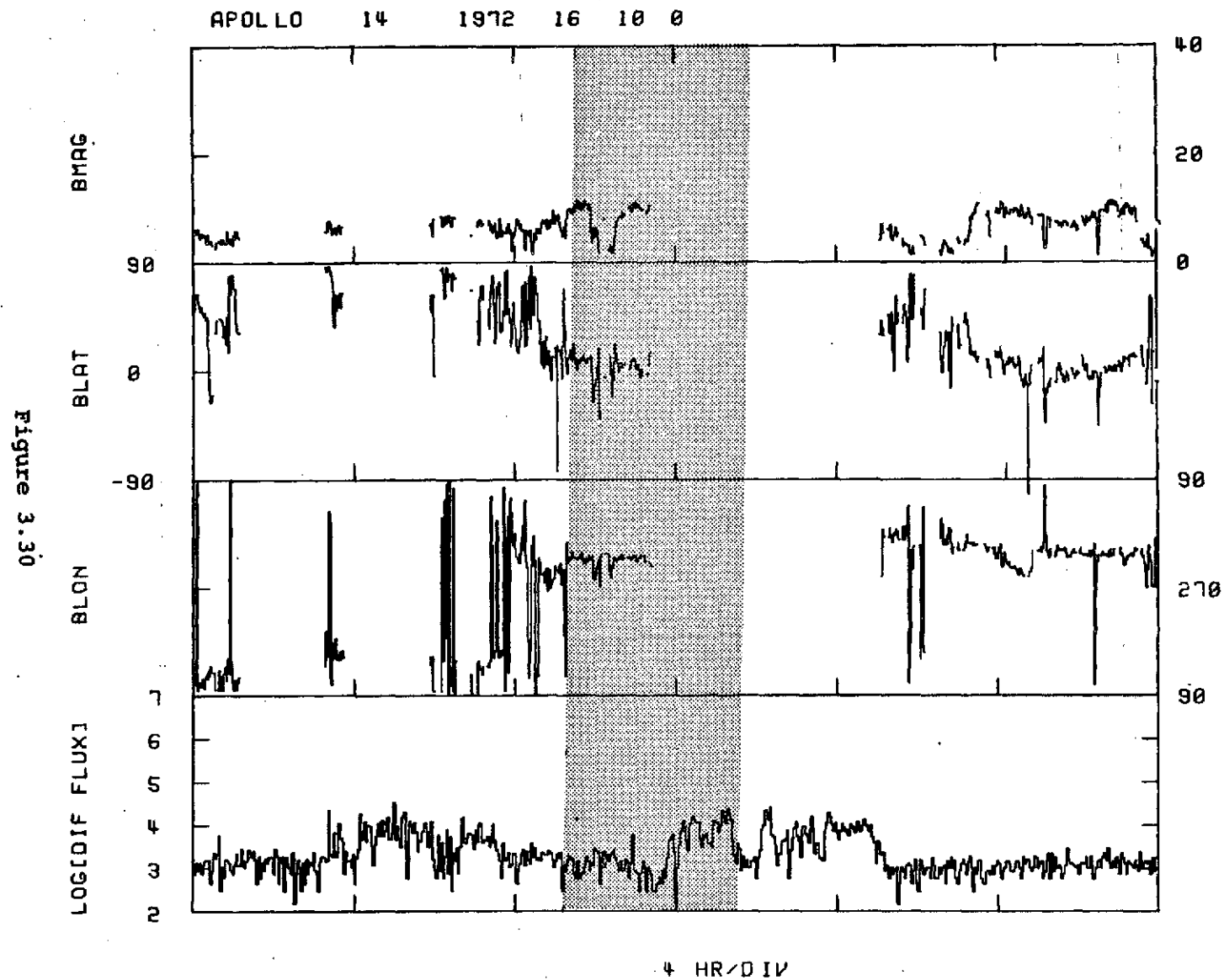


Figure 3.30

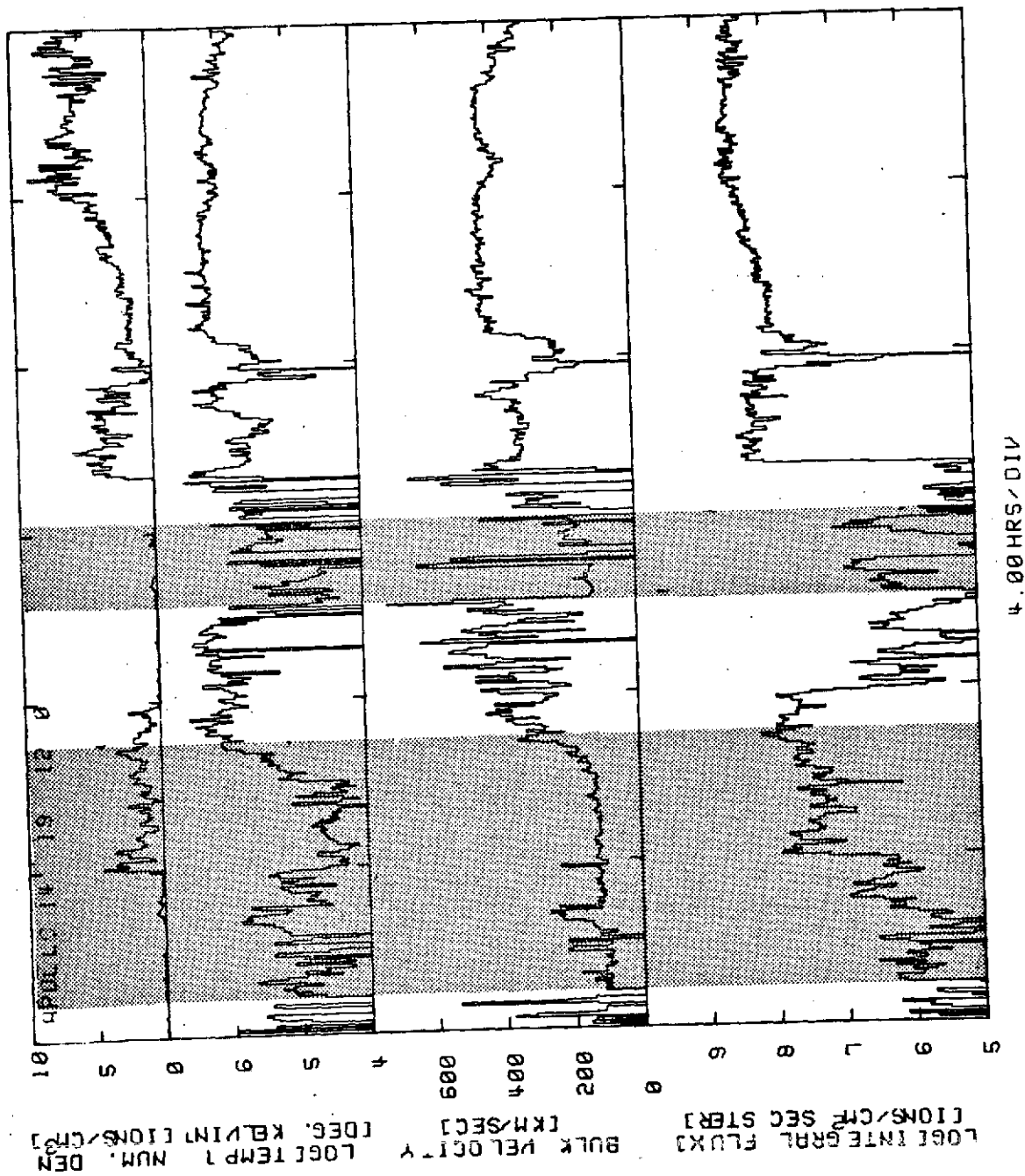
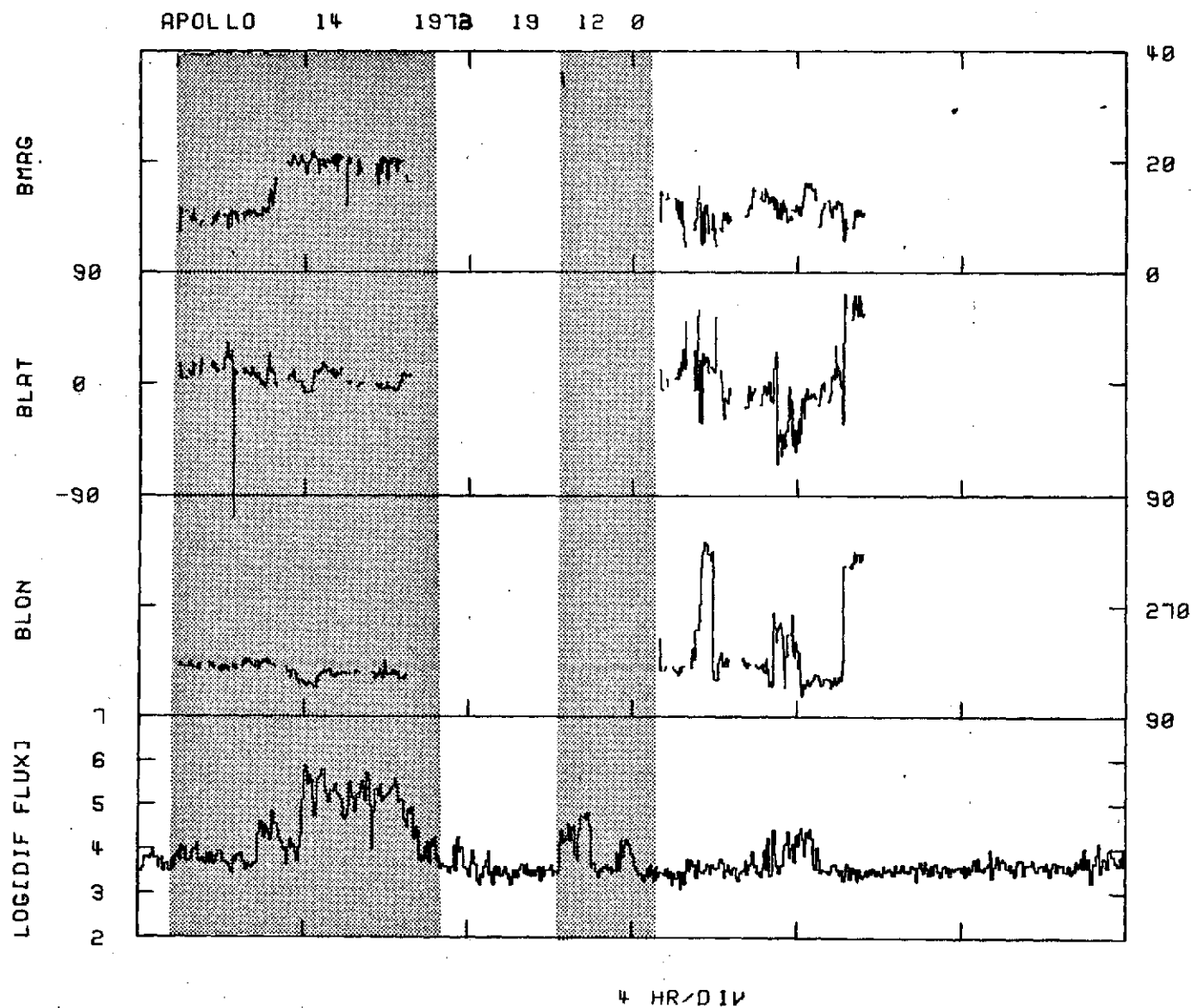


Figure 3.31

Figure 3.32



START 16 22 90

END 20 0 7

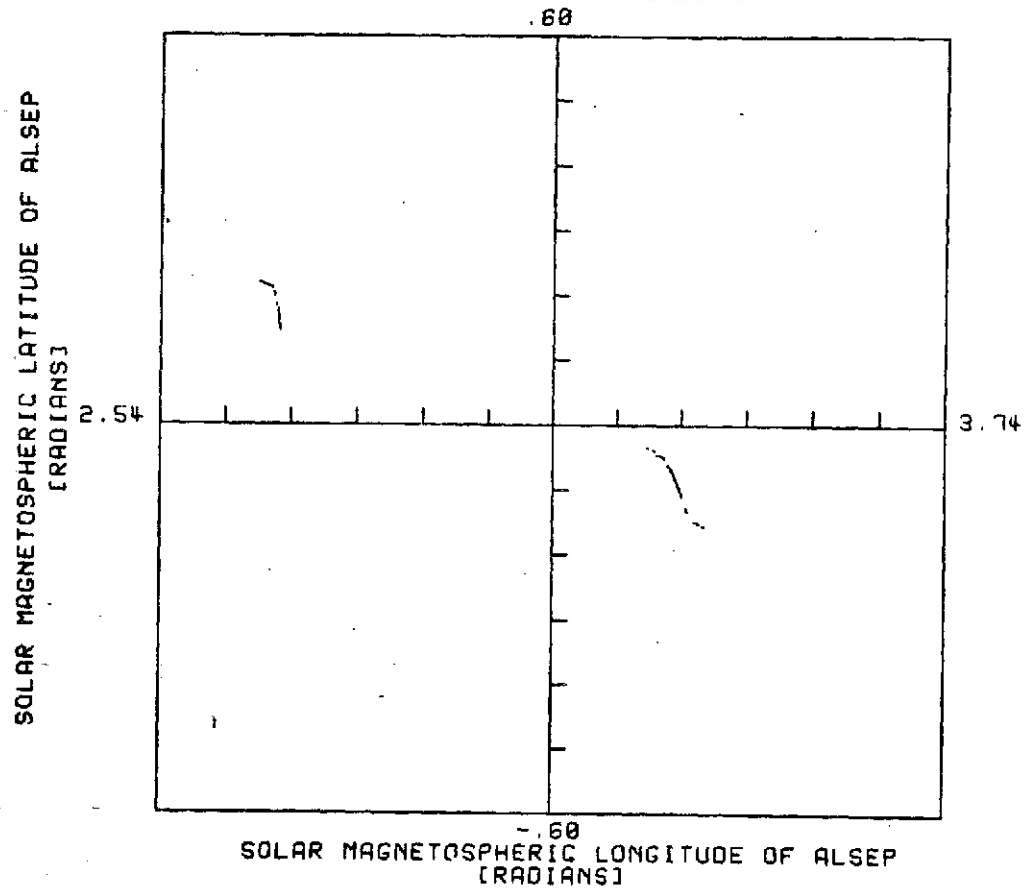


Figure 3.33

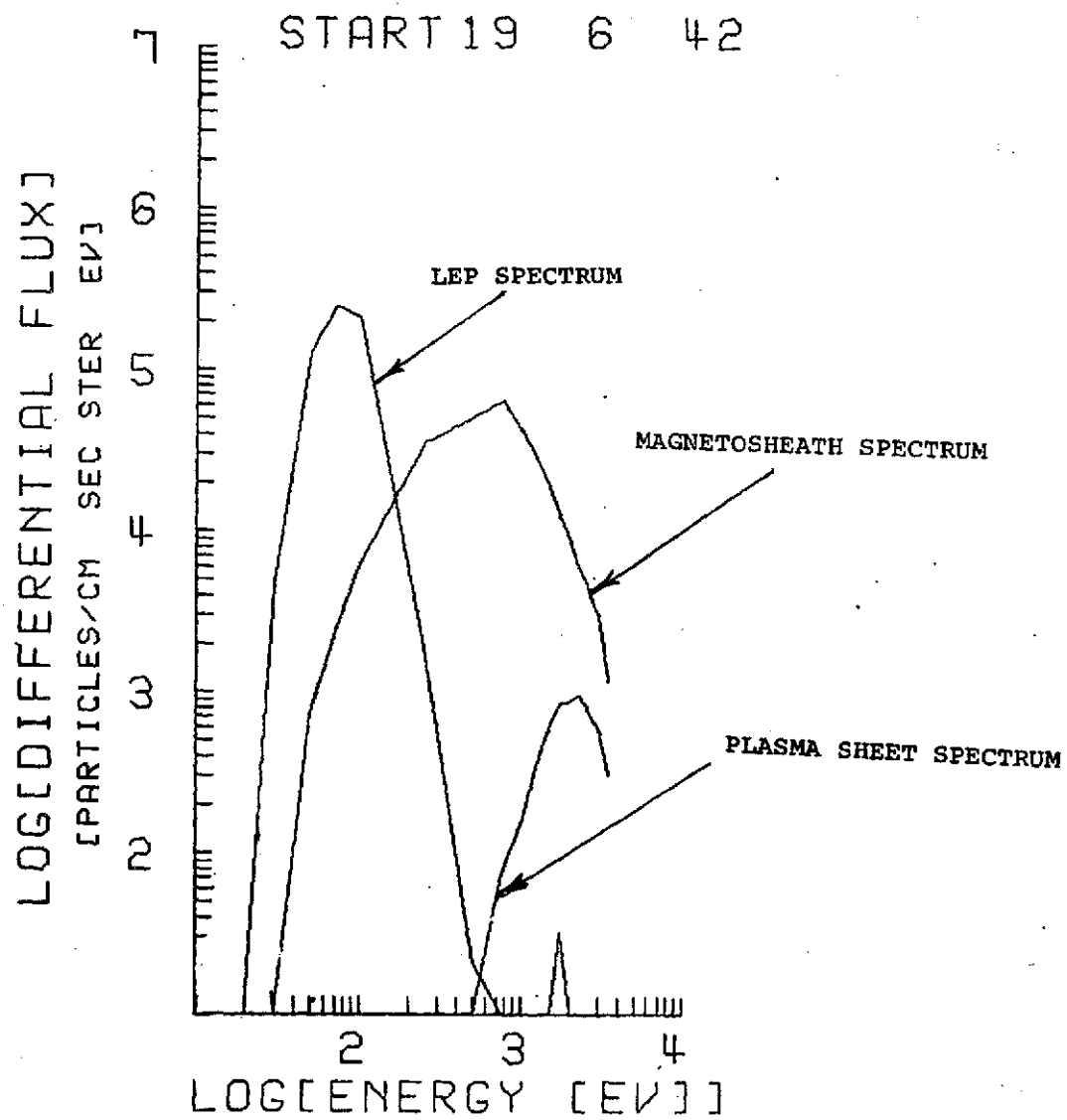


Figure 3.34

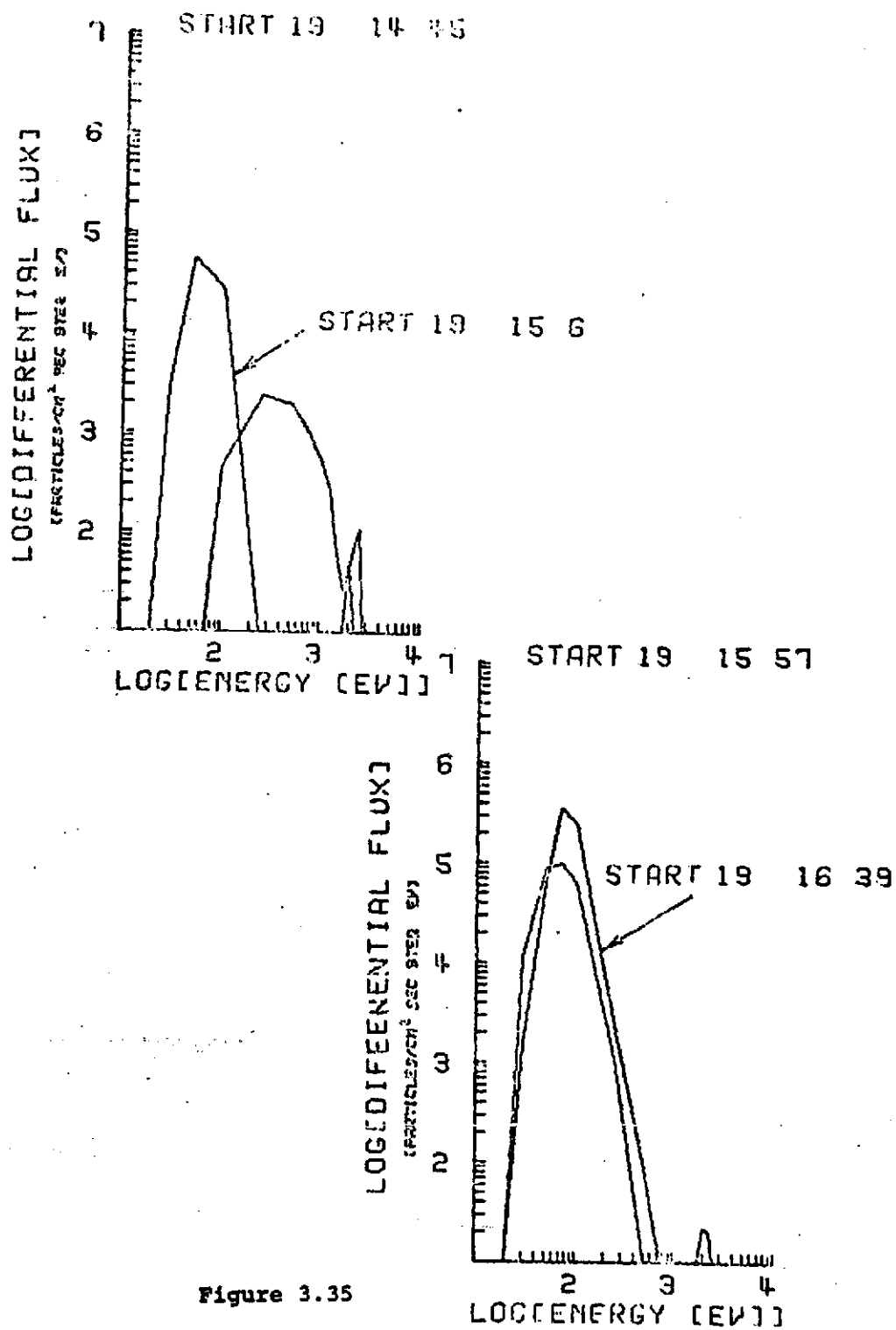


Figure 3.35

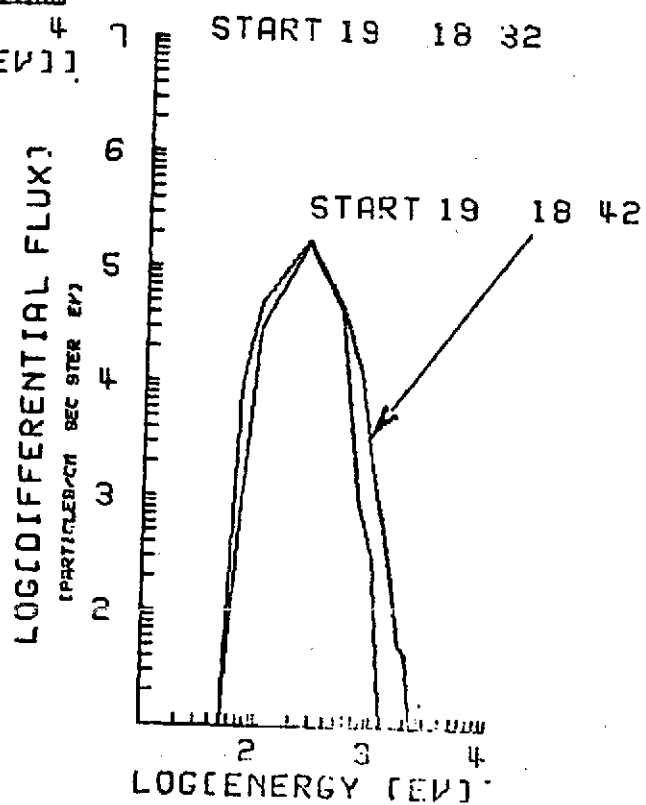
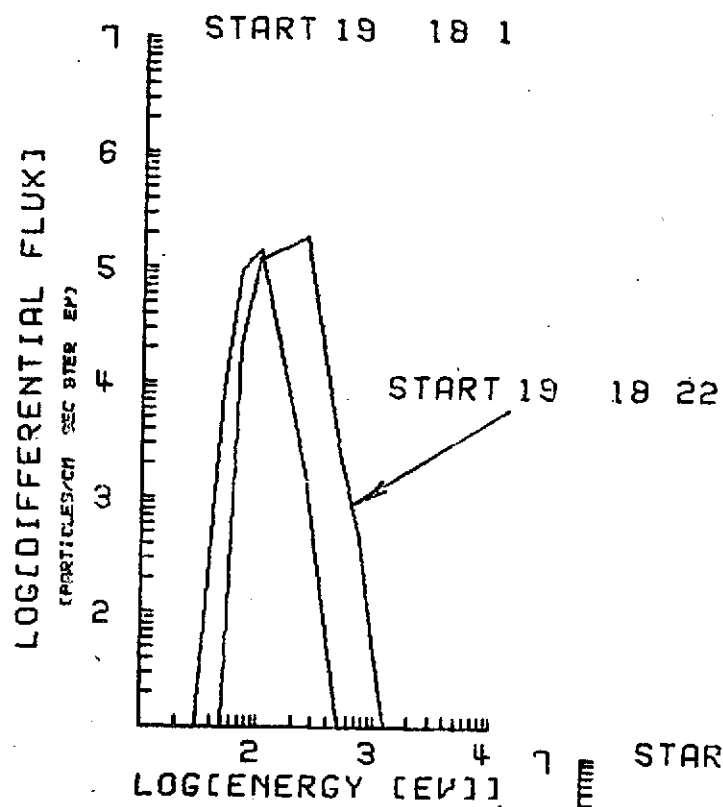


Figure 3.36

3.6 Lunation 3

One other tail passage of special interest will be mentioned here because of the duration of the LEP events observed. Lunation 3 is the orbit for which the most hours of observation of the LEP events were found. Nearly 60% of the time of the tail passage for this orbit was dominated by LEP spectra. Figure 3.30 shows that the events appear spatially across much of the range the moon traversed in the Y_{sm} and Z_{sm} directions. Particularly on the outbound portion of the tail passage, the LEP events are nearly continuous over $14 R_e$ in the Y_{sm} direction and $7 R_e$ in the Z_{sm} direction.

Figures 3.38 and 3.39 show the behavior of the events for the two days prior to the moon's entry into the magnetosheath. The LEP events are dominant for 34 hours of this time exhibiting a bulk velocity of 100 to 200 km/sec, an integral flux of $1 - 6 \times 10^7$ ions/cm² - sec-ster, a temperature of 6×10^4 to 2×10^6 K and number densities of .1/cm³ to 2/cm³. The most striking feature of this period is the relative stability of the LEP events over such an extended period of time and over such a vast spatial extent.

3.7 General Observations

In order to gain some insight as to the overall spatial features of the phenomenon it is useful to plot the position of the moon in solar magnetospheric coordinates for the times when the LEP's were observed. (See Figure 3-41a) For comparison the complete orbits for the fifteen lunations also have been plotted in the SM coordinate system. (Figure 3-41b) It is of note that the envelope for the space swept out by the moon de-

Figure 3.37

Twenty minute averages of the counting rates for the 20 channels of the TID plotted as functions of the time for the tail passage of lunation 3. The different particle regimes encountered are labeled MS, for magnetosheath, PS for plasma sheet, and LEP for low energy protons.

Figure 3.38

The location of the moon in solar magnetospheric coordinates for the times when the LEP events were observed. ($.1 \text{ radian} = 6 R_e$)

Figures 3.39&3.40

The plasma parameters for the outbound LEP events in the tail passage for lunation 3. Shaded regions correspond to the times for the LEP events.

APOLLO 14 1972
START TIME 90 5 44
20 MIN AV
24.00HR/DIV

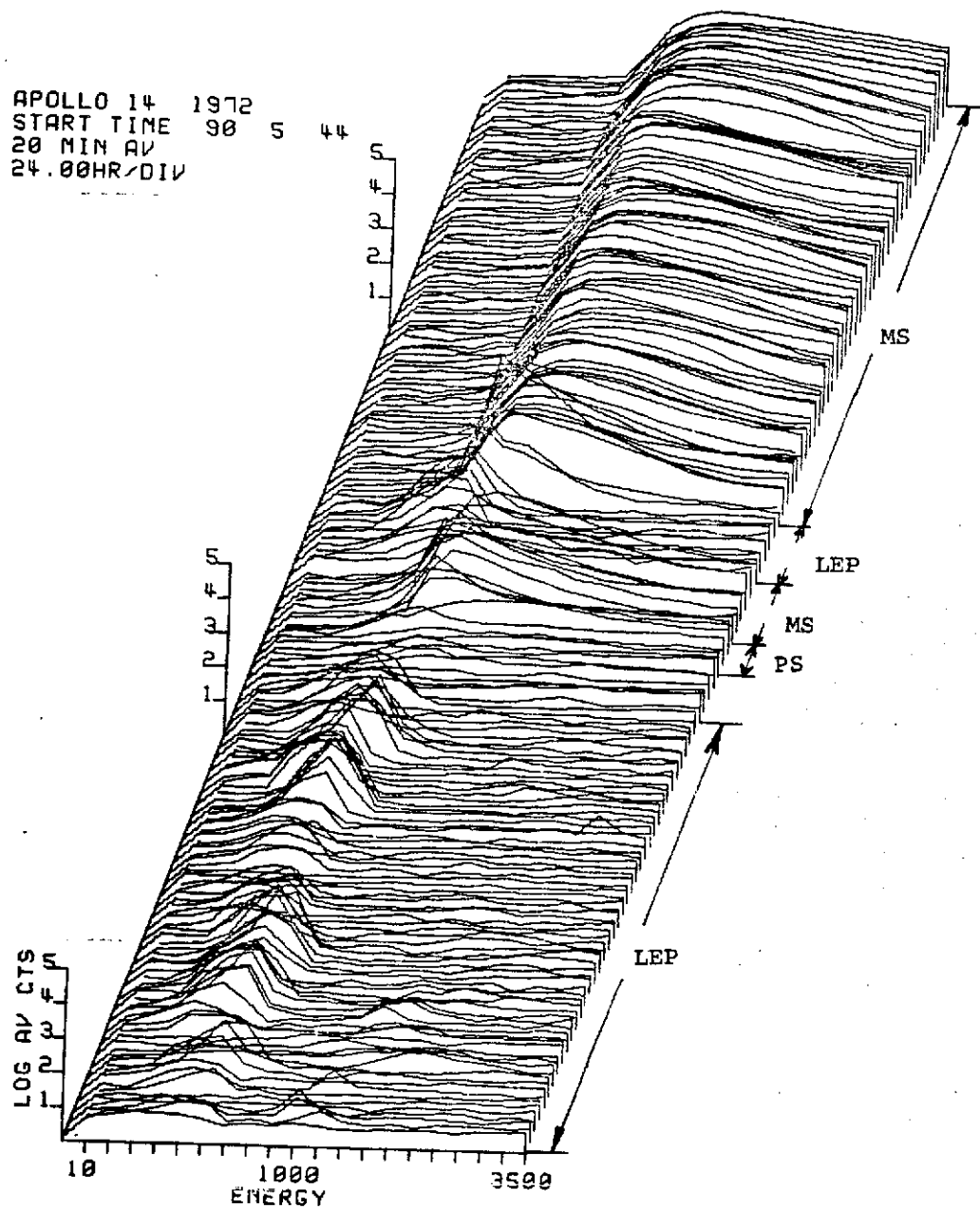


Figure 3.37

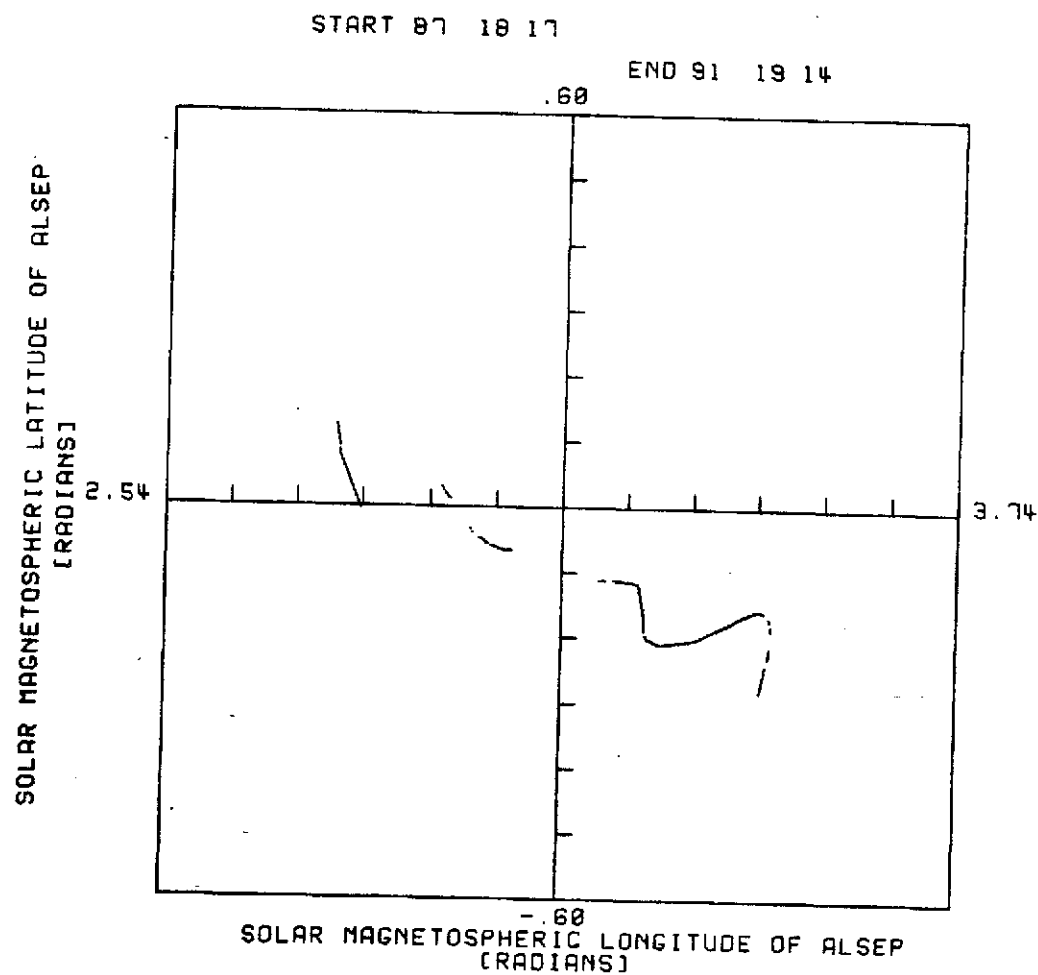


Figure 3.38

4.00 HRS / DIV

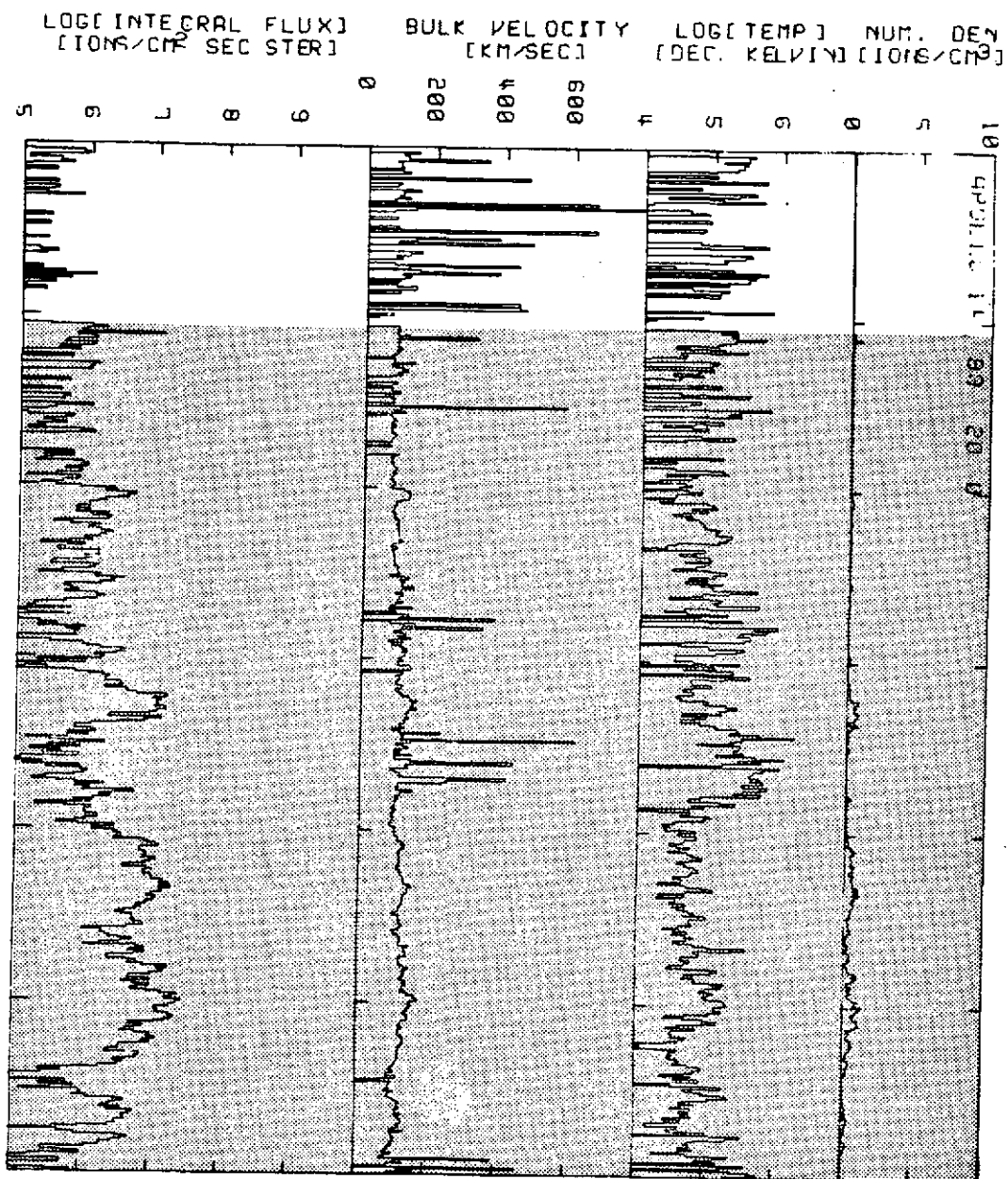


Figure 3.39

4 CORRESPOND

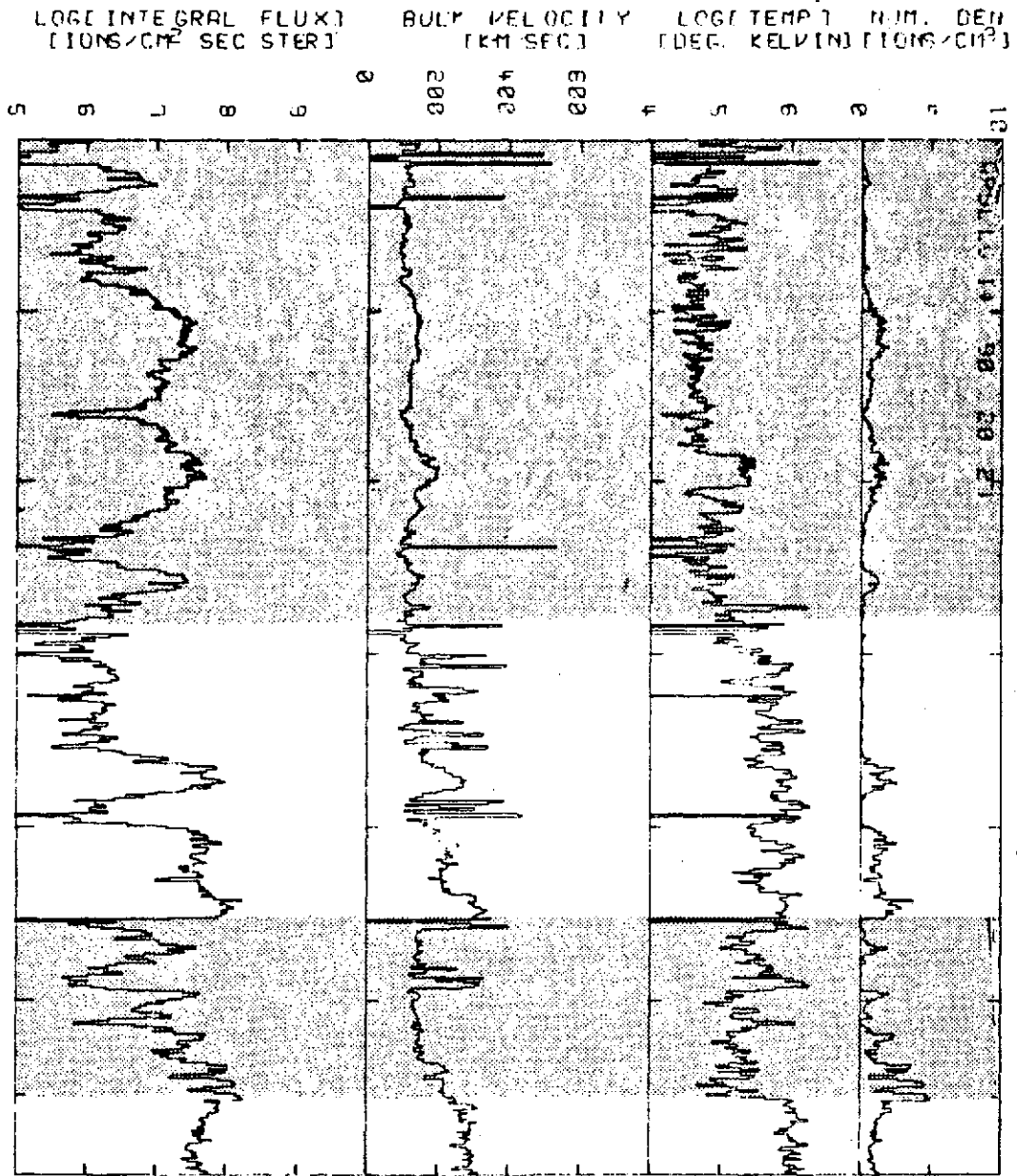


Figure 3.40

defined by these orbits is not symmetric about the point $Y_{sm} = Z_{sm} = 0$. This asymmetry is produced by the moon's five degree inclination to the ecliptic and the apparent yearly ± 23 degree wobble of the earth's spin axis in solar ecliptic coordinates.

The net effect of this asymmetry is to produce a higher density of coverage over a smaller spatial extent for solar magnetospheric longitudes less than 180 degrees than for longitudes greater than 180 degrees. Inbound the moon is restricted to a region relatively close to the $(XY)_{sm}$ plane. There are more than twice as many crossing of the $(XY)_{sm}$ plane on the inbound portions of the orbits as opposed to the outbound portions. This means that inbound the moon has a higher probability than outbound of being near the $(XY)_{sm}$ plane during times when the plasma sheet is either thin or displaced. This behavior is reflected in Figure 3-41a which shows that numerous events are seen near the $(XY)_{sm}$ plane inbound while no LEP events are seen near the plane outbound. The complete lack of LEP events near the $(XY)_{sm}$ plane outbound is, however, somewhat anomalous and may indicate another mechanism operating to exclude the particles from this region. What all the above indicate is that the phenomenon has potentially a very large spatial extent since observations are found from $+17 R_e$ to $-17 R_e$ in the Z_{sm} direction and from $-36 R_e$ to $+33 R_e$ in the Y_{sm} direction. It must be kept in mind, however, that the region for the particles is separate from the plasma sheet. The observation of LEP's near the $(XY)_{sm}$ plane must therefore correspond to times when the plasma sheet was either very thin or displaced from its expected location.

Figure 3.41a

The position of the moon during each of the 265 LEP events studied has been plotted in solar magnetospheric coordinates. (.1 radian = $6 R_e$)

Figure 3.41b

The orbit of the moon for the fifteen orbits studied has been plotted in solar magnetospheric coordinates in the SM longitude range from 2.54 to 3.74 radians. (.1 radians = $6 R_e$)

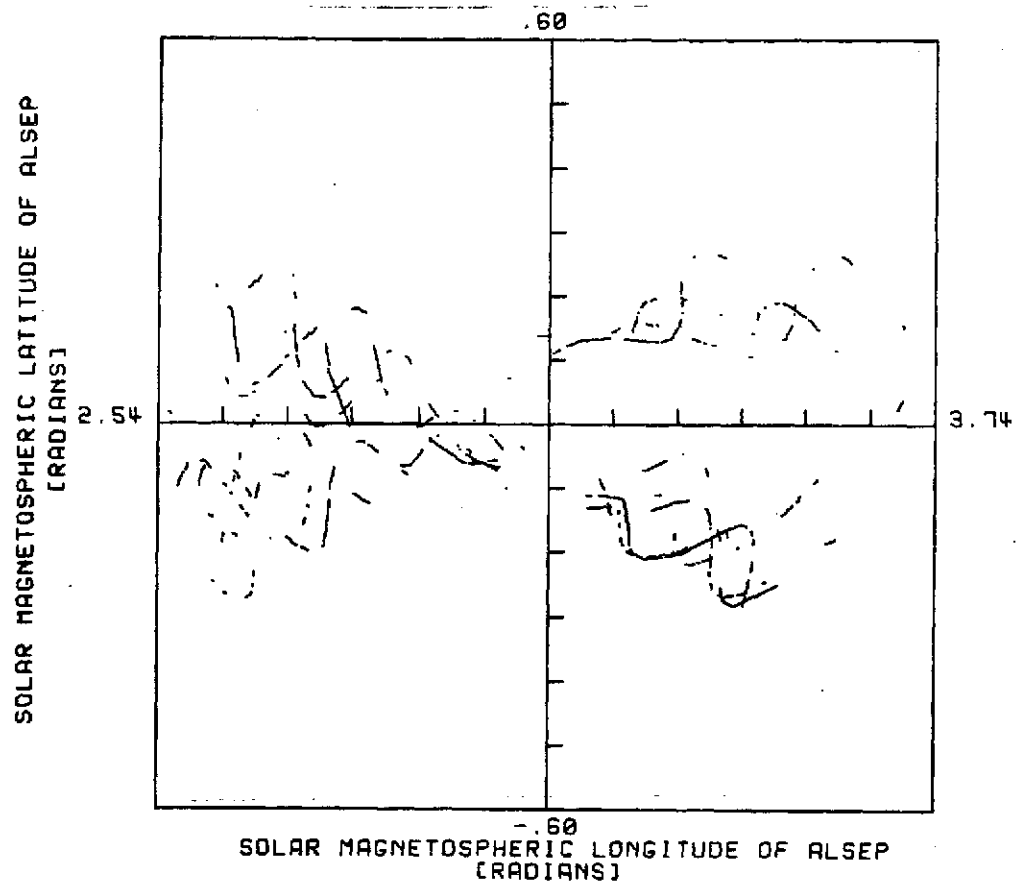
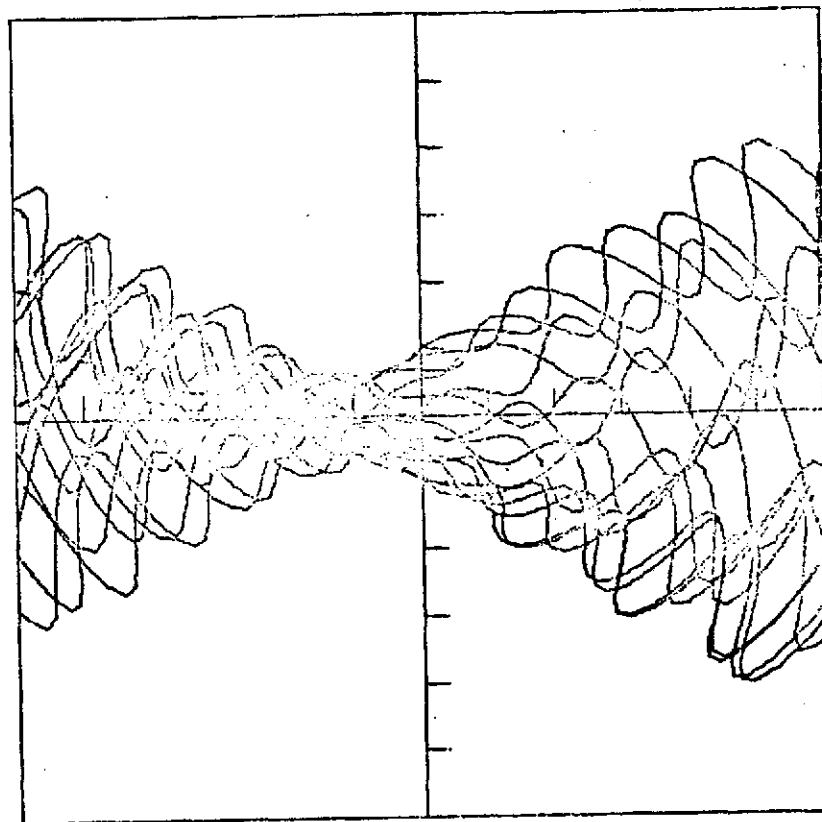


Figure 3.41a

C-2

SOLAR MAGNETOSPHERIC LATITUDE OF ALSEP
[RADIAN]

2.54



.60

-.60

SOLAR MAGNETOSPHERIC LONGITUDE OF ALSEP
[RADIAN]

3.74

Figure 3.41b

This still leaves the question as to in what region exclusive of the plasma sheet these events are found. First, it must be determined if the LEP events are confined to a relatively thin "boundary layer" at the flanks of the tail and along the boundary between the plasma sheet and the lobes, as suggested by Akasofu. This suggestion seems contradicted by the Side data. If one considers again lunations 3 and 9 which were discussed earlier one sees that continuous LEP events are observed during times in which the moon traveled distances of $18 R_E$ or more in the Y_{sm} direction and $9 R_E$ or more in the Z_{sm} direction. Such observations are not reconcilable with a thin "boundary layer". That the events are instead either homogeneous throughout the lobes or comprise a thick "boundary layer" appear more in keeping with the data but no definitive statement can be made without further analysis.

One may also study the incidence of the events as a function of the look angle of the instrument. Since the LEP events are observed to take place on the ordered field lines of the tail lobes, it is logical to investigate their incidence as a function of the angle between the detector and the field line. For this purpose we assumed the field lines to be aligned in the perfect antisolar direction, i.e., the longitude of the field to be exactly 180 or 360° and the latitude to be exactly 0 degrees. From the magnetic field data which has been presented this appears to be a reasonable assumption for the LEP events.

To accomplish this angular study, the extent over which the events were observed was divided into a series of five degree wide bins. The number of minutes a given event was in a given bin was calculated and that number stored in that bin. The process was repeated for all 265 events with the total number of minutes in each bin then

being summed. The results of this analysis are shown in Figure 3.42. The two dark vertical lines in the figure represent the average angle of the detector with respect to the field line for the entry and exit of the moon from the tail.

This graph points out several important facts. First, the LEP events must have an angular extent of at least the 50° over which the Apollo 14 SIDE sees the events otherwise the observation of so many events at both the inbound and outbound flanks of the tail could not be explained. Secondly, there appears to be more LEP events occurring at times when the angle between the magnetic field and the detector was large (angles greater than $+10^\circ$) than when it is small. This can be attributed to three factors. First, part of this is due to the fact that the Apollo 14 instrument looks back approximately at the earth. Thus the bins for the smallest angles of the detector with the respect to the field represent periods when the moon was approximately in the middle of the tail and close to the location of the neutral sheet. This would normally correspond to times when the moon was in the plasma sheet. Since we have already seen that the LEP events do not occur in the plasma sheet, few observations of the LEP events should be made during this time; as is the case. Secondly, part of the observations at large angles arises from the fact that the moon sweeps through a larger and larger region of space in solar magnetospheric coordinates with increasing distance, $|Y_{SM}|$ from the center of the tail. This increases the probability of an encounter with the LEP's and thus the total number of events observed. Lastly, the peaking of the frequency of events away from the center of the tail may indicate an increase in spatial extent of the events near the magnetopause. This last conclusion will

Figure 3.42

Distribution of the observations of the LEP events as a function of the angle between the detector and the magnetic field lines of the lobes of the geomagnetic tail.

Figure 3.43

Distribution of the duration of the LEP events as a function of the angle between the look direction of the TID and the field lines of the lobes of geomagnetic tail.

Figure 3.44

Plot of the average K_p for the times of the LEP events in a lunation versus what percentage of the tail passage was dominated by the observation of LEP events.

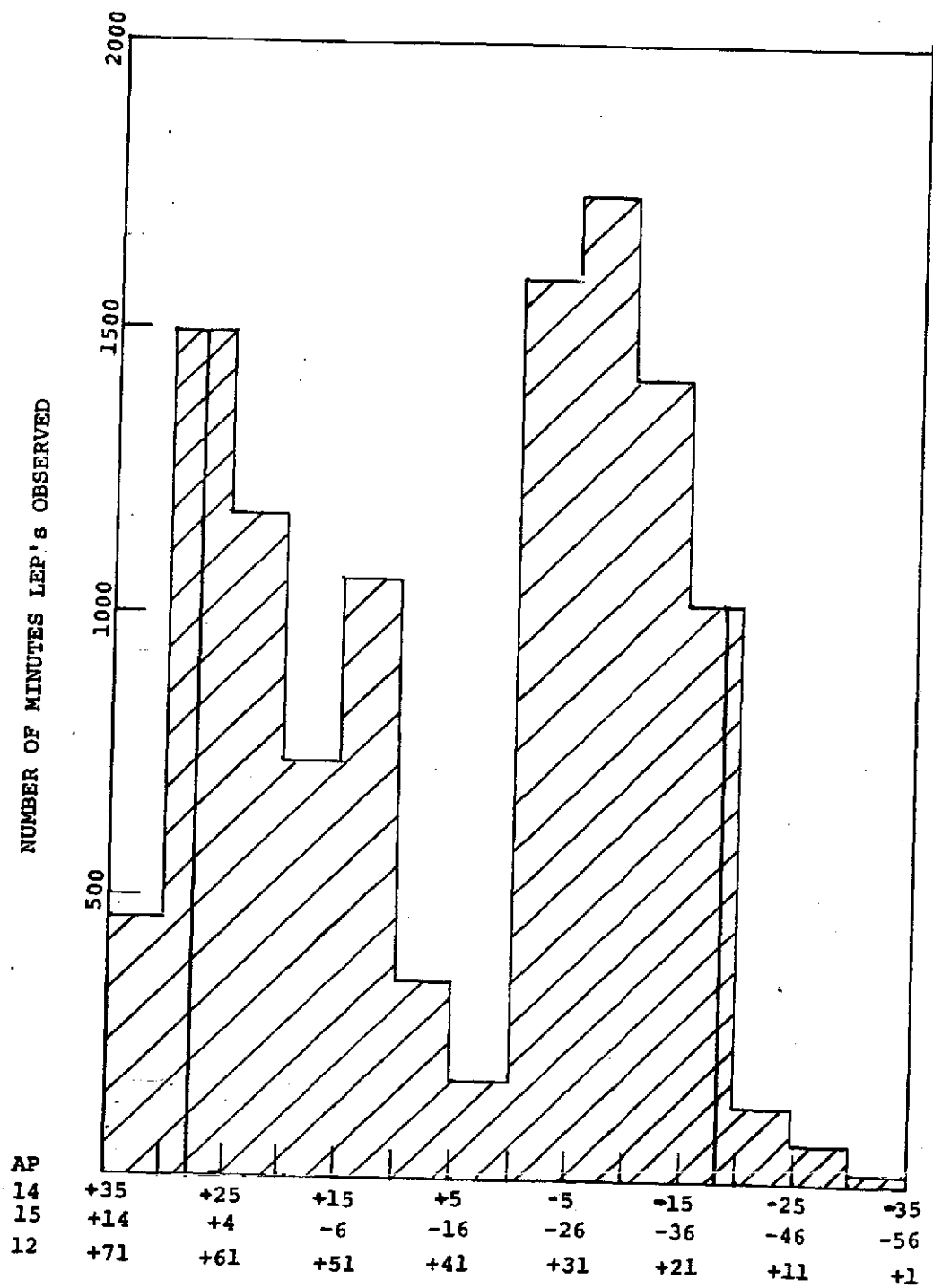
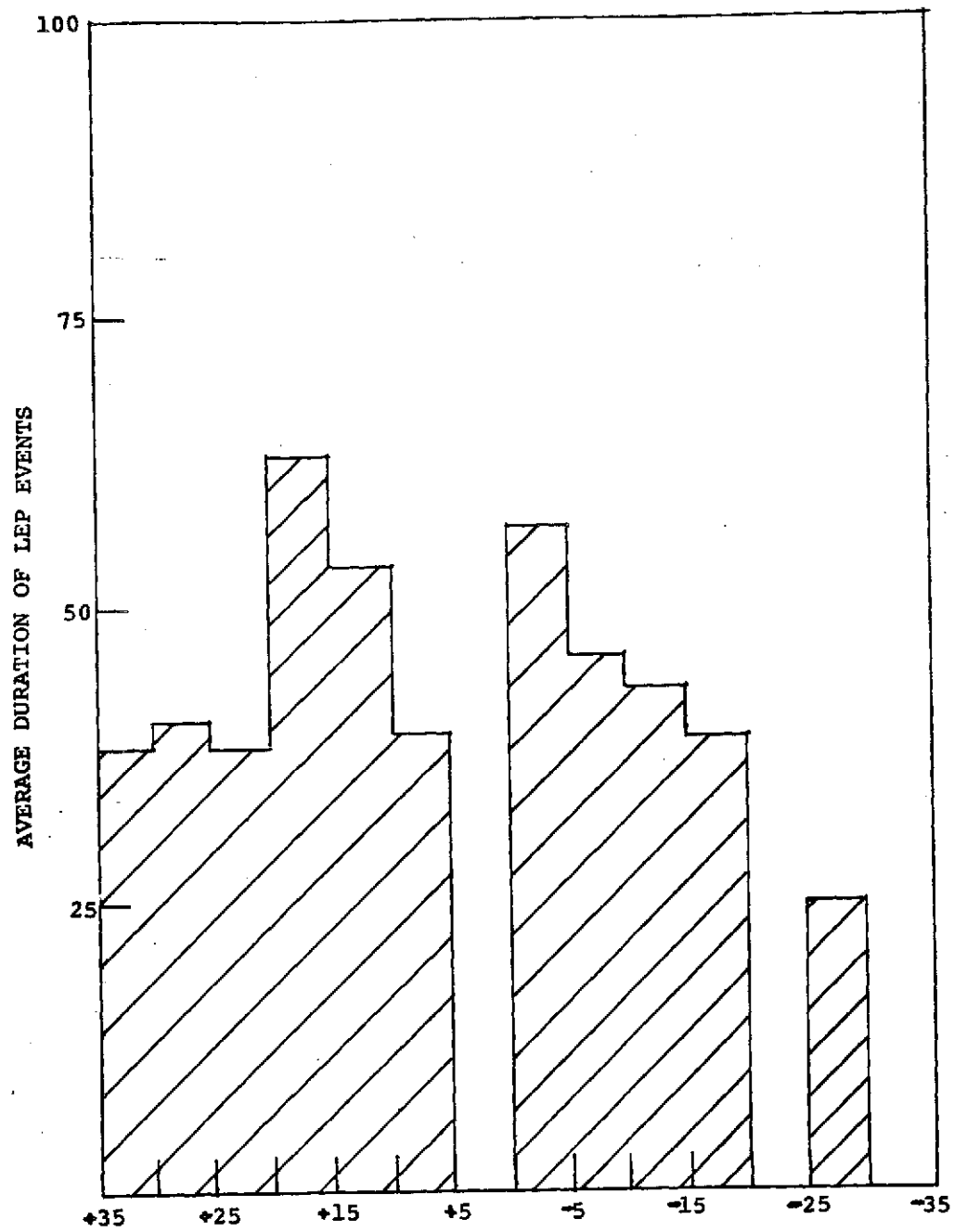
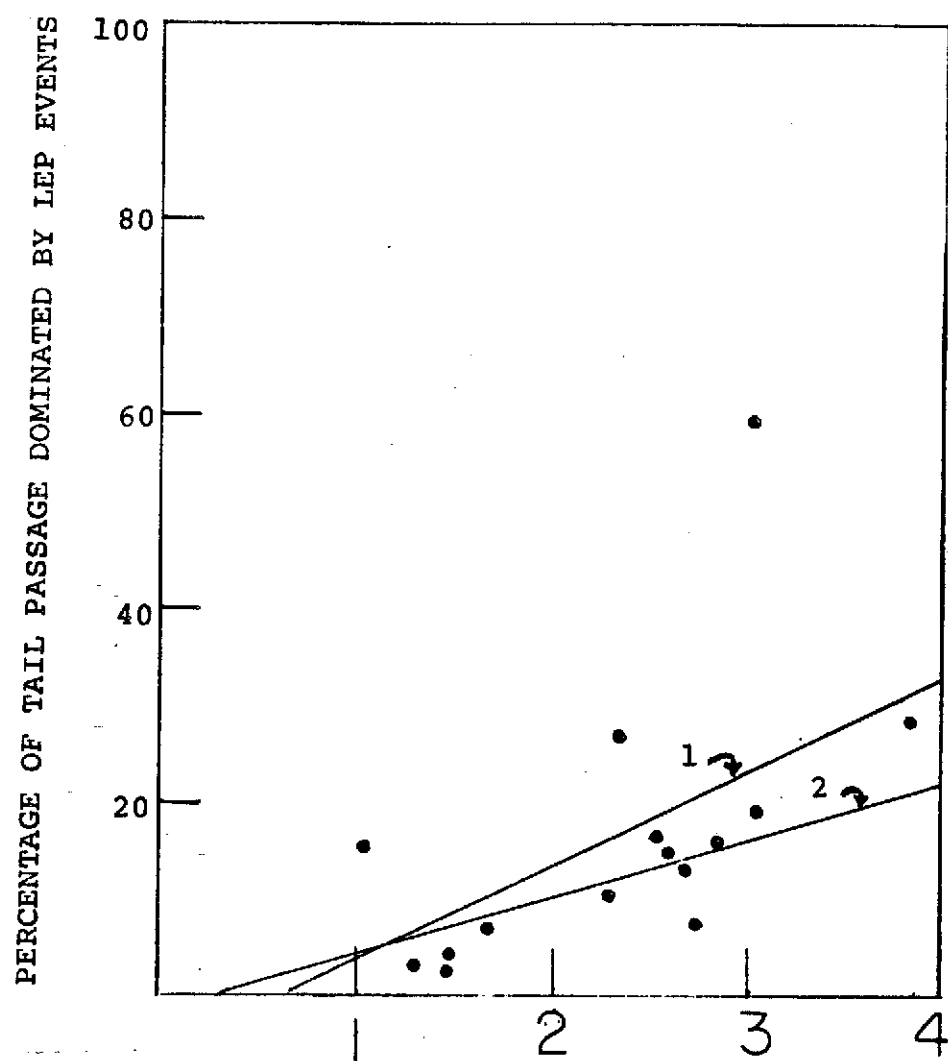


Figure 3.42



ANGLE BETWEEN MAGNETIC FIELD AND LOOK DIRECTION OF SIDE
(degrees)

Figure 3.43



AVERAGED KP OVER LEP EVENTS IN A LUNATION

Figure 3.44

be by no means certain, however, until the motional and positional effects mentioned above have been more completely studied.

In spite of the above the look direction is not completely insignificant. Figure 3.42 shows that outbound the majority of the events occur in an angular range of 0 to 15° relative to the field lines. These outbound LEP events tend to be the most intense observed; in general displaying considerable higher integral flux than the inbound events where the angle between the detector and the field lines is much greater. Similarly the high observation rate in the -15 to -10° bin can be principally attributed to the two most intense events inbound; one in day 118 of 1972 and the other in day 77 of 1973.

This is further supported by the distribution of durations as shown in Figure 3.43. In this figure each angular bin has been divided by the total number of events it contained and the average duration has been plotted as a function of angle. Two bins have been deleted, since they each contained only two events which was deemed too small a sample on which to base an average. One sees that the longer term events are associated with smaller angles relative to the field lines than was true in the total observations distribution. This is especially true on the outbound portion where the average duration is seen to decrease with increasing angle. This is sensible in terms of flow along the field lines since it would become increasingly difficult for the instrument to detect low intensity events the further its look direction moved away from zero with respect to the field lines.

More information can be acquired by considering the other two instruments for which data is available. As stated previously, when simultaneous data was available, and has been analyzed, the events were

seen by all three instruments. In Figure 3.42 below the angular bins for the Apollo 14 instruments are listed the comparable angular bins in which the events would be found for the Apollo 12 and 15 instruments. One sees that this greatly increases the angular extent over which the events are seen. The angular extent now is on the order of 100° . The answer is somewhat rough, however, since few comparably Apollo 12 events have been found due to a scarcity of tail data for the instrument.

Finally the dependence of the events on geomagnetic activity can be investigated. So far no relationship has been found between K_p and the intensity or duration of the events. There does, however, appear to be a relationship between the amount of the tail passage which is dominated by the IEP events and the K_p averaged over the time when the IEP events occurred. Table 2 shows the total hours of observation of the event for each lunation, what percentage of the tail passage that time comprises, and the K_p averaged over that period. In Figure 3.44, this averaged K_p has been plotted versus the percentage of the passage that was dominated by the event. One can see that the percentage tends to increase for increasing K_p . When a linear regression is run on the data a correlation coefficient of $r = .55$ is obtained. Such a correlation has a three percent probability of arising from a random data set. The corresponding line to this least square fit is labelled one in the graph.

The one point which deviates most from the data is that arising from lunation three. If this one lunation is treated as atypical; a fair assumption since it has twice as many hours of observation as any other tail passage, and if the linear regression is run again, we obtain a correlation factor of $r = .670$. This has a probability of

Table 2

Lunation	Hours of LEP observations	percentage of passage dominated by LEP events	Kp averaged over LEP events
1	16.167	18.37	2.54
2	14.50	15.42	1.03
3	42.683	59.28	2.97
4	16.350	16.35	2.86
5	2.10	2.01	1.45
6	3.083	3.90	1.47
7	13.650	13.38	2.60
8	5.667	6.75	1.683
9	20.132	26.84	2.32
10	8.00	10.39	2.31
11	6.232	7.16	2.73
12	3.81	4.01	1.30
13	11.733	14.49	2.70
14	17.117	18.66	3.02
15	17.533	28.28	3.90

less than 1% of arising from uncorrelated data. The line labelled two represents the least square fit to this condition.

It appears, therefore, that the frequency of occurrence does depend on the general geomagnetic activity as measured by Kp. This has two possible explanations. First, an increase in Kp could correspond to an increase in the motion of the magnetotail. This could move the LEP events past the moon more often than in periods of low activity. This approach fails to explain the long periods of continuous observation which are normally associated with the more prominent LEP events. Such an explanation would require that the induced motion in the tail mirror the motion of the moon in solar magnetospheric coordinates. This seems unlikely. The second approach would require some mechanism tied to geomagnetic activity which would increase the number of particles placed on these field lines. In other words the means by which the particles get on to these field lines must be tied to the general geomagnetic activity with an increase in activity increasing the number of particles that are fed onto these field lines.

Lastly since the events are related to Kp this explains some of the scatter of the data in the Z_{sm} direction. During periods of high Kp the location and thickness of the plasma sheet and neutral sheet can vary greatly thus destroying any possible ordering of the events in solar magnetospheric coordinates. This, coupled with the deviations in the location of the tail caused by variations in the solar wind parameters, is probably responsible for much of the scatter. This does fail, however, to explain the anisotropy between the inbound and outbound portions of the tail; unless this is merely a statistical artifact.

3.8 Observational Conclusions

Considering all of the above the following observational conclusions can be made as to the nature of the phenomenon.

1. The events represent a phenomenon uniquely separate from the other particle regimes traversed by the moon. The spectrum for the events, normally exhibiting a peak between 50 and 250 eVs, is both narrower and of lower energy than either the magnetosheath or the plasma sheet. This is reflected in the LEP's low bulk velocity (100 to 250 km/sec) and low temperature (less than 5×10^5 °K). Similarly they have a number density of .2 to 5.0/cm³ which is intermediary between the other two particle regimes.

2. The LEP events are found to occur only on the well ordered field lines associated with the high and low latitude lobes of the geomagnetic tail. Magnetically they are not seen in close proximity to the location of the neutral sheet and little if any perturbation in the field is produced by either the advent, duration or cessation of the events. It appears impossible to locate the LEP events from the field data. Also abrupt changes in the spectra observed can be made to correspond to a traversal from one magnetic region to another, i.e., from transitions between the tail lobes, the plasma sheet and the magnetosheath.

3. There are numerous cases where there exists a shifting in the spectral characteristics of the events associated with passage from regions of ordered field where the low energy spectra are seen, to regions of disordered fields where magnetosheath spectra are observed. This transition is marked by a gradual broadening of the spectrum and a shifting of its peak towards higher energy.

4. Spatially the events occur over a wide region extending very deep into the tail (greater than $15 R_e$ in the Y_{sm} direction) and to the maximum extent of observation in the Z_{sm} direction. The heaviest density of events is, however, associated with regions closer to the magnetopause.

5. The LEP events have a broad angular extent. They are observed over an angle of at least 50° and perhaps greater than 100° .

6. The events display no systematic ordering in solar magnetospheric coordinates. Whether this is due to the failure of the coordinate system at such large distances from the earth where solar wind effects on the location of the tail would tend to be important, or due to the intrinsic nature of the events will require more field data. The LEP events, nonetheless, are found only exterior to the plasma sheet.

7. The frequency of observation increases with increasing K_p either indicating increased motion of the tail or an injection mechanism whose operation either arises from or is reflected by geomagnetic activity.

8. The events appear to be sporadic within the sensitivity of the instrument, i.e., the events do not seem to point to a region of fixed size where the constant flow of particles along field lines take place, but rather it appears as if there are regions to which particles are given access on some occasions by some as yet unspecified mechanism. If this were not true there would not be lunations in which practically no observations of the LEP events were made.

3.9 Theoretical Considerations

From the above data one can make some statements as to the possible ways in which these particles may gain access to the region in which they are observed. Two somewhat interconnected theories have been proposed to explain the existence of such particles. Hones has suggested (Hones et al., 1972) that the region in which these particles are observed is a mapping back into the tail of the field lines of the cusp where, through magnetic merging, particles have been allowed to enter. This fits fairly well his observations at $18 R_e$ where most of the events are found in close proximity to the magnetopause. At lunar distances the more extended region over which the particles are seen makes this theory untenable.

A somewhat more inclusive theory has been offered by R. A. Wolf (private communication). In this theory as in Hones, particles are allowed to enter by merging through the cusp. This produces particles flowing backward on the field line close to the magnetopause and possessing some distribution in velocity. These particles will be exposed to the cross tail electric field and as a result they will execute $E \times B$ motion convecting them downward towards the neutral sheet. The slower moving particles being exposed to the tail field for a longer period of time will be convected further down than the faster moving particles. This would predict only lower energy particles deep in the tail.

Some crude calculations can be made to test this theory. If one assumes that the cross tail potential is on the order of 5×10^4 volts and that the tail has a diameter of $\sim 45 R_e$, a number in keeping with the SIDE observations, one may calculate a rough number for the

Figure 3.45

Cross section of the tail, assumed circular, showing the region in which ions of energy less than 100 eV would be expected to drift by the time they reached lunar distance assuming a cross tail potential drop of 5×10^4 volts.

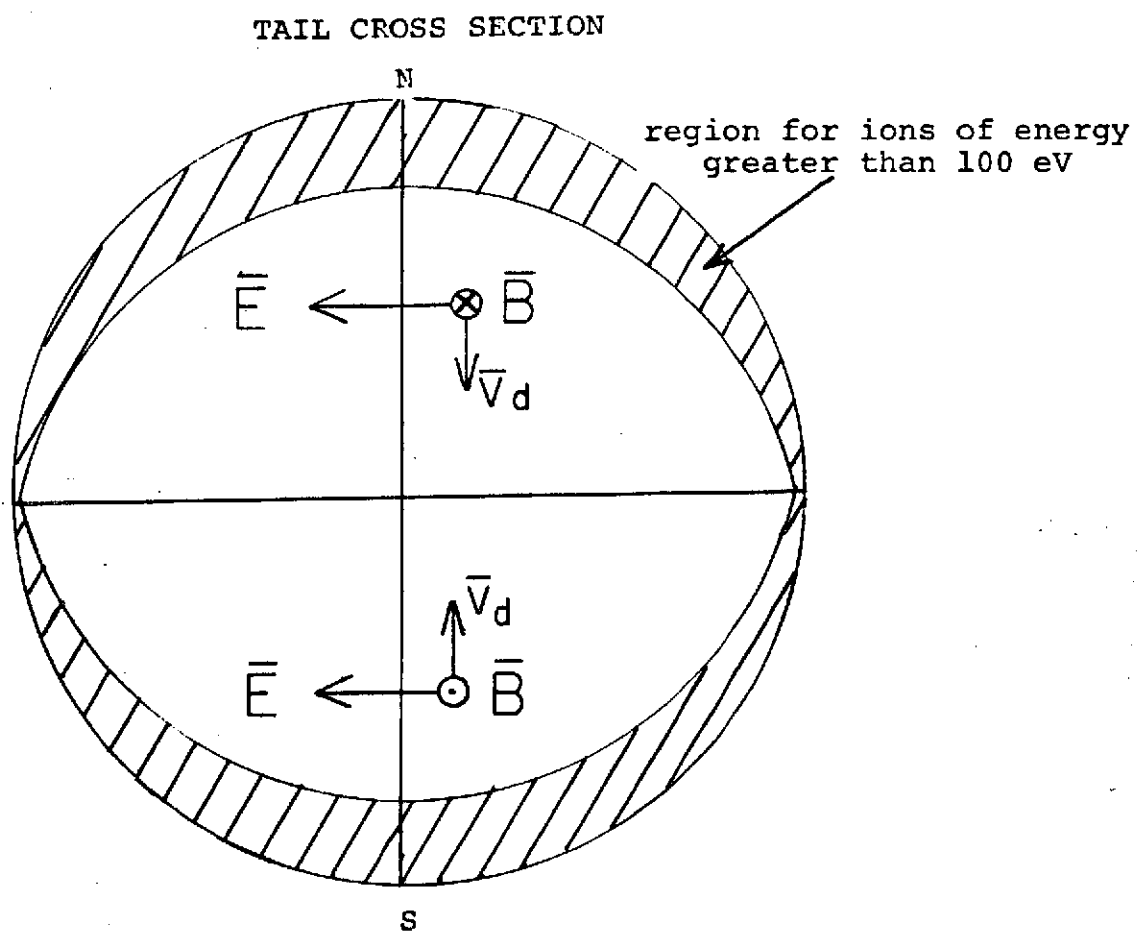


Figure 3.45

field strength. Assuming the field to be homogeneous one gets

$$E = .174 \text{ volts/km} .$$

Using a field strength of 15 gammas (1.5×10^{-4} Gauss) one derives an $E \times B$ velocity of approximately 11.6 km/sec. For a 100 eV particle, assuming most of its energy is in flow motion, one computes a velocity of 138 km/sec and a transit time to the moon of 46 minutes. This means that the particles could $E \times B$ drift towards the neutral sheet a distance of $\sim 5 R_e$. Figure 3.45 shows the region in which one would expect particles with energy greater than or equal to 100 eV.

Similar calculations for the 50, 70, and 250 eV particles give distances of $\sim 7 R_e$, $6 R_e$, and $3.16 R_e$, respectively. This process at first glance does not appear to give the particles enough motion in the Z_{sm} direction to account for the observed distribution.

There are two ways in which this difficulty might be overcome. First, it is known that during substorms the magnitude of the cross tail potential increases to values as high as 235 kilovolts; a potential drop almost five times the value used in the previous calculations. Such a potential drop would imply a $E \times B$ velocity of 60 km/sec and a convective distance for 100 eV particles of $\sim 25 R_e$. This is more than enough to account for the appearance of the events deep in the tail. Alternatively the potential drop might not be uniform across the tail with a higher field region over a smaller extent giving the particles the necessary cross field motion. Thus there is so far no insurmountable contradiction.

If the mechanism described above is responsible for the motion of the particles one would expect that, if the magnitude of the potential drop was kept constant, then the number of LEP events observed would increase for decreasing diameter of the tail. This is due simply to an increase in the field caused by the same potential drop being applied across a shorter distance. This increase in observations with decreasing tail diameter is somewhat supported by the data. The three lunations in which the most hours of observations are found, lunations 3, 9, and 15 are also the lunations with the smallest apparent diameters, $38.6 R_e$, $40.26 R_e$ and $33.28 R_e$, respectively. The diameters in this case were determined by calculating the distance traversed from the last magnetopause crossing inbound to the first outbound.

The data for all fifteen lunations is plotted in Figure 3.46. We have plotted here the diameters of the tail versus the percentage of the tail passage dominated by the events. Performing a linear regression on this data we obtain a correlation factor of $r = -.49804$ which is surprisingly good considering the crudeness of the method used to determine the diameters.

There are two other points which are supportive of the theory. First, it can explain the apparent correlation between K_p and the number of observations of LEP events. This is true since, if the events arise from particles entering through magnetic merging at the cleft, an increase in merging rate and therefore an increase in the time over which particles enter would be reflected in an increase in geomagnetic activity and therefore K_p . Secondly, it can explain the apparent burst like behavior of the events. Since the merging rate is dependent on the orientation of the interplanetary field relative to the earth field

one would expect to see events only episodically, i.e., when the orientation for merging was optimum.

The theory runs into some difficulty, however, in accounting for the spectral behavior of the events. It predicts that the lower the initial flow energy of the particles the further they will drift towards the neutral sheet by the time they reach lunar distances. In Figure 3.48 are shown the regions corresponding to the maximum drift distance that could be covered by 50, 70, 100, and 250 eV particles assuming a cross tail potential of 100 kilovolts. The assumption was made that the particles entered in a region of one earth radius thickness at the edge of the tail. The particles of a given energy are, therefore, confined to a relatively small region in the Z_{sm} direction. Superimposed on Figure 3.47 is a representative lunar orbit shown in solar magnetospheric coordinates. Since the distribution in energy should be continuous there should actually be a gradient in energy in the positive Z_{sm} direction above the neutral sheet and in the negative Z_{sm} direction below the neutral plane. Thus as the moon follows the orbit shown in the figure it should observe a shifting in the energy of the event as it travels up and down in the Z_{sm} direction and as it travels towards the center of the tail.

This sort of behavior is not supported by the data analysis which has been done to date. Spectral variations of any significance are the exception not the rule, with the spectrum in most cases showing no variations over the period of observation. The few cases where significant variation in the peak or width of the spectrum has been noted have been associated either with motion in the wrong direction for the shifting to agree with theory or with the shifting associated

Figure 3.46

Approximate diameters of the tail plotted versus the percentage of the tail passage dominated by the LEP events. The line represents the least square fit to the data.

Figure 3.47

Cross section of the tail showing the regions in which 250 eV, 100 eV, 70 eV, and 50 eV particles would be observed assuming the cross tail potential drop was 100 kilovolts and that the particles entered in a region one earth radius thick at the magnetopause. A typical lunar orbit in solar magnetospheric coordinates is also shown.

Figure 3.46

Approximate diameters of the tail plotted versus the percentage of the tail passage dominated by the LEP events. The line represents the least square fit to the data.

Figure 3.47

Cross section of the tail showing the regions in which 250 eV, 100 eV, 70 eV, and 50 eV particles would be observed assuming the cross tail potential drop was 100 kilovolts and that the particles entered in a region one earth radius thick at the magnetopause. A typical lunar orbit in solar magnetospheric coordinates is also shown.

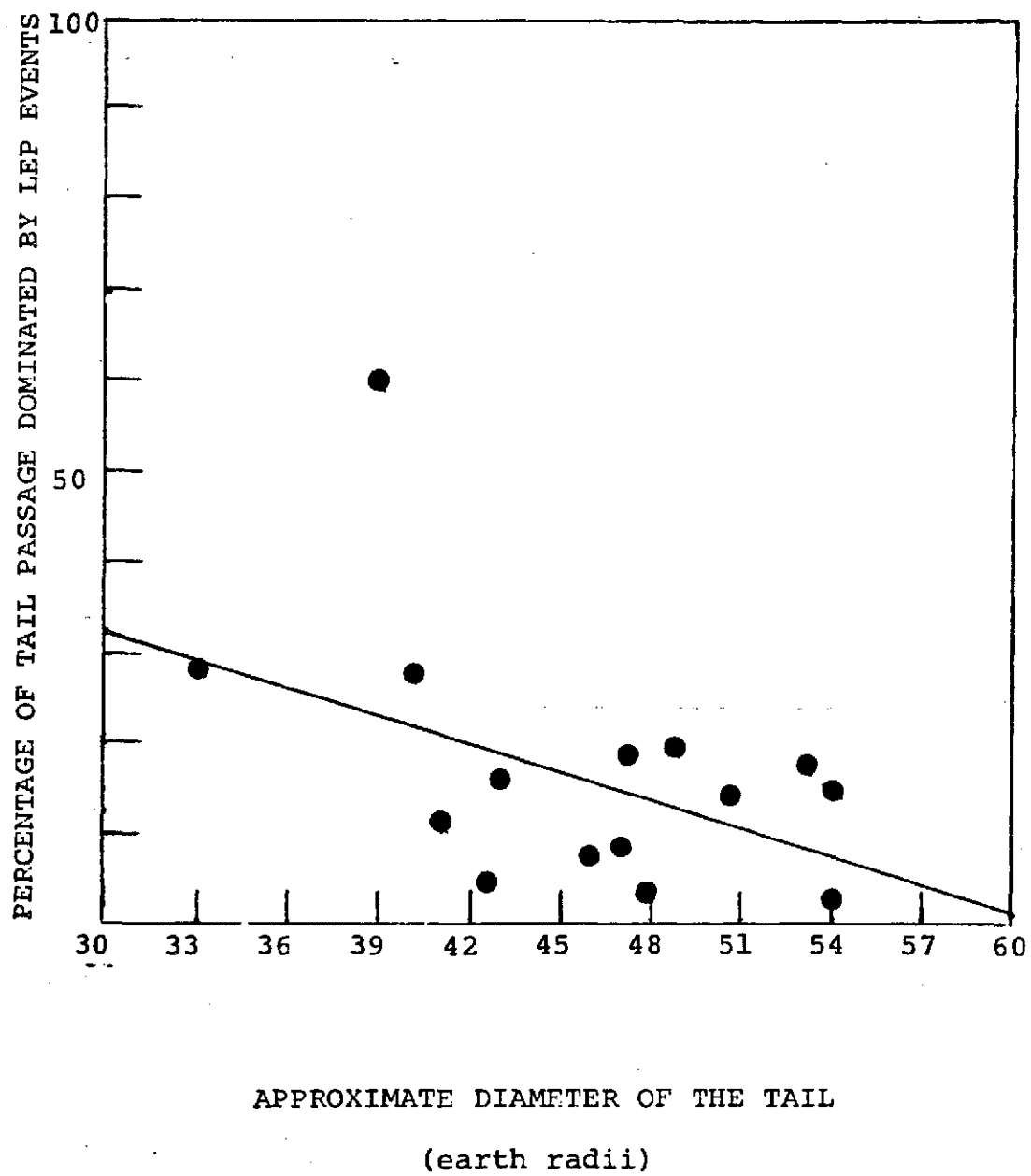


Figure 3.46

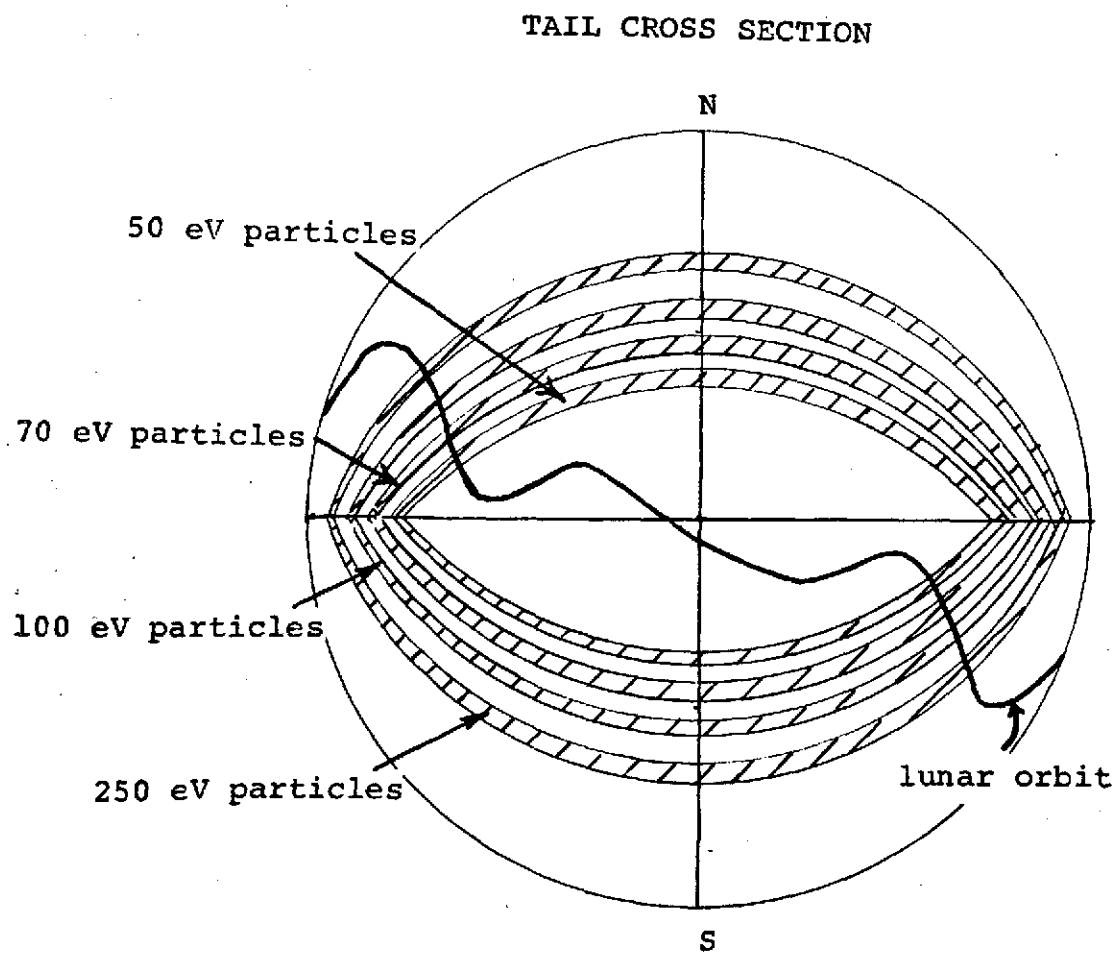


Figure 3.47

with the transition into the magnetosheath. The first case was seen in the lunation one where a hardening of the spectrum and shifting of the peak was associated with motion towards the neutral plane. The second case corresponds to the transition between the tail and magnetosheath seen in lunation two. There is evidence that the spectrum remains quite constant over distances as great as 6 earth radii in the Z_{sm} direction. All this is in contradiction to the predictions of the theory.

In conclusion it appears that while the theory is able to explain some aspects of the phenomenon observed there exist discrepancies between what is actually observed. This could be a basic incompatibility. We believe, however, that without further analysis the theory cannot be discounted.

3.10 Further Analysis

There are several further projects which are necessary to fully quantify and qualify the nature of the events.

1. An attempt should be made to fit a Maxwellian distribution to the data to determine the plasma characteristics more exactly. The numerical integration method used in this thesis represents only a first approximate method for determination of the parameters. We hope to considerably improve on them.

2. We hope to obtain more Explorer 35 magnetometer data or comparable data from the Apollo 15 Lunar Surface Magnetometer. Using this data the location of all the events relative to the observation of the magnetopause and neutral sheet can be compiled. It is possible that much of the disorder of the inbound portion of the tail passage is due to the inadequacy of the solar magnetospheric coordinates. By

ORIGINAL PAGE IS
OF POOR QUALITY

defining the locations of the LEP events in terms of real observations this difficulty will be partially eliminated and a more realistic spatial distribution will be obtained.

3. Using such a revised spatial distribution the region through which the moon passes may be divided into square elements of 1 or 2 earth radii each. The number of hours of observation of the events in each section can then be calculated and normalized to the total number of hours the moon actually spent in that region. This will give a very precise picture of the spatial distribution.

4. All of these above projects will require the analysis of more tail passages. We hope to double the amount of tail time that has been used.

5. The angular analysis needs to be done in finer detail with smaller bins. Also the relative intensity in the three instruments for simultaneous observations should be used to precisely define the angular extent.

6. There should be a careful analysis to see if there is a correlation between the occurrence of the events and the occurrence of substorms. This can be most easily accomplished by the use of the Auroral Electrojet (AE) index and the use of ground based magnetograms.

7. A more detailed analysis of the temporal behavior of the events must be undertaken to ascertain whether any energy gradient exists.

8. Some observations have been made of double peaked spectra associated with LEP events. These shall be studied further.

ORIGINAL PAGE IS
OF POOR QUALITY

ACKNOWLEDGMENTS

I wish to thank my thesis advisor, Dr. John Freeman Jr., for his help and support in the preparation of this work. My special thanks go to Dr. Kent Hills, Lynne Mutchler, and John Benson for their help in teaching a novice how to program and use the computer. Also, more importantly, I want to thank them for the many hours of discussion they provided both on my research and about things in general. This made my work easier and definitely more enjoyable. Most importantly I wish to thank my parents for their love and encouragement without which this work would have been impossible.

My appreciation to Steve Bowling for many valuable discussions, to Dr. D. S. Colburn for providing magnetic field data and to Barbara Ballou for typing this thesis. This research was supported by NASA contract NAS 9-5911.

REFERENCES

- Akasofu, S. I., E. W. Hones, Jr., S. J. Bame, J. R. Asbridge and A. T. Y. Lui, Magnetotail and boundary layer plasma at a geocentric distance of approximately $18 R_E$; Vela 5 and 6 observations, J. Geophys. Res., 78, 31, 7257, 1973.
- Axford, W. I., Viscous interaction between the solar wind and the earth's magnetosphere, Planet. Spac. Sci., 12, 45, 1964.
- Bame, S. J., J. R. Asbridge, H. E. Felthaus, E. W. Hones, I. B. Strong, Characteristics of the plasma sheet in the earth's magnetotail, J. Geophys. Res., 72, 113, 1967.
- Behannon, K. W., Mapping of the earth's bow shock and magnetic tail by the Explorer 33, J. Geophys. Res., 73, 3907, 1968.
- Behannon, K. W., Geometry of the geomagnetic tail, J. Geophys. Res., 75, 4, 743, 1970.
- Burke, W. J., F. J. Rich, and D. L. Reasoner, Effects on the geomagnetic tail at $60 R_E$ of the geomagnetic storm of April 9, 1971, J. Geophys. Res., 78, 25, 5477, 1973.
- Cahill, L. J., Preliminary results of magnetic field measurements in the tail of the geomagnetic cavity, IGB 79, 45, 231, 1964.
- Dessler, A. J., Length of the geomagnetic tail, J. Geophys. Res., 69, 19, 3913, 1964.
- Dungey, J. W., The length of the magnetospheric tail, J. Geophys. Res., 70, 1753, 1965.

Fenner, M. A., Magnetosheath plasma at $60 R_e$, M. S. thesis, Rice University, 1971.

Fenner, M. A., J. W. Freeman, Jr., and H. K. Hills, The electric potential of the lunar surface, Proceedings of the Fourth Lunar Science Conference, 3, 2877, 1973.

Fenner, M. A., Observations of magnetosheath plasma at the lunar orbit, Ph. D. thesis, Rice University, 1974.

Freeman, J. W., Jr., H. Balsiger and H. K. Hills, Suprathermal ion detector experiment (Lunar ionosphere detector), Apollo 12 Preliminary Science Report, NASA SP-235, 1970.

Garrett, H. B., T. W. Hill, and M. A. Fenner, Plasma sheet ions at the lunar distance preceding substorm onset, Planet. Space Sci., 19, 1413, 1971.

Heppner, J. P., N. F. Ness, T. L. Skillman, and C. S. Scearce, Explorer 10 magnetic field measurements, J. Geophys. Res., 68, 1, 1963.

Hess, W. M., The Radiation Belt and Magnetosphere, Blaisdell Publishing Co., Waltham, Mass., 1968.

Hones, E. W., Jr., J. R. Asbridge, S. J. Bame, M. D. Montgomery, S. Singer, S.-I., Akasofu, Measurements of magnetotail plasma flow made with Vela 4B, J. Geophys. Res., 77, 28, 5503, 1972a.

Hones, E. W., Jr., S.-I. Akasofu, S. J. Bame, and S. Singer, Outflow of plasma from the magnetotail into the magnetosheath, J. Geophys. Res., 77, 34, 6688, 1972b.

- Hruska, A., A. Hruskova, Transverse structure of the earth's magnetotail and fluctuations of the tail magnetic field, J. Geophys. Res., 75, 13, 1449, 1970.
- Intriligator, D. S. and J. H. Wolf, Evidence of a diffuse magnetopause boundary, J. Geophys. Res., 77, 28, 5480, 1972b.
- Johnson, F. S., The gross character of the geomagnetic field in the solar wind, J. Geophys. Res., 65, 3049, 1960.
- Meng, C. I. and J. D. Mihalov, On the diamagnetic effect of the plasma sheet near $60 R_e$, J. Geophys. Res., 77, 25, 4668, 1972.
- Meng, C. I., and J. D. Mihalov, Average plasma sheet configuration near $60 R_e$, J. Geophys. Res., 77, 10, 1739, 1972.
- Nishida, N., E. F. Lyon, Plasma sheet at lunar distance: structure and solar wind dependence, J. Geophys. Res., 77, 22, 4086, 1972.
- Ness, N. F., The earth's magnetic tail, J. Geophys. Res., 70, 2989, 1965.
- Ness, N. F., The geomagnetic tail, Rev. of Geophys., 1, 97, 1969.
- Piddington, J. H., Geomagnetic storm theory, J. Geophys. Res., 65, 93, 1963.
- Prokash, A., Detection of earthward flow of Kev protons in the geomagnetic tail at lunar distances, J. Geophys. Res., 77, 28, 5633, 1972.
- Reasoner, D. L., W. J. Burke, Characteristics of the lunar photoelectron layer while in the geomagnetic tail, J. Geophys. Res., 77, 34, 6671, 1972.

Rich, F. J., Plasma in the geomagnetic tail observed by the charged particle lunar environment experiment, Ph. D. thesis, Rice University, 1973.

Roederer, J. G., The earth's magnetosphere, Science, 183, 37, 1974.

Russel, C. T., K. I. Brody, Some remarks on the position and shape of the neutral sheet, J. Geophys. Res., 73, 6104, 1967.

Winningham, J. D. and W. J. Heikkila, Characteristics of magnetosheath plasma at low altitudes in the dayside cusp, TAM Geophys., 52, 4, 320, 1971.